University of St Andrews

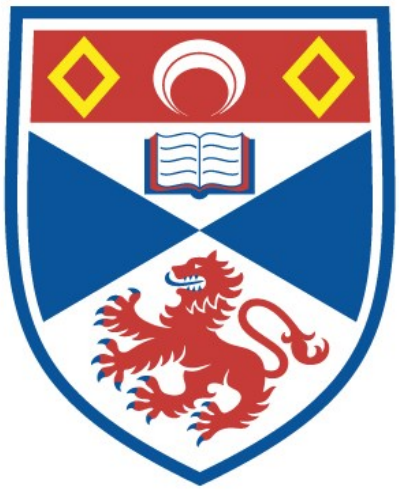

Full metadata for this thesis is available in
St Andrews Research Repository
at:
http://research-repository.st-andrews.ac.uk/

This thesis is protected by original copyright

FIELD PENETRATION INTO TYPE I SUPERCONDUCTING CYLINDERS

A Thesis

presented by

Rögnvaldur Ólafsson, B.Sc.

to the

University of St. Andrews

in application for the Degree

of Doctor of Philosophy.

Th 5853

DECLARATION

I hereby certify that this thesis has been composed by me, and is a record of work done by me, and has not previously been presented for a Higher Degree.

The research was carried out in the School of Physical Sciences in the University of St. Andrews, under the supervision of Professor J.F. Allen, F.R.S.

Rögnvaldur Ólafsson

CERTIFICATE

I certify that Rögnvaldur Ólafsson, B.Sc., has spent nine terms at research work in the School of Physical Sciences in the University of St. Andrews under my direction, that he has fulfilled the conditions of the Resolution of the University Court, 1967, No.1, and that he is qualified to submit the accompanying thesis in application for the Degree of Doctor of Philosophy.

Research Supervisor

CAREER

I first matriculated in the University of St. Andrews in October 1963, and obtained Third Class Honours in Physics in 1967.

In October 1967 I was enrolled as a research student under Ordinance 12, and was transferred to the Resolution of the University Court, 1967, No.1, in October 1968 as a candidate for the Degree of Doctor of Philosophy.

ACKNOWLEDGEMENTS

The author wishes to express his gratitude to Professor J.F. Allen, F.R.S. for his patient guidance and invaluable encouragement during this work.

He is grateful to Professor D.C. Baird for initiating the problem during a year in St. Andrews.

He thanks members of the Laser Group at St. Andrews for their help with the laser, and Mr. J. McNab for skilful technical assistance.

He is indebted to the Icelandic Government for providing maintenance grants through various channels.

Abstract

This thesis is concerned with the first stage of magnetic field penetration into short cylinders of type I superconductors.

The penetration has been studied experimentally by observing the magnetic field pattern on the top surface of indium and tin cylinders. The flux pattern has been made visible both by using Faraday rotation in a thin cerium metaphosphate glass disc and the diamagnetism of very fine superconducting vanadium powder. The first method allows the dynamics of the penetration to be studied but has rather a poor resolution. The powder method is largely confined to observing static field patterns but its resolution is good.

The penetration has also been studied mathematically for cylinders of length/diameter ratio from 0.2 to 2.0. Computer programs have been written that solve the field equations outside the superconducting region and show how the penetration proceeds as the applied field is increased. The field equations are solved numerically using successive overrelaxation and the penetration profiles have been found by iterative methods. The mathematical methods are discussed at some length.

The first stage of the penetration was found to consist of penetration of the corners of the cylinders. How far the penetration

proceeds is determined on the one hand by the condition that the field on the normal superconducting boundary should be equal to the critical field, and on the other hand by the pressure of demagnetization effects.

For very low applied fields the penetration has radial symmetry but as the field behind a convex boundary is necessarily lower than the field on the boundary, superconducting laminae soon spread from the superconducting centre region into the penetrating region. The penetration therefore takes the form of thin radial laminae, perpendicular to the advancing penetrating front. The period of the laminae is determined by the local value of the magnetic field and the surface energy of the metal, and can be described by Landau's unbranched model of the intermediate state, suitably modified.

It is also shown that the second stage of field penetration is reached when the two penetrating regions meet and just penetrate the equator of the specimen.

It is suggested that this form of penetration is not confined to short cylinders but is characteristic of cases where the penetration has a convex interface.

Lastly both the magnetic moment and the average magnetic induction in the cylinders have been computed for a number of applied fields up to the start of the second stage of penetration.

CONTENTS

LIST OF ILLUSTRATIONS

LIST OF SYMBOLS

A	area
B	magnetic flux density
B_a	flux density of applied magnetic field
B_c	critical flux density
B_i	flux density inside specimen
D	demagnetization constant
d	diameter of cylinder, or thickness of infinite plate
E	electric field strength
f_n	free energy per unit volume of normal phase
f_s	free energy per unit volume of superconducting phase
H	magnetic field strength
H_a	applied magnetic field strength
H_i	field strength inside specimen
g_n	Gibbs free energy per unit volume of normal phase
g_s	Gibbs free energy per unit volume of superconducting phase
H_c	critical magnetic field strength
H_{c1}	lower critical field of type II superconductor
H_o	critical magnetic field strength at $0^{\circ}K$
h	reduced magnetic field strength ($=H/H_c$)
h_a	reduced applied magnetic field strength ($=H_a/H_c$)
I	magnetization (magnetic moment per unit volume)
J	current density
J_s	surface current density

l	length of cylinder, or mean free path of electrons
M	total magnetic moment of a specimen
N	normal
S	superconducting
T	temperature
T_c	superconducting transition temperature
t	reduced temperature ($=T/T_c$)
V	volume
α	surface energy per unit area
$\Delta(t)$	surface energy parameter at temperature t ($\alpha = (H_c^2/8\pi)\Delta$)
η	volume fraction of normal material, or fraction of length
ξ	coherence length
κ	Ginzburg - Landau parameter
λ	penetration depth, or wavelength
$\lambda(0)$	penetration depth at $0^{\circ}K$
μ	permeability
σ	electrical conductivity
ϕ	magnetic scalar potential
ψ	magnetic flux (see page 50)
ρ	reduced length along the radius of a cylinder ($=r/r_o$; r_o = radius of cylinder), or resistivity
ω	relaxation constant, or order parameter

CHAPTER 1 - INTRODUCTION

1.1 Discovery and basic properties of superconductors

In 1908 Kamerlingh Onnes succeeded in liquefying helium and thereby created lower temperatures than were previously available. He was naturally eager to use his new technique to study various properties of materials at these low temperatures and among other things he measured the resistance of metals. During this work he observed that at about $4.2^{o}K$ the resistance of mercury suddenly fell very sharply to an immeasurably small value (fig. 1.1), and in fact it looked as if mercury lost its resistance completely at that temperature (Kamerlingh Onnes (1911) and (1913)). In the following years he studied this most curious behaviour further and found that not only was the superconductivity, as the phenomenon was called, destroyed by a high temperature but it was also destroyed when a sufficiently high magnetic field was applied (Kamerlingh Onnes (1913)). He found this critical field H_c to be a function of temperature, rising approximately parabolically from $H_c = 0$ at the transition temperature T_c to its maximum value H_o at $T = 0$ according to the relation $H_c = H_o (1-t^2)$, where $t = T/T_c$.

Soon after the discovery of superconductivity in mercury, sufficiently pure lead and tin were found to be superconductors

and today about half the metallic elements and a large number of alloys are known to exhibit superconductivity. Of the metallic elements niobium has both the highest transition temperature ($T_c = 9.3^{o}K$) and the highest critical field ($H_o = 1944$ Oe) but some alloys remain superconducting up to $18^{o}K$ and have critical fields of tens of thousands of Oersteds.

One of the most interesting questions that inevitably rose was whether superconductors had in fact zero resistance or a resistance just smaller than the sensitivity of the apparatus used. Naturally there is no answer to this question, the resistance could always be just smaller than what can be measured, but it is possible to find its upper limit. This was first done by Kamerlingh Onnes and Tuyn (1923) and their experiment showed that the resistance is so small that at least for practical purposes it can be neglected.

They used the fact that perfect conductors have the rather unusual property that the magnetic field inside them remains constant in time (or $\dot{\underline{B}} = 0$). This follows directly from Ohms law $\sigma \underline{E} = \underline{J}$ and the Maxwell equation curl $\underline{E} = -\dot{\underline{B}}/c$ when $\sigma \longrightarrow \infty$. This means that if a perfect conductor is subjected to a changing external field, internal currents that oppose the change will be induced and, as there is no

resistance, they do not die away and the magnetic field inside the body remains constant. They made use of this property by suspending a superconducting sphere by a torsion string above a superconducting ring. Both samples carried induced supercurrents and as long as these currents remained constant the specimens could be expected to behave like permanent magnets and repel each other by a constant force. The experiment lasted several hours and the force remained the same, showing that the resistance was indeed very small.

Since 1923 this experiment has been repeated every now and then with increasing sensitivity. The latest value for the upper limit of the resistance is 10^{-23} ohm-cm found by Quinn and Ittner (1962) by looking at the decay of a supercurrent in a tiny thin walled tube. As the low temperature limit of the resistance of pure copper is about 10^{-9} ohm-cm it seems fully justified to consider superconductors to be perfect conductors, that is without resistance.

For twenty years after their discovery superconductors were assumed to be nothing more than perfect conductors and their magnetic properties were thought to be only a result of their infinite conductivity. It was not until 1933 that Meissner and Ochsenfeld (1933) found them to have the additional property of never having an internal magnetic flux, regardless of

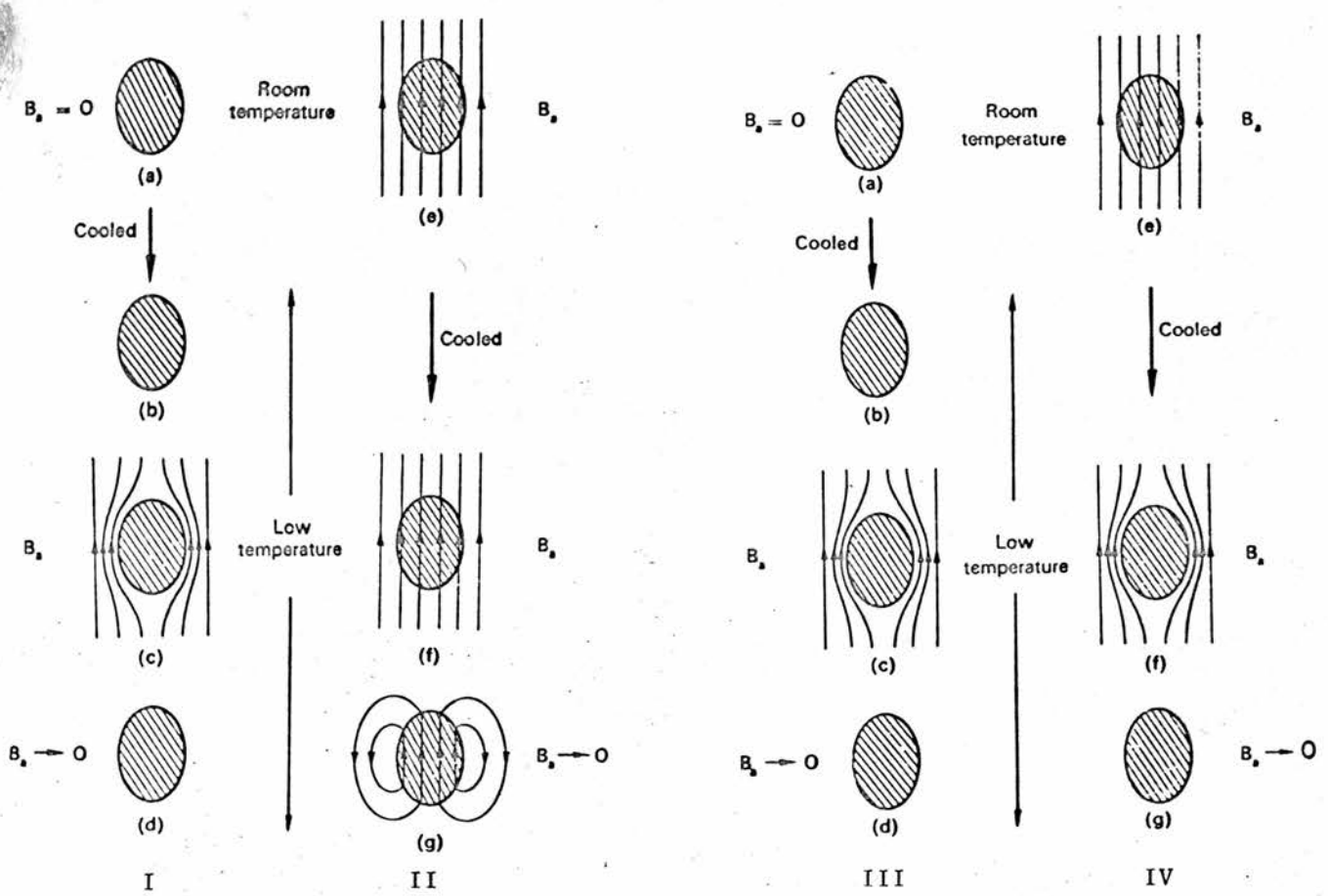

Fig. 1.2

The magnetic behaviour of a perfect conductor (left) and a superconductor (right). If the field is applied below T_c the behaviour is identical (I and III), but totally different when it is applied above T_c (II and IV). [From Rose-Innes and Rhoderick (1969)].

how the superconducting state is reached, that is inside a superconductor not only is there no variation of flux with time ($\dot{\underline{B}} = 0$), as would be expected for a perfect conductor, but there is also no internal flux ($\underline{B} = 0$). This has become known as the Meissner effect.

The difference between a superconductor and a perfect conductor is clearly demonstrated when both are cooled down in a magnetic field. At high temperatures both are threaded by flux but when the transition temperature is reached the superconductor expels the flux. The flux in the perfect conductor is on the other hand unchanged. If the applied field is now removed the superconductor remains non-magnetic, but in the perfect conductor currents are induced so as to prevent any change in the internal field and an internal magnetic flux equal to the applied flux remains (fig. 1.2).

It might seem strange that this fundamental property remained undiscovered for such a long time but apart from the fact that superconductivity was thought to be adequately explained by the perfect conductor theory, so no one looked for other effects, the Meissner effect is seldom perfect especially when the metal is not homogeneous and the sample of non-ellipsoidal dimensions.

This is because flux is easily trapped inside the superconductor both by imperfections and also when a superconducting path forms enclosing flux as often happens with cylinders and other shapes. The material then behaves as a perfect conductor.

1.2 Theory of superconductivity - A historical survey

Long before the discovery of the Meissner effect attempts had been made to apply thermodynamics to the transition from normal to superconducting state (Keesom (1924), Gorter (1933)) but as the transition in magnetic field had to be considered as essentially irreversible the validity of these theories was considered doubtful. The odd thing was however that the agreement between the theories and the experimental results was so good that it very much looked as the transition from superconducting into normal state was reversible.

After the discovery of the Meissner effect there could be no doubt that the transition was like any other phase transition and thermodynamics could be applied. Gorter and Casimir (1934 a,b) subsequently worked out a thermodynamic treatment and a two fluid model and F. and H. London (1935 a,b) developed a model describing the Meissner effect.

The two fluid model is based on two assumptions. Firstly a superconducting system possesses an order characterized by an order parameter ω varying from zero at $T = T_c$ to unity at $T = 0^{o}K$. This parameter can be considered as being the fraction of the conduction electrons that are superconducting. Secondly the entropy of the system is considered to be solely due to the non-condensed electrons which behaviour is considered as being similar to that of the electrons in the normal metal.

London's model assumes basically that the magnetic field inside a superconductor decays exponentially from the surface in the same manner as its time derivative does in a perfect conductor. This means that magnetic field penetrates the superconductor such that it decays to 1/e of its value in a characteristic distance λ called the penetration depth. Typical values of λ are about 10^{-5} cm. For large specimens this effect can clearly be neglected but for thin wires and films, and most important for this work, in the intermediate state, the penetration is important.

These two theories are highly successful in cases where size and surface effects are not important and in fact most of the present work is based on them.

H. London (1935) pointed out that the total exclusion of an external field does not lead to the state of lowest energy unless there is a surface energy on the boundary between the superconducting and normal phases. His argument was that as the energy of a superconductor increases by $H_a^2/8\pi$ per unit volume in the presence of an excluded magnetic field it would be more favourable for a superconductor to split up into a very large number of alternate normal and superconducting layers such that the width of the superconducting layers is less than the penetration depth λ and the width of the normal ones very much smaller. The free energy contribution of the superconducting layers would be reduced because of the penetration of the magnetic field and the normal regions, being extremely narrow, would not significantly contribute to the free energy. The resulting free energy would therefore be lower than that for a total exclusion of the field. The existence of the Meissner effect shows that this is not the case and London concluded that a large surface energy must exist on the phase boundary.

Among other things this high surface energy led Pippard (1950, 1951, 1953) to propose a modification of the London

model according to which the order parameter ω does not change abruptly at the surface but gradually over a length ξ which he called the range of coherence of the superconducting wave function. He found ξ to be about twenty times the penetration depth or of the order of 10^{-4} cm. As any change in the thermodynamic functions extends over the same region as changes in the order parameter this model overcame the difficulty in the London model of a very high field-induced entropy density at the surface. The coherence length, together with the penetration depth, also explained the surface energy on the superconducting-normal boundary as will be shown below.

Ginzburg and Landau (1950) developed a compatible theory by using quantum mechanics to predict the effect of the magnetic field.

Then in 1957 Bardeen, Cooper, and Schrieffer (1957) developed a microscopic theory of superconductivity (BCS theory) based on the so-called Cooper pairs (Cooper (1956)). These are formed from electrons of opposite spin and momentum condensing into a lower energy state. The BCS theory leads to the correct thermal and electromagnetic behaviour of superconductors. As the BCS theory is not important in this

work it will not be discussed further.

1.3 Surface energy - Type I and type II superconductors

As mentioned earlier London (1935) pointed out that expulsion of flux would not lead to the lowest energy state unless a rather high positive surface energy existed on the boundary between the superconducting and the normal phases. This idea was further strengthened by Pippard's theory of coherence and the Ginzburg-Landau theory. Indeed for a long time all superconductors were thought to exhibit Meissner effect and have a positive surface energy and although deviations were noted in certain superconductors and alloys these were considered to be impurity effects and consequently of little scientific interest. It was not until Abrikosov (1957) pointed out, that there might be superconductors with properties different from those that had been considered up to then, that it was realized that the apparently anomalous properties of some superconductors were in fact inherent properties of a new class of superconductors ~~which~~ whose behaviour was quite different from that of the old type. It soon became obvious that the difference was due to these new, type II as they

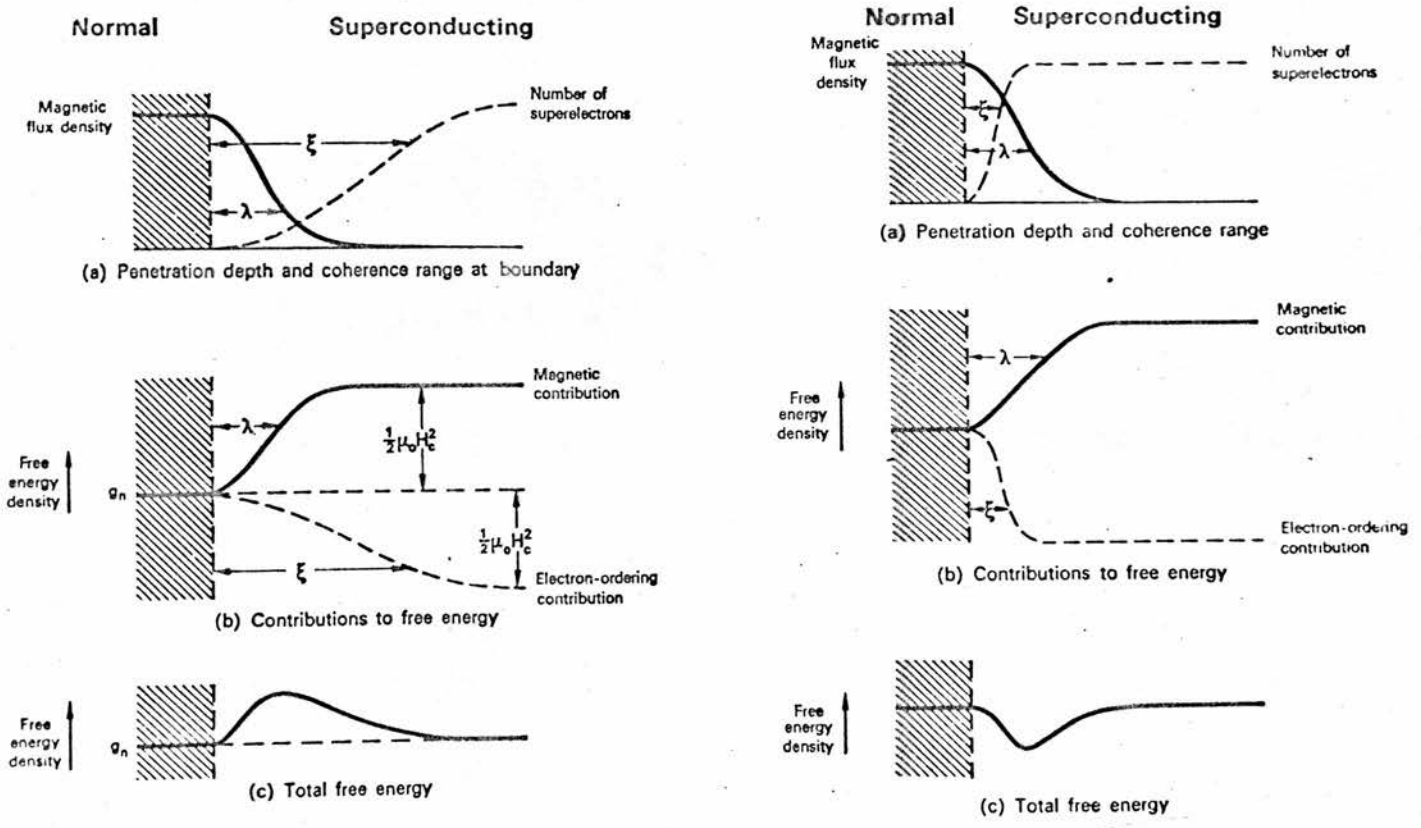

Fig. 1.3

Surface energy in type I (left) and type II (right) superconductors can be explained as the difference in magnetic and condensation energy near the interface. [From Rose-Innes and Rhoderick (1969)].

were called, superconductors having a negative surface energy instead of the positive surface energy of the old, type I, superconductors.

The existence of surface energy and the difference between type I and type II superconductors can be explained in terms of the penetration depth λ and the coherence length ξ and their relative sizes. Inside a superconductor some of the conduction electrons have condensed into Cooper pairs and thereby reduced the free energy of the metal. At the normal-superconducting interface the density of these superelectrons naturally falls to zero, but because of the coherence length the drop is spread over a length ξ (fig. 1.3). This means that the lowering of free energy occurs gradually from the interface and only reaches its full value at a depth ξ inside the superconducting region.

When a superconductor is placed in a magnetic field its energy is increased because of its apparent magnetization, or expelled flux, but this energy does not reach its full value until at a depth inside the superconductor equal to the penetration depth λ. Far inside the superconducting region these two energy contributions cancel each other but

near the interface there can be a net contribution of free energy, the size of which depends on the relative values of the penetration depth and the coherence length. In most pure metals the coherence length has a value of about 10^{-4} cm but the penetration depth is only about 5×10^{-6} cm and they therefore have a positive surface energy and are type I superconductors. In impure metals and alloys the mean free path and consequently the coherence length is reduced and can easily become less than the penetration depth. In that case the substance has a negative surface energy and is a type II superconductor.

In fact a detailed treatment shows that the change in behaviour does not occur when the ratio of penetration depth λ and coherence length ξ is equal to one (this is called the Ginzburg-Landau parameter $\varkappa = \lambda / \xi$) but rather when it is $1/\sqrt{2}$.

As mentioned above, type II superconductors should not exhibit Meissner effect but instead find it favourable to split up into a large number of normal filaments. Experimentally this is found to be the case and in an applied magnetic field they go into a so called "mixed state" that essentially consists of a large number of normal filaments

or current vortices in the otherwise superconducting material. It should be stressed that the mixed state is a fundamental property of the type II superconductor and, in spite of the apparent similarity, is quite different from the intermediate state of type I superconductors which is essentially only a result of the shape of the superconductor and is not a real "state" but a mixture of normal and superconducting regions, the exact nature of which depends on the geometry of the system, rather than on the superconducting properties. Although in certain macroscopic circumstances it may be justifiable and useful to treat the intermediate state as a separate phase it should not be forgotten that it is in fact a macroscopic mixture of two phases.

1.4 Magnetic behaviour of type I superconductors

In a bulk superconductor, where penetration can be neglected, the Meissner effect, that is the vanishing of magnetic flux inside the superconductor, can be attributed to induced surface currents whose direction and magnitude is such that they create an internal field that just cancels out the applied field inside the specimen. A superconductor in an applied field

$\underline{H}_a$ is therefore described by the following:

in the interior	$\underline{B}_i = \underline{H}_i = \underline{I} = 0$
at the surface	$\underline{J}_s \neq 0$
outside	$\underline{B}_e = \underline{H}_a + \underline{H}_s$

where $\underline{H}_s$ is the field due to the surface currents.

This is the formally correct description but ordinary electrodynamics (see for example Stratton (1941), chapter IV) show that from outside a magnetic body it is impossible to distinguish between magnetic effects due to surface currents and those due to bulk magnetization. Consequently the field outside a superconductor is equally well described by:

in the interior	$\underline{B}_i = 0,\ \underline{H}_i \neq 0,\ \underline{I} \neq 0$
at the surface	$\underline{J}_s = 0$
outside	$\underline{B}_e = \underline{H}_a + \underline{H}_s$

where now $\underline{H}_s$ is the field due to the magnetization of the sample.

As $\underline{B} = \underline{H} + 4\pi\underline{I}$ this is equivalent to attributing to the superconductor a magnetization $\underline{I} = -(1/4\pi)\underline{H}_i$, that is considering the superconductor to have the ideal diamagnetic

susceptibility of $-(1/4\pi)$.

Each description has its merits and in this work both are used. The latter has the advantage that simply by putting the susceptibility equal to $-(1/4\pi)$ standard electromagnetic treatments can be applied to superconductors in a magnetic field.

1.5 An introduction to the intermediate state

When a superconductor of any shape other than a long needle is placed in a magnetic field the flux pattern around it is changed by its induced magnetic field and at some point on its surface the local magnetic field becomes higher than the applied field. The problem is well known from ordinary electromagnetism and is in general complicated. Analytical solutions are only known for specimens with high symmetry, such as spheres, ellipsoids, and a long rod in a transverse field. For these the induced magnetization $\underline{I}$ is uniform and parallel to the applied field. The internal field $\underline{H}_i$ is then given by $\underline{H}_i = \underline{H}_a - 4\pi D\underline{I}$ which for a superconductor, where $\underline{I} = -(1/4\pi)\underline{H}_i$, reduces to $\underline{H}_i = (1/(1-D))\underline{H}_a$. The constant D is called the demagnetization factor and its

value depends on the shape of the specimen. (D=0 and 1/2 for infinite cylinders in axial and transverse fields respectively, and D = 1/3 for a sphere). On the surface of a superconductor the ordinary electromagnetic boundary conditions hold, that is the tangential component of $\underline{H}$ and the normal component of $\underline{B}$ are continuous across the boundary. The field on the outer surface is therefore highest at the equator where it is equal to the internal field. Here it exceeds the applied field by a factor $1/(1-D)$ and therefore reaches the critical value H_c long before the applied field does. As soon as that happens the superconductivity at that point is destroyed and flux penetrates the sample in such a way as to keep the field critical on the phase boundary. The specimen is now in the intermediate state. The same thing happens for any shape where flux lines are curved because of the induced field and the sharper the curvature the sooner the field becomes critical.

When superconductivity is destroyed and the critical field boundary penetrates the specimen the field just behind it is lower than H_c and it therefore soon becomes

energetically favourable to recreate there the superconducting phase and the specimen goes into a complicated mixture of superconducting and normal regions. As a superconducting phase is only created with difficulty inside a normal region (Faber (1952)) it seems more likely that superconducting fingers spread from the main superconducting region through the interface into the normal region. If this is the case one would expect the penetration to take the form of normal laminae perpendicular to the penetrating front. This was first pointed out in 1934 by Gorter and Casimir (1934a) but little attention has been paid to it since.

Finding the geometry of the intermediate state normally requires the solution of a very complicated free boundary problem, that is a problem where the shape of the regions is unknown and has to be determined from a condition on the surface, in this case the condition that $H=H_c$. This kind of problem is bad enough in a simple form and utterly impossible where there are a number of boundaries and a limited symmetry, as is usually the case for superconductors.

Convinced that an exact solution was not possible Peierls (1936) and London (1936) developed a zero-order approximation

that only took account of the relative volumes of superconducting and normal phases but neglected their geometrical distribution. They took the mean value of the induction over volumes larger than the intermediate state structure, found the ratio of normal to superconducting volume, and then found the free energy from the sum of the energies of both phases. In this way they found a relation between the average values of $\underline{H}$ and $\underline{B}$ in the intermediate state from which other thermodynamic quantities could be derived. F. London pointed out, that it is not the microstructure but the mean values that are given by macroscopic measurements, so although the theory is "grossly macroscopic" it is still useful in explaining the experimental results.

Gorter and Casimir (1934a, b) had already applied thermodynamics to the superconducting transition and found the free energies of the normal and superconducting phases. To avoid complications due to demagnetizing effects they considered a long superconducting rod in a longitudional field ($D = 0$). The magnetic free energy per unit volume for such a system is given by ordinary electromagnetism as

$$f(T, \underline{B}) = f(T, 0) + (1/4\pi) \int_0^{\underline{B}} \underline{H} \cdot d\underline{B}$$

As generally $\underline{H}$ rather than $\underline{B}$ is adjustable the important quantity is not $f(T, \underline{B})$ but $g(T, \underline{H})$, that is the Gibbs free energy or the thermodynamic potential. It can be found from the above equation using $g = f - \frac{\underline{H} \cdot \underline{B}}{4\pi}$ and comes to

$$g(T, \underline{H}) = g(T, 0) - (1/4\pi) \int_0^{\underline{H}} \underline{B}(\underline{H}) \cdot d\underline{H} \qquad (1.1)$$

Now making use of the Meissner effect

$$\underline{B}(\underline{H}) = \begin{cases} 0 & \text{for } |\underline{H}| < H_c \\ \underline{H} & \text{for } |\underline{H}| \geqslant H_c \end{cases}$$

one gets by integrating (1.1)

$$g(T, \underline{H}) = g(T, 0) \qquad \text{for } |\underline{H}| < H_c$$

$$g(T, \underline{H}) = g(T, 0) - \frac{1}{8\pi} (\underline{H}^2 - H_c^2) \quad \text{for } |\underline{H}| \geqslant H_c$$

which with a suitable shift of origin, gives

$$g_s(T, \underline{H}_a) = -(1/8\pi) H_c^2$$

$$g_n(T, \underline{H}_a) = -(1/8\pi) \underline{H}_a^2 \qquad (1.2)$$

where the subscripts s and n refer to the superconducting and normal states respectively.

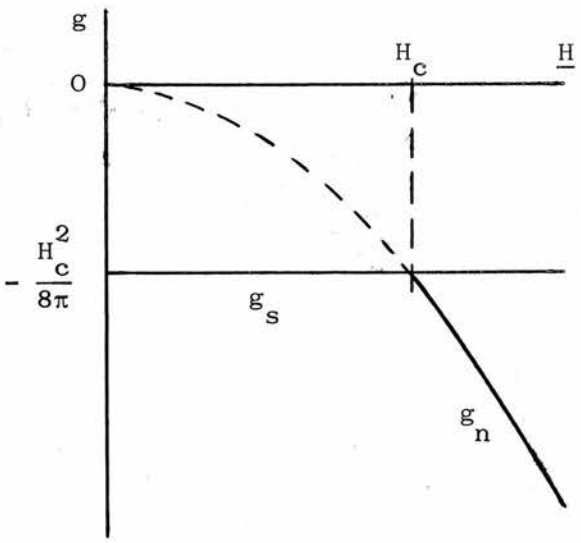

Fig. 1.4

Gibbs free energy as a function of H for a superconductor

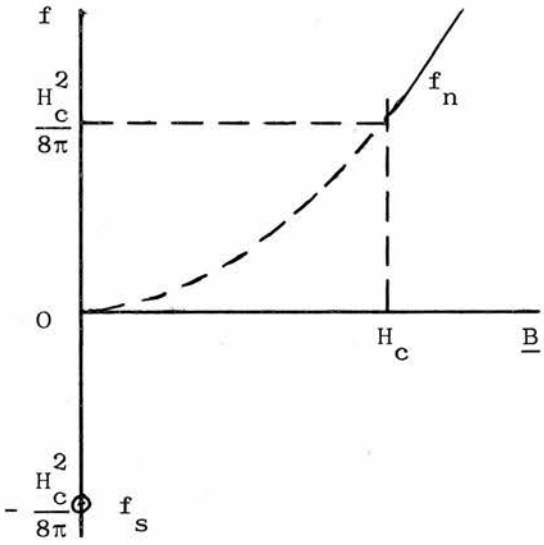

Fig. 1.5

Free energy as a function of B for a superconductor

The free energies of the two states can be found from (1.2) and $f = g + (1/4\pi)\underline{H}\cdot\underline{B}$, remembering that $\underline{B} = 0$ in the superconductor,

$$f_s(T, 0) = -(1/8\pi)H_c^2$$
$$f_n(T, \underline{B}_a) = +(1/8\pi)\underline{H}_a^2 \qquad (1.3)$$

From (1.3) the condensation energy of the superelectrons is found by considering the difference in the free energy of the two states in zero field

$$f_s(T, 0) - f_n(T, 0) = -(1/8\pi)H_c^2 \qquad (1.4)$$

As the external field is kept constant the equilibrium condition is that the Gibbs free energies of the two states should be equal. Equation (1.2) shows that this is at $\underline{H}_a = H_c$.

The above treatment allows the thermodynamic quantities in the purely superconducting and normal states to be calculated but it does not say anything about the intermediate state or how the specimen goes from being purely superconducting, with $|\underline{H}| = H_c$ and $\underline{B} = 0$, to being fully normal with $|\underline{H}| \geqslant H_c$ but $\underline{B} = \underline{H}$. The macroscopic theories of Peierls and London bridged this gap by finding the relation between $\underline{H}$ and $\underline{B}$ in the intermediate state. Their derivation was similar to that below.

Calling the volume fraction of normal material η and remembering that the local field in the normal regions must be equal to H_c when the two phases coexist, one gets for the average flux in the intermediate state

$$|\underline{B}| = \eta H_c + (1 - \eta) \cdot 0 = \eta H_c$$

Neglecting surface energy and magnetic energy due to the distortion of field as it enters and leaves the specimen the free energy per unit volume is the sum of the condensation energy in the superconducting volume and the magnetic energy of the normal fraction and is found from equation (1.3) to be

$$f(T,\eta) = (1-\eta)(-\frac{H_c^2}{8\pi}) + \eta\,\frac{H_c^2}{8\pi}$$

which in terms of B becomes

$$f(T,\underline{B}) = -\frac{H_c^2}{8\pi} + \frac{|\underline{B}|\cdot H_c}{4\pi} \qquad (1.5)$$

The thermodynamic field $\underline{H}$ is given by

$$df = \frac{\underline{H}\cdot d\underline{B}}{4\pi}$$

so differentiating (1.5) gives

$$\underline{H} = \frac{H_c}{|\underline{B}|}\,\underline{B} \qquad (1.6)$$

which shows, firstly that the field inside the intermediate state has everywhere the same direction as $\underline{B}$, and secondly that the field has the absolute value H_c everywhere in the specimen.

Equation (1.6) is equivalent to the equation $\underline{B} = \mu\underline{H}$ in a diamagnetic or paramagnetic medium but differs from it in that it is a non-linear relation.

Although the macroscopic model was in many ways useful it did not explain the pattern of normal and superconducting regions observed in the intermediate state. The first and still the most successful theory that tried to do that is due to Landau (1937). (For a detailed derivation see Landau and Lifshitz (1960), chapter VI.) To simplify the problem he considered an infinite

plate in a transverse magnetic field. He then assumed the plate to split up into alternate superconducting and normal strips as shown on fig. 1.6 and found the laminar period by minimizing the free energy with respect to the size of the domains.

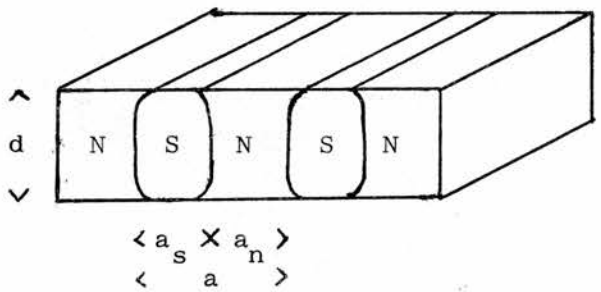

Fig. 1.6

Landau's model of intermediate state

The free energy is taken as the sum of a structure-independent macroscopic part, equal to the zero-order approximation in London's model (equation (1.5)), and a structure-sensitive microscopic contribution, i.e. a correction due to the actual intermediate state structure.

The microscopic free energy is conveniently expressed as energy per unit area of the plate and consists of three parts.

(1) A surface energy $2\alpha d$ per strip or

$$\frac{2d\Delta}{a} \cdot \frac{H_c^2}{8\pi}$$

per unit surface, where Δ is the surface energy parameter given by $\alpha = \Delta H_c^2/8\pi$.

(2) The flux lines spread out as they leave the sample and the superconducting domains become rounded off. This gives an additional condensation energy.

(3) The rounding off also adds a factor to the magnetic free energy.

The second and third terms are complicated functions of the periodicity and the reduced applied field $h = H_a/H_c$ and can in general not be found. For the special case of an infinite plate they have been computed numerically and expressed in terms of a and f(h) where f(h) is a tabulated function (Lifshitz and Sharvin (1951)). The microscopic free energy is then given by

$$g_m = 2\frac{H_c^2}{8\pi}\left[\frac{d\Delta}{a} + a \cdot f(h)\right] \qquad (1.7)$$

The condition that the free energy is a minimum is now found by differentiating (1.7) with respect to a, and is

$$a = \left(\frac{d\,\Delta}{f(h)}\right)^{\frac{1}{2}} \qquad (1.8)$$

A typical value of the function is $f(h) \approx 10^{-2}$ for $h \approx 0.7$ so for a 1.0 cm thick sample with surface energy parameter $\Delta \approx 10^{-5}$ cm

the laminar period should be about 0.3 mm which, as will be shown later, is similar to what is found experimentally.

In this model the field is critical on the interface but somewhat lower in the normal region just below the surface (point A on fig. 1.7a). This caused Landau (1943) to propose another model where the

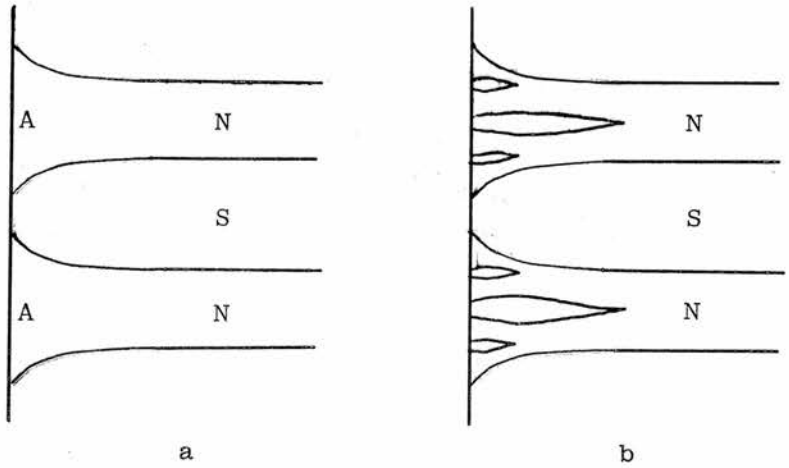

Fig. 1.7

Landau's unbranched (a) and branched (b) model of intermediate state.

normal laminae branch repeatedly (see fig. 1.7b). The branching becomes infinitely fine towards the surface so that the flux is homogeneous as it leaves the body. This overcame the difficulty of supercooling but naturally increased the surface energy.

When experiments showed that branching usually did not occur Lifshitz and Sharvin (1951) reexamined the theories of

Landau and concluded that for surface energy parameters of the order of 10^{-4} cm and sample dimensions of the order of 1 cm the normal layers would probably not branch at all and in any case not more than once or twice. This is because the reduction in free energy by the elimination of supercooling is outweighed by the increase in surface energy.

A number of attempts have been made to improve on Landau's model but with limited success. Andrew (1948) proposed a branching model similar to that of Landau but where the normal regions were threads rather than laminae. Cochran and Kaeser (1957) measured the magnetic moment of a synthetic intermediate state consisting of alternate plates of superconducting and normal metals and from the measurements derived expressions for the magnetic energy and the equilibrium spacing. Kuper (1951) also proposed an unbranched laminar state.

An interesting alternative to the branching was suggested by Balashova and Sharvin (1956). They noted that the intermediate state pattern in a narrow slit between two tin hemispheres was different from the pattern on the surface in that it consisted of rather wide straight layers while the layers on the surface were narrower and corrugated. They concluded that this was an alternative way of spreading the flux.

The free energy and the periodicity of this configuration were worked out by Faber (1958). The difference between his values and those of Landau are small.

Generally it can be said that the difference in free energy between the various configurations is very small and it is therefore not unlikely that the configuration taken depends on how the equilibrium state was reached and even that more than one could exist in the same sample.

1.6 Direct observation of intermediate state

The intermediate state structure has been experimentally observed by three methods. These make use of the magneto-resistance in small probes, fine magnetic powders, and Faraday rotation. The first is now of historical interest only but the other two are in use and constantly being improved. These methods will be described here in a historical order.

Motivated by Landau's theory of the intermediate state Meshkovsky and Shalnikov (1947) attempted to observe the intermediate state pattern between two hemispheres of superconducting tin. After trying unsuccessfully to imprint the structure on a magnetic steel band and to record it in magnetic powder spread between

the hemispheres they finally measured the field with minute bismuth probes. Bismuth has a high magnetoresistance and by continuously recording the probe resistance while moving it in the gap they could map the flux regions. The results largely confirmed Landau's theory that inside the specimen the intermediate state consisted of alternate superconducting and normal layers. The experiment was only designed to show the internal structure and did not distinguish between the branching and non-branching theory.

Balashova and Sharvin (1956) were the first to observe the flux pattern on the surface of a superconductor. They used ferromagnetic nickel powder of about 1 μm average dimensions which they blew with a jet of helium into the cryostat containing the sample. The magnetic powder fell under gravity along the flux lines and collected on the normal regions. The sample, again a split sphere, could then either be photographed in the cryostat or, as the powder clung rather firmly to the surface, could be warmed up and removed for observation. The experiment showed the normal regions to be corrugated near the pole of the sphere but quite straight near the equator. As already mentioned they interpreted the corrugations as a way of minimizing field energy and therefore an alternative to branching. Near the equator the field

component parallel to the surface straightens out the corrugations.

To prove this corrugation theory they sprinkled nickel powder in the narrow gap between the hemispheres before a run and let it take up what they thought would be the internal pattern. They considered the experiment at least partially successful. This kind of experiment should though be very carefully interpreted because flux moves in and out of the sample in flux bundles, inside which the field is equal to the critical field, and any method that responds to the flux well enough to take up the intermediate state pattern is also likely to respond to the outward drift of flux. The final pattern may therefore show flux paths rather than patterns.

The straight parallel layers observed near the equator of the sphere led Sharvin (1957) to consider the intermediate state structure in a flat plate where the applied field made an acute angle with the plate surface. He used nickel powder and found that the tangential field component did indeed subdue branching and corrugations and the pattern consisted of straight parallel laminae. By modifying Landau's unbranched model to take account of the component parallel to the surface he was able to make use of this simplified structure to get quite good values for the surface energy parameters of indium and tin.

Shawlow pointed out that ferromagnetic particles had large local fields around them and could therefore possibly influence the intermediate state pattern. Moreover the particles tended to form their own pattern in the magnetic field. He and his coworkers (Shawlow et al. (1954, 1956, 1958, 1959)) did therefore use superconducting niobium powder of about 60 μm average dimensions. Being superconducting the powder is strongly diamagnetic and is expelled from the flux regions and comes to an equilibrium on the superconducting domains. In equilibrium no forces act on the powder and it should not disturb the intermediate state pattern.

Faber (1958) used a similar technique and tin powder to measure surface energy in tin and aluminium plates with excellent results. The technique was also used by Haenssler and Rinderer (1959, 1960, 1965a, b) to study flux flow and intermediate state in type I superconductors.

The powder technique has recently been considerably improved by evaporating iron and other magnetic metals directly into small droplets inside the cryostat and letting them fall on to the specimen, the same way as fine powders (Träuble and Essmann (1966a, b) and Sarma and Moon (1967)). The droplets are very small and a resolution of 100 Å is claimed. When the droplets

fall on to the surface they become immobile and the sample can be warmed up and the pattern examined under an optical or an electron microscope.

The resolution of the powder method is ideally equal to a few particle diameters. Some of the coarser powders move reasonably freely on the surface and follow changes in the magnetic flux. When used with care they can therefore give a fairly good record of dynamic processes. Other powders, particularly the very fine ones (1 μm), stick to the surface and only record the pattern as it is when they are applied. In fact they often adhere so strongly that the pattern is not disturbed by heating the sample up and it can then be examined outside the cryostat.

The use of Faraday effect in a transparent paramagnetic material was developed by Alers (1957), (1959) to observe the intermediate state. The method is based on the property of some materials of rotating the polarization plane of polarized light that is passed through them parallel with a magnetic field. When a thin sheet of such material is placed on the surface of a superconductor in the intermediate state the magnetic field will have approximately the same structure in the sheet as in the specimen. If polarized light is then shone through the sheet and

reflected from the metal surface its plane of polarization will be rotated depending on the magnetic field strength. By passing the light through an analyser this pattern can be changed into a pattern of varying light intensity which can be seen or recorded on film. The method has been used by DeSorbo (1960, 1962, 1964, 1965) and Baird (1964, 1965) using a disk of cerium metaphosphate glass (CMP), 0.2 - 0.5 mm thick. Baird (private communication) has also successfully used a slice of terbium aluminium garnet which has a considerably higher rotating power.

Recently thin evaporated films of europium compounds have been used in the same way. Kirchner (1968a, b and 1969) used 50/50 mixtures of EuS/EuF_2 and Huebener et al. (1970 a, b) used a 75/25 mixture of the same materials. Salomon and Harris (1970) on the other hand used EuSe/EuF_2 mixtures. These films are both thin and have a very high rotating power and consequently the resolution is much better than what is obtained with CMP. For example Kirchner claims a resolution of about 2 μm for his experiments which is two orders of magnitude better than the 200 μm typically obtained with CMP.

The magneto-optic method has two advantages. The rotation varies linearly with the field strength so the local field in the

material is easily determined. The method is furthermore ideally suited to dynamic processes and a continuous record of these is easily obtained on cine film.

1.7 Intermediate state in short cylinders

The present work is concerned with intermediate state in superconducting cylinders and in particular with the superconducting to normal phase transition at constant temperature. The problem has previously been studied by Faber (1958), Baird (1964, 1965), and DeSorbo and Healy (1964). The general features of the penetration were most clearly described by Baird (1964, 1965, and private communication), who used the magneto-optic method to observe the flux penetration on the top surface.

As the applied field is increased, penetration takes place in two stages. First flux penetrates along the periphery and proceeds radially inwards as the field is increased. This stage is reversible in that if the field is reduced the penetration recedes. At a well defined value of the applied field the width of the annular penetration region ceases to increase; this is the end of the first stage. Further increase of field causes flux to break away from the perimeter and to migrate towards the axis of the cylinder, and at the same time the width of the annular

penetration region begins to shrink. This is the second stage and it is not reversible.

Baird observed that the inner perimeter of the penetration was not a uniform circle but was corrugated, or possessed "fingers", from the tips of which bundles of flux were generated in stage two.

Faber (1958) and Baird (1964) suggested models for the penetration. Faber showed how flux bundles could form from the ends of laminae but his explanation of the annular penetration involved metastable phase boundaries and weak points and was not satisfactory. Baird similarly pointed out that due to demagnetizing factors the field at the edge of the cylinder would soon exceed the critical value and suggested that flux would penetrate the corners in such a way as to keep the field critical on the interface (fig. 1.8a). He further suggested that the second stage was reached when the two normal regions met and just penetrated the equator. At that stage flux lines would be completely within the sample and would presumably minimize the free energy of the system by moving, as bundles of flux, towards the centre of the disk (fig. 1.8b), probably in the way suggested by Faber. As the

bundles collect in the centre, the flux lines at the edge straighten up and the radius of the annular penetration region increases again.

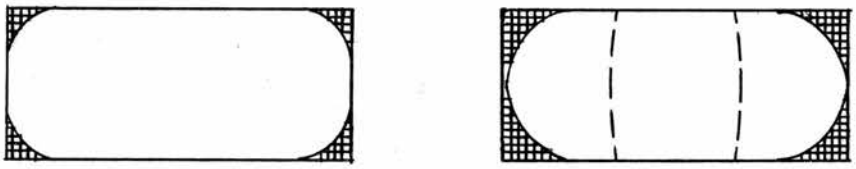

a b

Fig. 1.8

A diametral section through a superconducting cylinder showing the first stage of penetration (a) and formation of flux bundles in the second stage (b). [After Baird (1964)].

Its minimum radius does therefore coincide with the start of the second stage. Baird assumed the penetration region to be in a supercooled normal state and he did not explain the "fingers" but stressed their role as flux generators.

This work was started in collaboration with Baird and its main purpose was to compute numerically the field distribution inside the cylinder and so determine, whether the limit of the first stage of penetration coincided with field penetrating the equator. Later it was decided to investigate experimentally, the "fingers", or the fine structure of the penetration, and try to correlate the findings with the field computations.

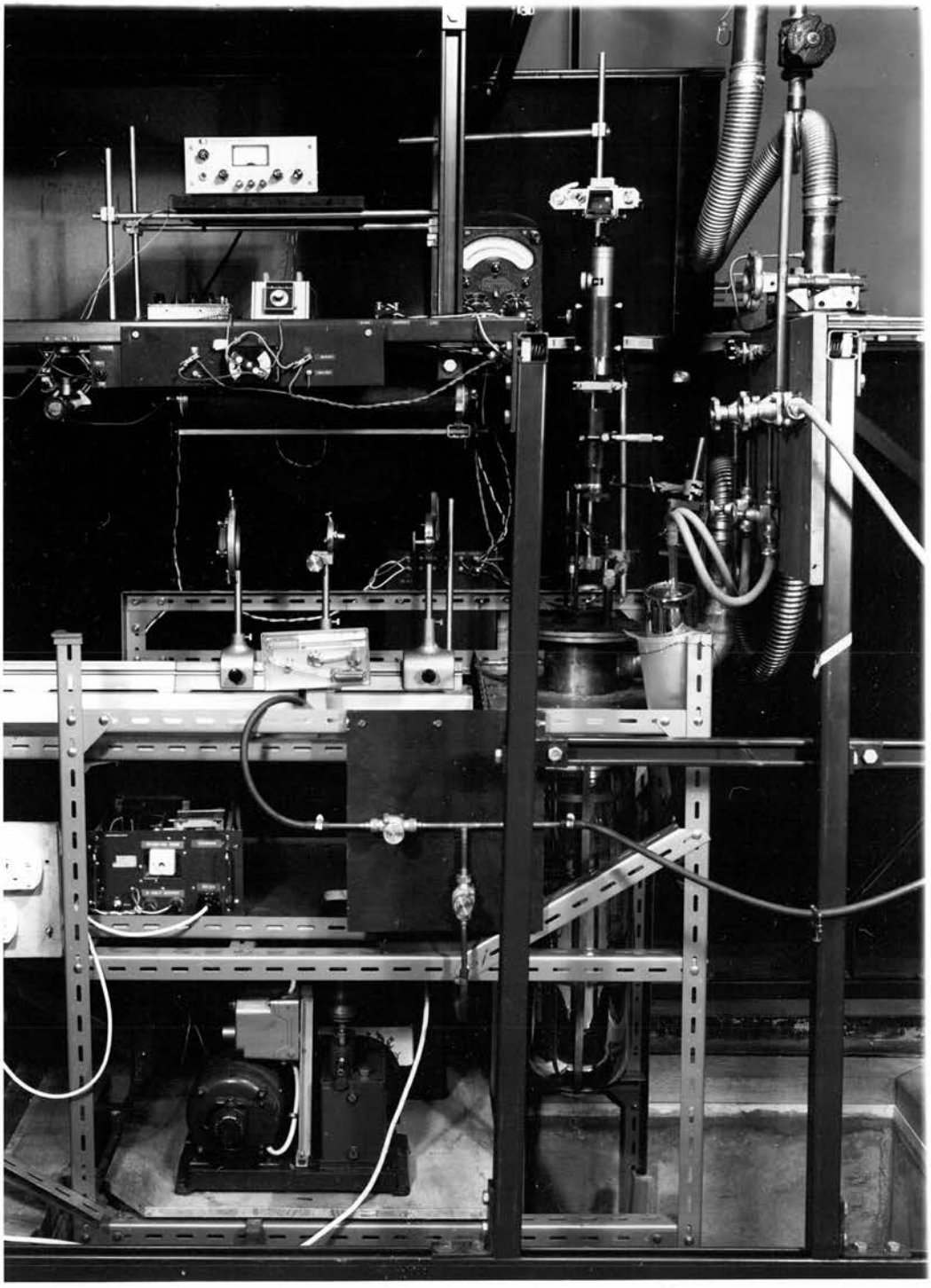

Fig. 2.1

The apparatus.

CHAPTER 2 - APPARATUS AND EXPERIMENTAL DETAILS

2.1 Introduction

The apparatus used resembled that of DeSorbo and Healy (1964), and Baird (1964). The general features were the same for the magneto-optical and powder method. These are described in section 2.2. The special requirements of each method are discussed in sections 2.3 and 2.4. A general view of the apparatus is shown on fig. 2.1 and 2.2. A schematic diagram is shown on fig. 2.4.

2.2 Cryostat

The cryogenic part of the apparatus was mounted inside large (25" long 4 1/4" internal diameter) glass dewars. These were fitted in the normal manner to a brass top-plate. The apparatus stood on a large concrete block that rested on springs on the foundations of the building. Vibrations from the pumping line were eliminated by two flexible plastic hoses (see fig. 2.1). The cryostat was virtually free from external vibrations.

The temperature was measured with a mercury manometer. Temperatures down to 1.3^{o}K could be reached by pumping on the helium. Measurements were normally done below λ point.

Optical access was through a 2" diameter glass window on the top-plate. The glass was uncoated but fixed at a 15^{o} angle to throw reflections out of the way.

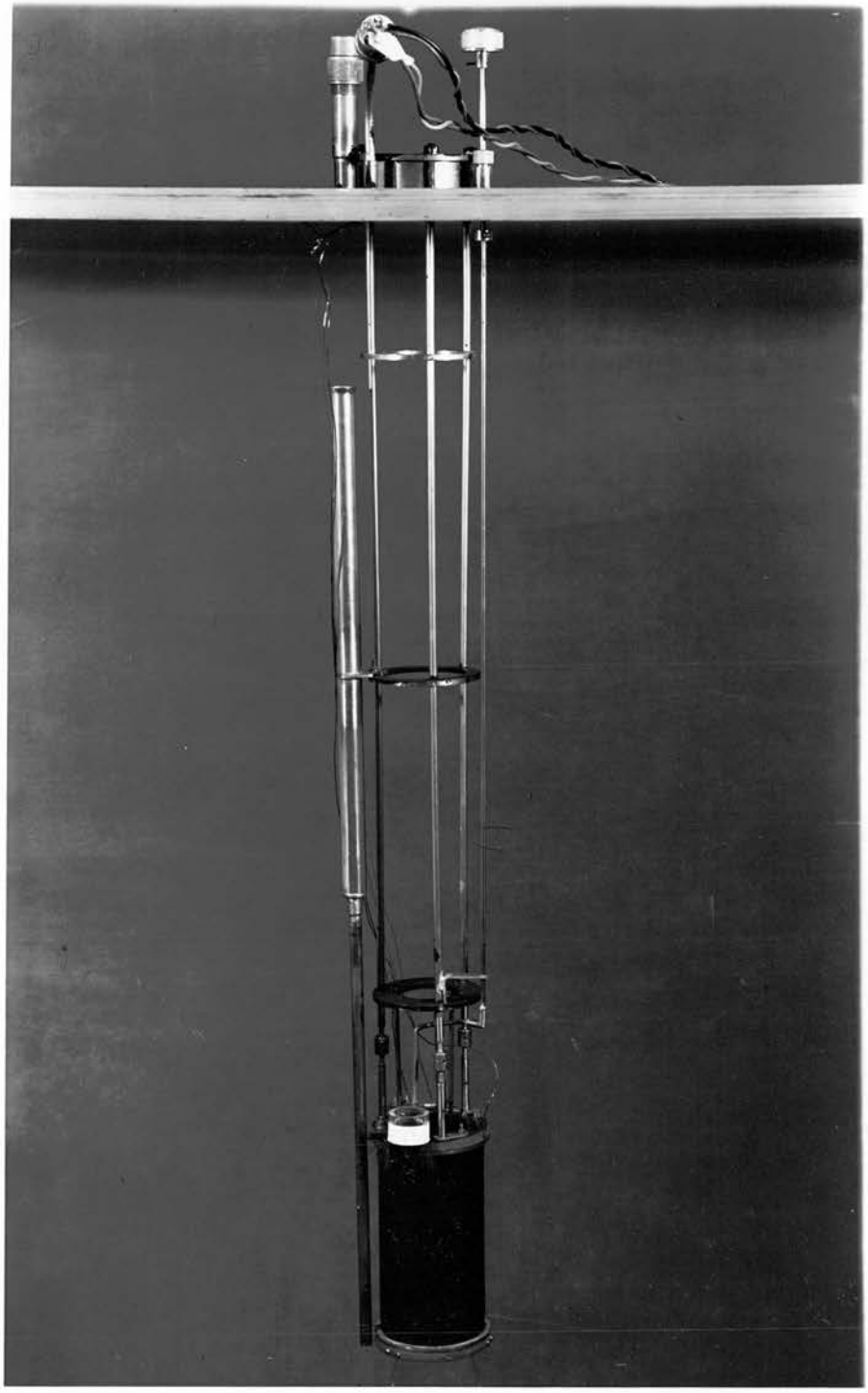

Fig.2.2

Cryogenic part of apparatus.

The sample holder and the superconducting solenoid were supported from the topplate by three 5 mm diameter stainless steel tubes. The sample holder is shown on fig. 2.3. The upper plate could be adjusted with respect to the bottom one by three screws.

A home-made superconducting solenoid was used. It gives a field of H/I = 0.456 Oe/mA. The wire was Niomax-S 25/40 superconducting wire made by I.M.I. and supplied by The Oxford Instrument Company Ltd. It has a 0.25 mm inner core of a superconducting alloy (56% niobium, 44% titanium) coated by copper. The outer diameter is 0.40 mm. The wire had a Formvar insulation. It was wound with an "Avo Automatic Coil Winder" on to a copper former, 2" diameter, 15 cm long and 1/16" wall thickness. Copper end flanges 3" diameter and 1/16" thick were fitted. A similar flange of 1/4" thick insulating material provided support for terminals etc. The former was insulated with a 3 thou thick Mylar film. The same insulation was used between wire layers. The coil took 916 m of wire, had 16 layers and 4836 turns.

The power supply for the solenoid is shown on fig. 2.5. Only low fields (< 1000 Oe) were needed so both the current required and the energy stored in the field were small. No special precautions had therefore to be taken. Two power sources were used. For low fields a Hewlett Packard model 6284 A constant voltage/constant current D.C. supply. It gave a maximum of 3 A (about 1500 Oe).

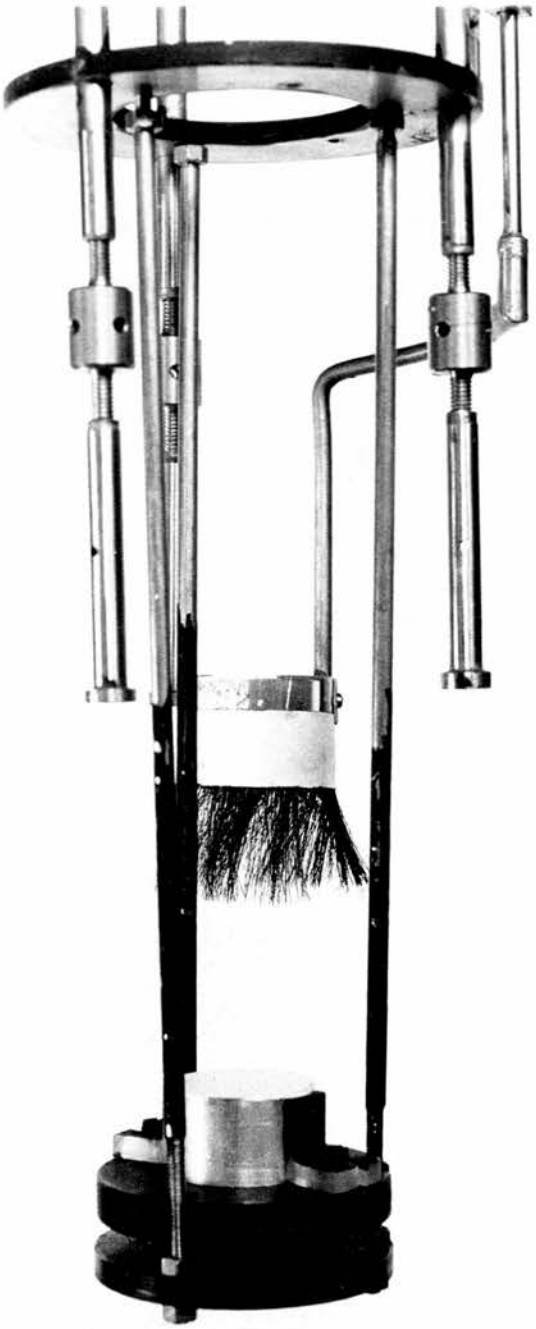

Fig. 2.3

Sample holder.

For higher fields a heavy duty 6 V car accumulator was used with two rheostats. A low resistance was connected across the superconducting coil to dissipate the field energy in case the coil went normal. Two antiparallel diodes protected the H.P. power supply against reverse currents and spikes by preventing voltages higher than 0.5 V from developing across the coil. The coil current was measured with an Avo multimeter and the field found from the computed H/I ratio.

2.3 Magneto-optical experiment

The rotation of the plane of polarization obtained with the CMP glass is generally of the order of a few degrees. The light intensity on passing through the analyser is therefore reduced by a factor of $\cos^2\theta$, where θ may be about 3°. The experiment therefore requires a high intensity source of polarized light. As the rotation is wavelength dependent the source should preferably be monochromatic.

These requirements led us to choose an argon laser. The laser (see fig. 2.6) was home made after a design by Mr. A. Maitland. The instrument gave 30 mW of plane polarized light at two sharp lines, 4879.86 Å and 5145.32 Å. The light was highly parallel with a beam diameter of about 0.6 mm. It was expanded to about 1" diameter with two common focal point lenses. The first was a

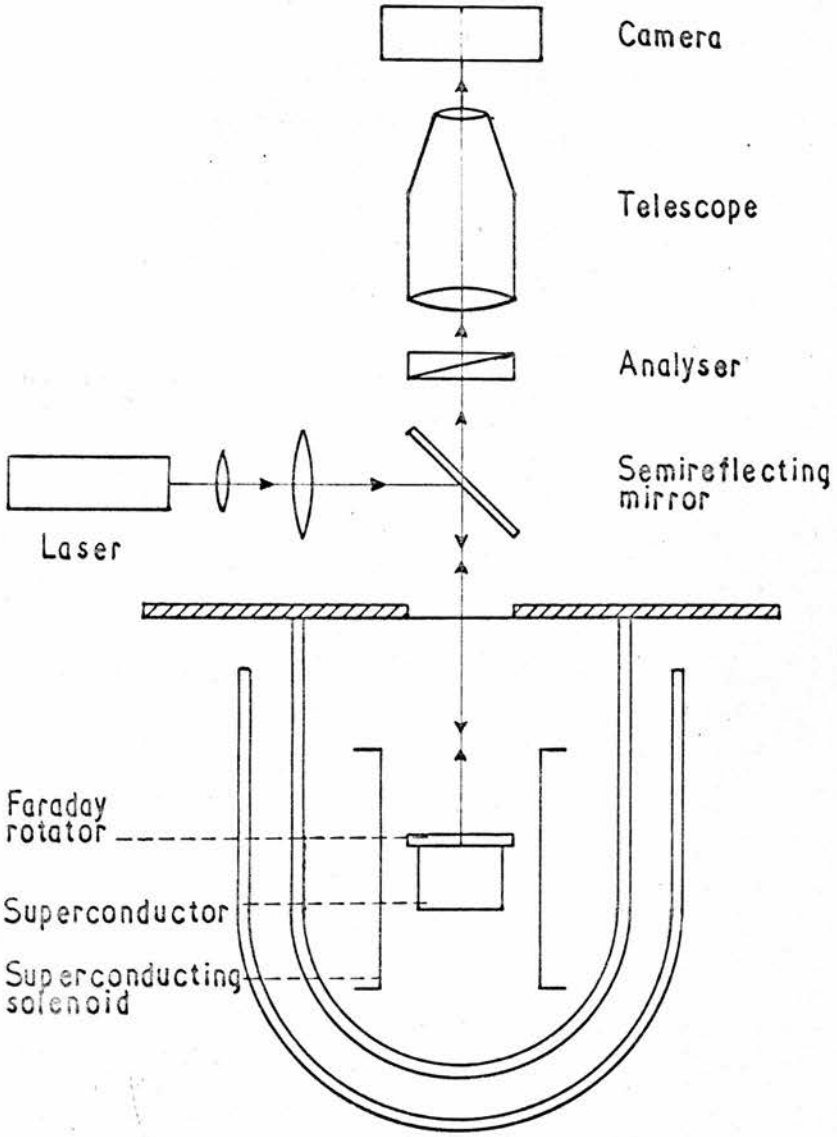

Fig. 2.4

A schematic diagram of the apparatus and the optical system.

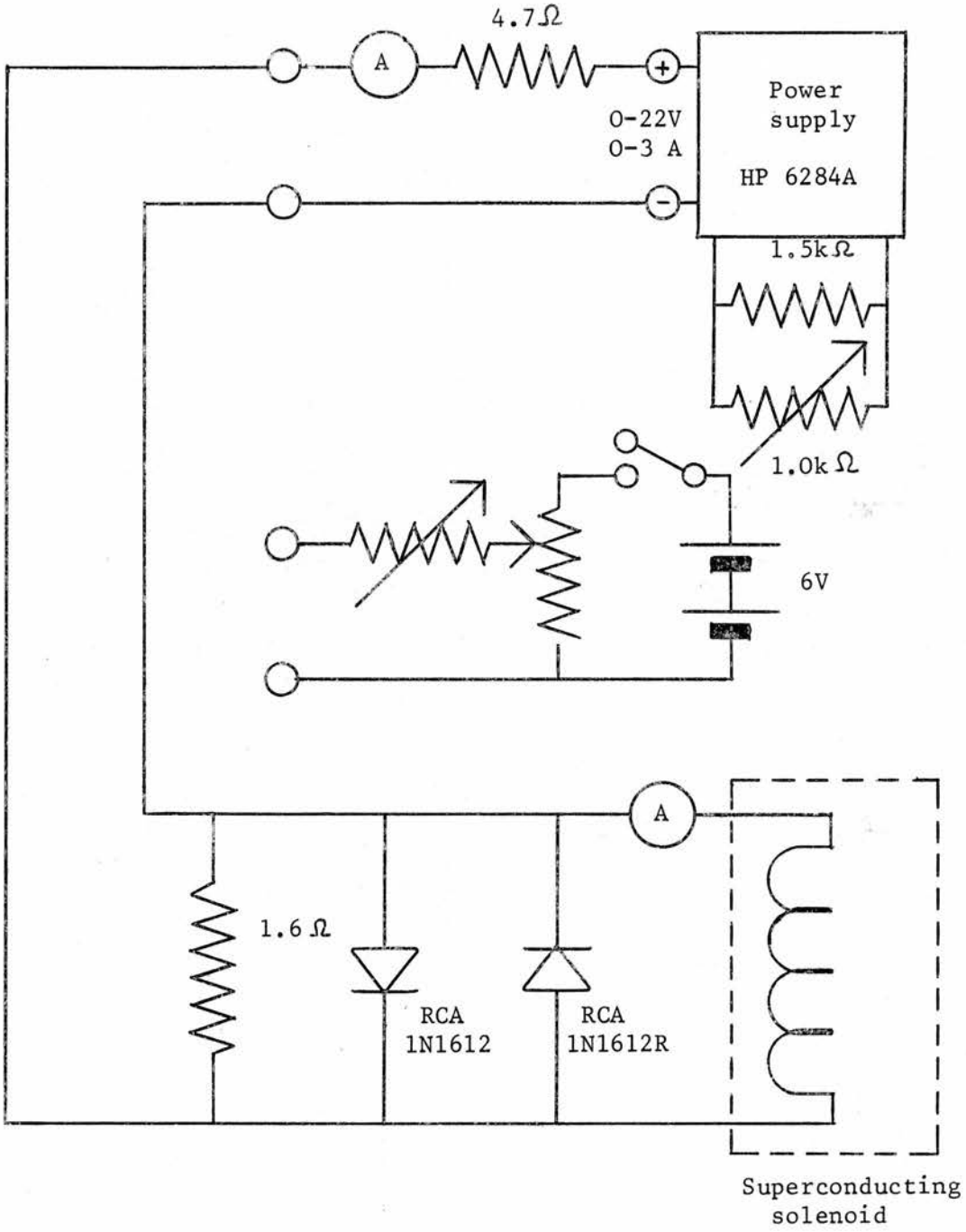

Fig. 2.5. A schematic diagram of the power supply for the superconducting solenoid.

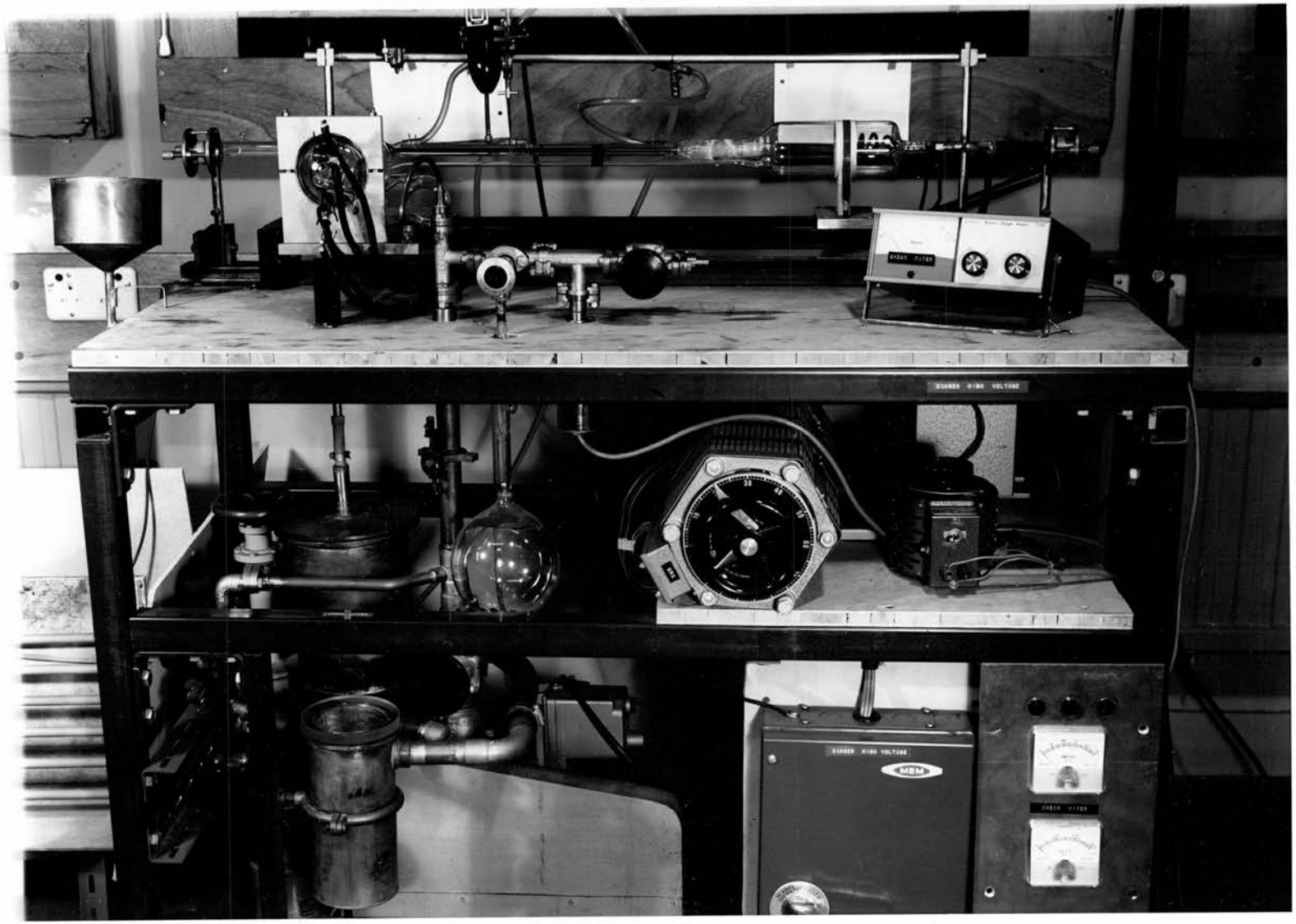

Fig. 2.6

The laser.

strainfree, coated microscope objective of 32 mm focal length from R. & J. Beck Ltd. The second was an acromatic, coated telescope objective of 168 mm focal length and 52 mm diameter.

The expanded beam is reflected into the cryostat by a 50/50 multilayer beam splitter of 2" diameter supplied by Grubb Parsons.

The magneto-optically active material was a 1" diameter, 0.5 mm thick glass disk made from a 80% solution of cerium metaphosphate (CMP) in glass. It was supplied by Bausch & Lomb Inc., Rochester, New York. The bottom side was coated with a reflecting aluminium layer and the top with an antireflective film.

The rotation of the plane of polarization by the CMP can be expressed as:

$$\Theta = \frac{A}{T} \int_0^1 H_x dx \qquad (2.1)$$

where A is a function of the material and the wavelength of the light ($A \propto 1/\lambda$), l the optical path length in the material and H_x the component of the magnetic field parallel to the light direction. The Verdet constant is defined as V = A/T. The constant A was measured for the laser light (λ = 5000Å) for temperatures from 1.4°K to 2.1°K. It was found to be 6.7×10^{-2} ang.deg. $^{o}K\ Oe^{-1}\ mm^{-1}$. This agrees with the values reported by Goodman et al. (1966) (6.5×10^{-2} ang. deg. $^{o}K\ Oe^{-1}\ mm^{-1}$ for λ = 5461Å) and Hearing et al. (1963) (8.0×10^{-2} ang. deg. $^{o}K\ Oe^{-1}\ mm^{-1}$ for

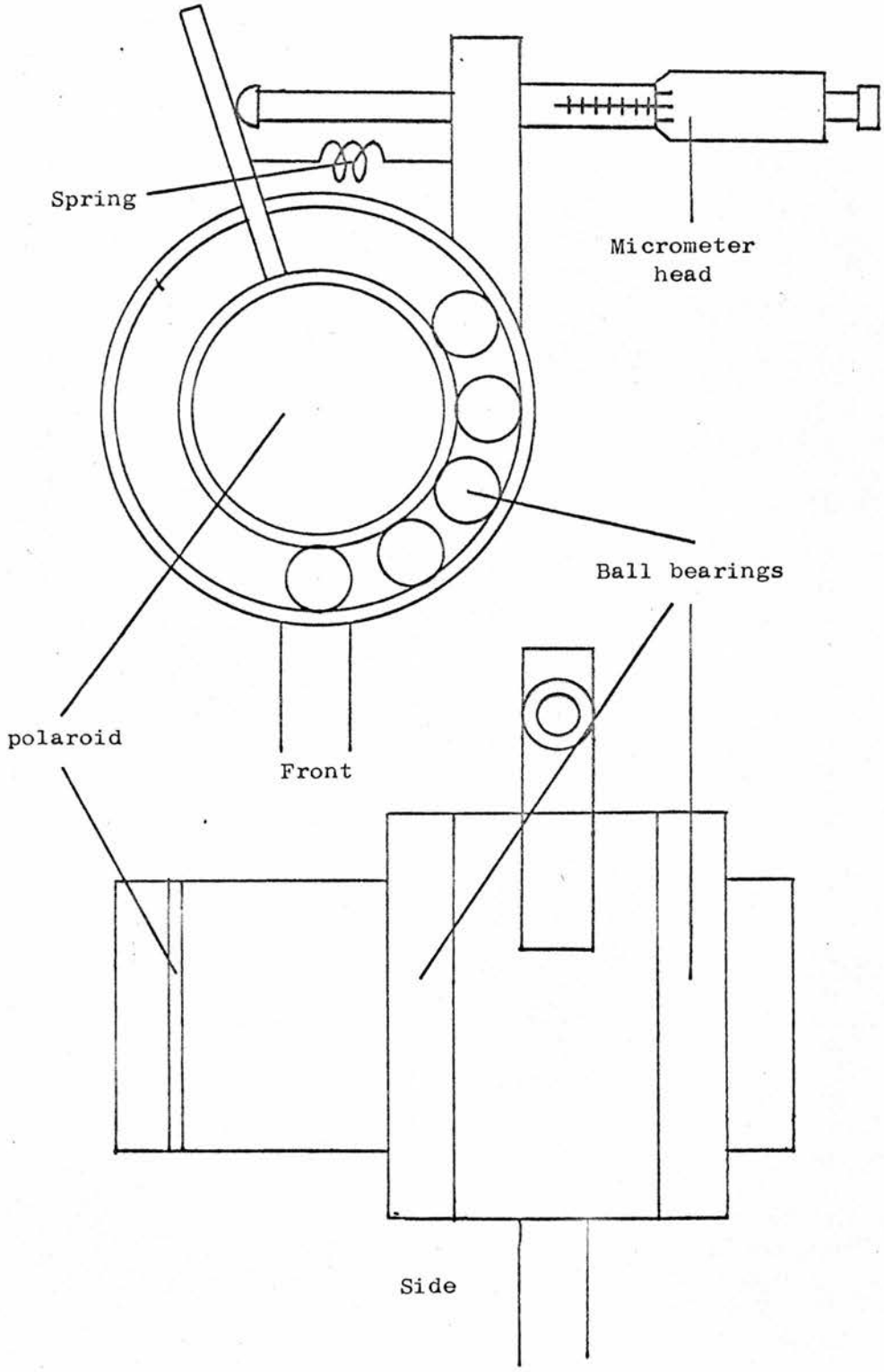

Fig. 2.7

Schematic diagram of analyser

λ = 4060Å).

The analyser was a type HN 22 polarizing filter from Polaroid Corporation between precision ground and polished glass. It was mounted inside a 2" diameter brass tube that was supported on ball bearings inside a larger tube (fig. 2.7). With a micrometer head the inner tube could be rotated with respect to the outer one. The rotation could be read off to about 0.01 degree.

The pattern was observed with a Hilger and Watt 'zero focus' telescope, type TA 14. It had a magnification of x25, an aperture of 37 mm and a focusing range of 25 mm to infinity. As laser light is dangerous to the eye the image could not be observed directly but had to be focused on a ground glass screen.

A Nikon F 35 mm reflex camera body was used for recording the flux pattern on to film. The image from the telescope was focused directly on to the film without intermediate lenses. Exposure times were determined by trial and error. There was ample light and exposure times of 1/60 - 1/250 seconds could be used.

2.4 The powder method

The illumination required is much less demanding than for the magneto-optical method. The losses are relatively low and any light source giving a high intensity beam of white or monochromatic light can be used. As the laser was rather cumbersome and difficult in operation it was replaced by a 12 V, 100 W halogen

projector lamp. The light was focused on to the sample by a small lens.

The beam splitter, being a multilayer filter, gave a ghost image when used with white light. It was therefore replaced by a fully reflecting mirror. The mirror was bypassed by the upcoming beam.

The analyser was no longer needed and was removed. Otherwise the optical system was unchanged.

We used superconducting vanadium powder (H_o = 1310 Oe, T_c = 5.3°K) of particle size 50μm for our experiment. The vanadium powder was found to be less sticky and more freeflowing than the previously used niobium powder (Schawlow et al. (1954), (1956), (1958), (1959) and Haenssler and Rinderer (1959), (1960), (1965a), (1965b)).

Before each run the powder was spread 3-5 layers thick on to the sample with a fine sieve. To some extent it followed changes in the flux pattern, i.e. moved off the normal regions, but usually it was necessary to assist this process by tapping the top-plate

The annular penetration tended to push the powder away from the sample edges into the centre. As the boundary advanced, little powder was left near the edge to show up the fine normal channels. It was therefore necessary to add powder during a run. For this purpose a small sieve of 50μm mesh was fitted inside the

cryostat (see fig. 2.3). The sieve could be moved both out of the light beam and up and down from outside the cryostat. No powder fell through when the sieve was undisturbed. The flow was therefore regulated simply by vibrating its support when powder was needed. Excess powder could be removed with a brush fixed to the bottom of the sieve.

2.5 Performance of apparatus

The apparatus worked quite satisfactorily for the magneto-optical experiment. The resolution of the method is limited by the spreading out of flux in the CMP disk and is therefore about the same as the thickness of the disk (500μm). As long as reasonable care was taken with the polarization of the light, this limit was reached.

The resolution of the powder method is naturally limited by the size of the vanadium particles (about 2-3 diameters, 100 - 150μm). This resolution was not obtained, mainly because of the long viewing distance (about 1.0 m). Although the theoretical resolution of the telescope at this distance is about 10μm its depth of focus is very shallow. The whole sample was therefore seldom in focus, even if great care was taken in aligning and focusing.

A very considerable loss of resolution was caused by glare

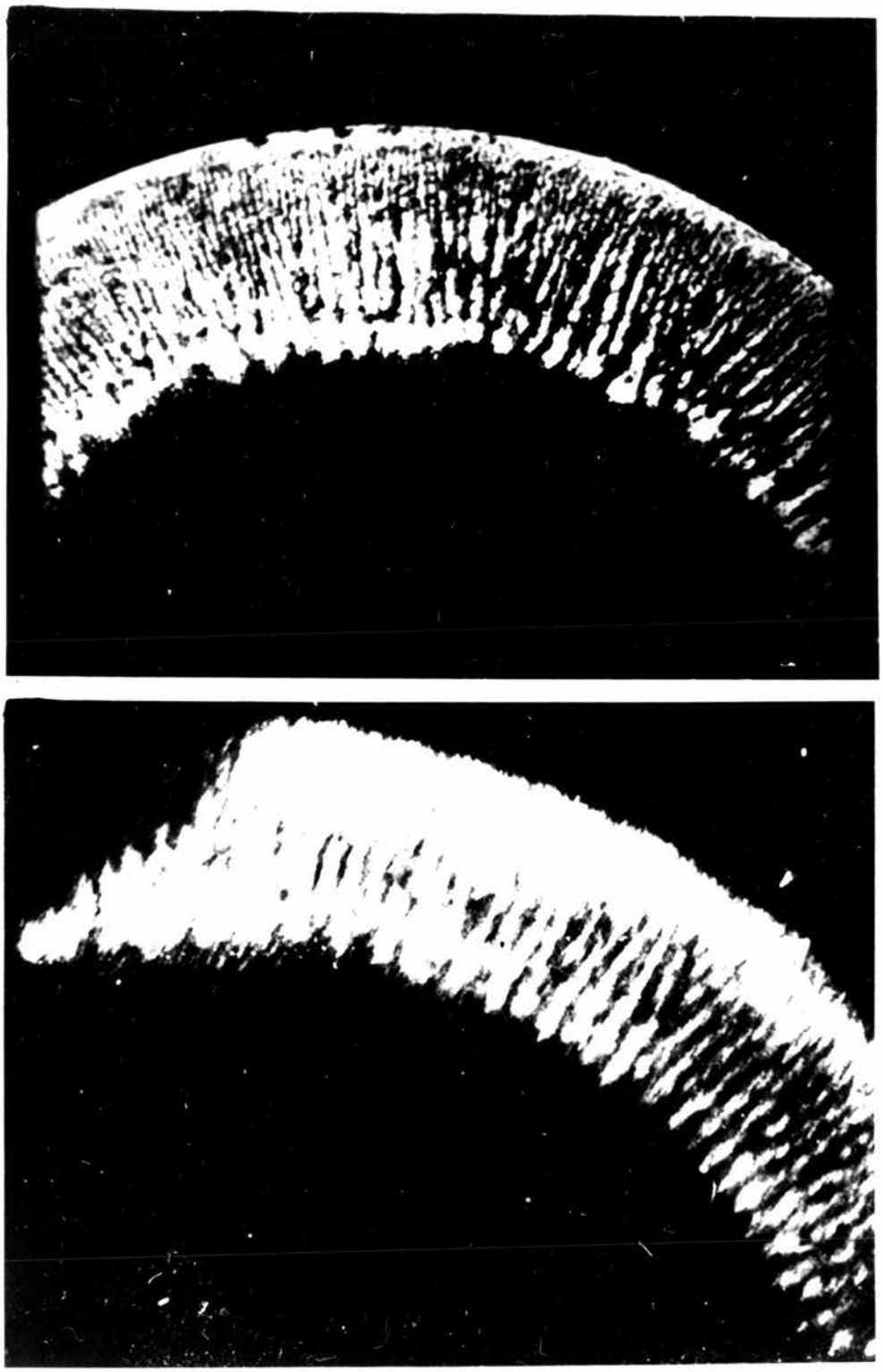

Fig. 2.8

Resolution; Top, through microscope; Bottom, in cryostat.

from the metal surface. The trouble was partly overcome by painting the sample surface with a thin coat of white water colours thus reducing its reflectivity.

Twice we succeeded in warming the sample up and taking it out of the cryostat without disturbing the powder pattern. This was done by reducing the mobility of the powder by letting the helium level drop below the sample surface and then carefully lowering the field. With some luck the pattern was undisturbed. Afterwards the sample was removed and photographed through a microscope. As fig. 2.8 shows the resolution obtained in this way was very much better than when the telescope was used.

CHAPTER 3 - SAMPLES

3.1 Introduction

The four metals suitable for work on intermediate state in type I superconductors are aluminium, indium, lead, and tin. Of these aluminium has the highest surface energy (Δ = 18 x 10^{-5} cm) and its intermediate state structure is therefore coarse and relatively easy to observe. Unfortunately it has a critical temperature of 1.2°K which was unobtainable with our apparatus. Lead has been used in the past but it has a high critical temperature (T_c = 7.2°K) and as temperatures above 4.2°K are not readily obtained in a helium cryostat the usable reduced temperature range is small. This leaves indium (T_c = 3.4°K) and tin (T_c = 3.7°K) which both have critical fields in the range 0 - 300 Oersted and surface energy parameters of 3.4 and 2.3 x 10^{-5} cm respectively. Both are readily available in a highly pure form and are easily pressed or melted into the required shape.

Most of the experiments were performed with indium since it anneals at room temperature and is therefore free from cold working strains and imperfections that might impede flux movement and thus prevent an equilibrium state being reached.

One tin sample was made in order to check the generality

of the results and to extend the range of surface energy values available for comparing with the theory describing the radial laminae.

The samples used were all polycrystalline, unannealed, short cylinders. Their dimensions are given in table 3.1.

Sample	Length	Diameter	$\frac{\text{Length}}{\text{Diameter}}$
	mm	mm	
In2	6.2	22.1	0.280
In4	13.4	22.0	0.609
In5	19.7	19.5	1.010
In6	11.8	19.5	0.605
Sn1	13.2	22.2	0.595

Table 3.1

3.2 Indium

The indium samples In2, In5, and In6 were made from Johnson and Matthey 99.999% pure indium. In4 contained 0.9 atomic % lead.

The samples In2 and In4 were cold pressed into their final shape in a precision ground stainless steel piston and cylinder of the required diameter using a hydraulic press. Before the indium was put into the cylinder it was etched in hydrochloric acid to

remove oxidation and then washed in distilled water and dried under vacuum.

The other two indium samples, In5 and In6, were vacuum melted into a rod in a glass cylinder of the required diameter. The glass was then broken off and the rod cut to length and its ends polished with a spark cutter. Finally the samples were etched in a reagent consisting of 20 cc hydrochloric acid, 4 g picric acid, and 400 cc ethyl alcohol.

No difference in superconducting properties was noticed between samples prepared in these different ways. All samples were free from flux pinning and their surfaces were smooth.

3.3 Tin

The tin sample Sn1 was made from 99.999% pure tin supplied by Koch-Light Laboratories. It was vacuum melted in the same way as In5 and In6 and cut to length in the spark cutter. The ends were then faced up in a lathe and polished lightly with fine emery paper. No attempt was made to anneal the sample although it showed some evidence of flux pinning, presumably due to the cold work. The pinning probably caused some irregularity in the radial fingers and it certainly hindered the drift of flux bundles into the centre of the sample but neither effect was important in these experiments and annealing was not considered worth while.

CHAPTER 4 - THEORY OF PHASE BOUNDARIES

4.1 Introduction

The purpose of the computations was to determine the mode of penetration of magnetic field into short superconducting cylinders and to test Baird's hypothesis about the first stage and the start of the second stage of penetration. This was done by finding mathematically the internal phase boundaries in the first stage.

The problem is complicated and to get anywhere at all, some simplification had to be made. This was done by neglecting any structure in the penetrating region and assuming the penetrating front and the field in the region to have angular symmetry. Furthermore the field on the interface was assumed to be equal to the critical field. This reduced the problem from three to two dimensions and made its solution seem possible.

In view of what will be said later about the intermediate state structure in the penetrating region, these assumptions might seem unrealistic. In fact the restrictions could be relaxed by considering the field in the specimen to be the average field over a region large compared with the intermediate state structure, but then the field on the interface could no longer be taken to be critical and a realistic value would be difficult to estimate.

To find the internal boundary from the condition that on it $H = H_c$ is what is called a free boundary problem. These are normally

solved by iteration, that is a boundary is guessed, the field on it computed, and the information used to make a better guess, and so on, until the field satisfies the boundary condition within given limits.

In order to find the boundary it is necessary to solve Laplace's equation in the region outside the sample, with the appropriate boundary conditions. In general this is complicated and has only been solved analytically for highly symmetric problems. The present problem had therefore to be solved numerically. Methods that might have speeded up the process, like conformal mapping and fast-converging matrix methods, were considered, but because the boundary was continuously changing, these would not have been successful. A finite difference method in the physical plane was therefore used.

Because of the symmetry of the system cylindrical coordinates were used. In these Laplace's equation takes the form

$$\nabla^2\phi = \frac{1}{\rho}\frac{\partial}{\partial\rho}\left(\rho\frac{\partial\phi}{\partial\rho}\right) + \frac{1}{\rho^2}\frac{\partial^2\phi}{\partial\theta^2} + \frac{\partial^2\phi}{\partial z^2} = 0$$

which, because of the angular symmetry, reduces to

$$\nabla^2\phi = \frac{1}{\rho}\frac{\partial}{\partial\rho}\left(\rho\frac{\partial\phi}{\partial\rho}\right) + \frac{\partial^2\phi}{\partial z^2} = 0 \qquad (4.1)$$

This equation has to be solved outside the superconducting region with the boundary conditions that $\underline{B}$ is tangential on the surface of the superconducting region, or $\frac{\partial\phi}{\partial n} = 0$, and that the field at infinity is equal to the applied field.

By the uniqueness theorem these boundary conditions are sufficient for the problem to have a unique solution for any shape of the boundaries. It is therefore considered likely that a shape satisfying the free boundary condition could be found. A rigorous proof of this would be very difficult and has not been attempted, but the fact that at least an approximate solution has been found is thought to justify the assumption.

Once the interfaces were found, $\underline{H}$ and $\underline{B}$ were known throughout the system and various quantities could be computed. One of the most important ones was the rotation of plane polarized light in a magneto-optic disc on the surface. This quantity could be measured experimentally and the results compared with the computations and it therefore constituted an important test of the validity of the computations. The magnetic moment of the cylinder and the free energy of the system were also computed.

The computations were done for four length/diameter ratios from about 0.2 up to 1.6 which was enough to make interpolation to other ratios in the interval reasonable. For each ratio a number of penetration profiles was computed and the predicted penetration on the top surface was compared with what was experimentally observed.

The computer programs were written in Fortran IV and developed on the IBM 1130 computer in the Physics Department at St. Andrews University. When the University acquired an IBM 360 computer in early 1969 the programs were transferred to that. All production runs

were subsequently done on the IBM 360.

The solution of Laplace's equation took 3-4 minutes on the IBM 360 but 15-20 guesses had usually to be made, before a boundary that satisfied the free boundary condition was found. A considerable amount of computing time was therefore used.

4.2 Theory

When solving Laplace's equation using finite differences the mesh and the boundaries should, as far as possible, be arranged so that the boundaries coincide with mesh lines. The same equation can then be applied throughout the region. In the present case a square mesh was used and by a suitable choice of mesh length all boundaries, except the free boundary, were made to coincide with mesh lines.

The boundary condition for the potential on the free boundary is that the normal derivative is given. On a curved boundary this is a very difficult condition and is usually best avoided, if at all possible. Very often this can be done by defining a new function, orthogonal to the potential function. The new function has its tangential derivative given on the free boundary, so by integration, the function values there can be found. The free boundary condition is in this way simplified and as it is also found that the differential equation for the new function is no more difficult to solve than the original one, the transformation has made the solution of the problem considerably easier. In the special case, where the normal derivative of the potential is zero, the boundary is

a flux line. Here the flux value on the sample surface is conveniently chosen as zero.

By analogy with the conjugate function in the two dimensional case the new function is called the flux, and it is defined ~~as~~ by

$$\rho \frac{\partial \phi}{\partial \rho} = \frac{\partial \psi}{\partial z} \qquad (4.2)$$

$$- \rho \frac{\partial \phi}{\partial z} = \frac{\partial \psi}{\partial \rho} \qquad (4.3)$$

Differentiating equations (4.2) and (4.3) with respect to z and ρ respectively and assuming the second derivatives to be continuous, that is $\frac{\partial^2 \phi}{\partial \rho \partial z} = \frac{\partial^2 \phi}{\partial z \partial \rho}$, leads to a new equation

$$\frac{\partial}{\partial \rho}\left(\frac{1}{\rho} \frac{\partial \psi}{\partial \rho}\right) + \frac{\partial}{\partial z}\left(\frac{1}{\rho} \frac{\partial \psi}{\partial z}\right) = 0 \qquad (4.4)$$

which has the same form as (4.1) and has to be solved in the same way.

The pair of equations (4.1) and (4.4) are said to be adjoint, and the pair of functions ϕ and ψ are called adjoint functions. The equations are a special case of quasi-plane-potential equations given by

$$\frac{\partial}{\partial x}\left(\chi \frac{\partial \phi}{\partial x}\right) + \frac{\partial}{\partial y}\left(\chi \frac{\partial \phi}{\partial y}\right) + \Phi = 0 \qquad (4.5)$$

where both Φ and χ are known functions of x and y.

When solving equation (4.4) numerically the region obviously

has to be finite and consequently a boundary is imposed just far enough out from the sample so that the effect of the induced magnetic field is negligible. The distance required can be estimated by considering a superconducting sphere in an applied magnetic field. It is found that at a distance of about six radii from the centre of the sphere the induced flux is only about 0.5% of the applied flux. As the accuracy of the computations could not be expected to be more than about 1%, putting the boundary at about six times the specimen size was considered enough. The boundary condition is that the flux should equal the applied flux, $H_a \rho$.

The region is reduced further by making use of the symmetry about the equatorial axis, $\frac{\partial \psi}{\partial z} = 0$ on $z = 0$, and the symmetry around the rotational axis of the system, $\frac{\partial \psi}{\partial z} = 0$ on $\rho = 0$. As the potential on the specimen has already been chosen to be zero, it follows, that $\psi = 0$ on the axis.

The problem has thus been reduced to solving equation (4.4) in a region ABCDEFGA on fig. 4.1, where AB and CD are on the surface of the specimen and the boundary condition is $\psi = 0$. BC is the normal-superconducting interface, whose coordinates are to be found, and where, apart from the electromagnetic boundary condition $\psi = 0$, there is the free boundary condition, $\frac{\partial \psi}{\partial n}$ = constant. DE is on the equatorial axis and has a symmetry condition $\frac{\partial \psi}{\partial z} = 0$. EF and FG are arbitrarily chosen and on them the boundary condition is that the flux should correspond to the undisturbed applied field, i.e. $\psi = H_a \rho$. GA is the rotational axis of the specimen with $\psi = 0$.

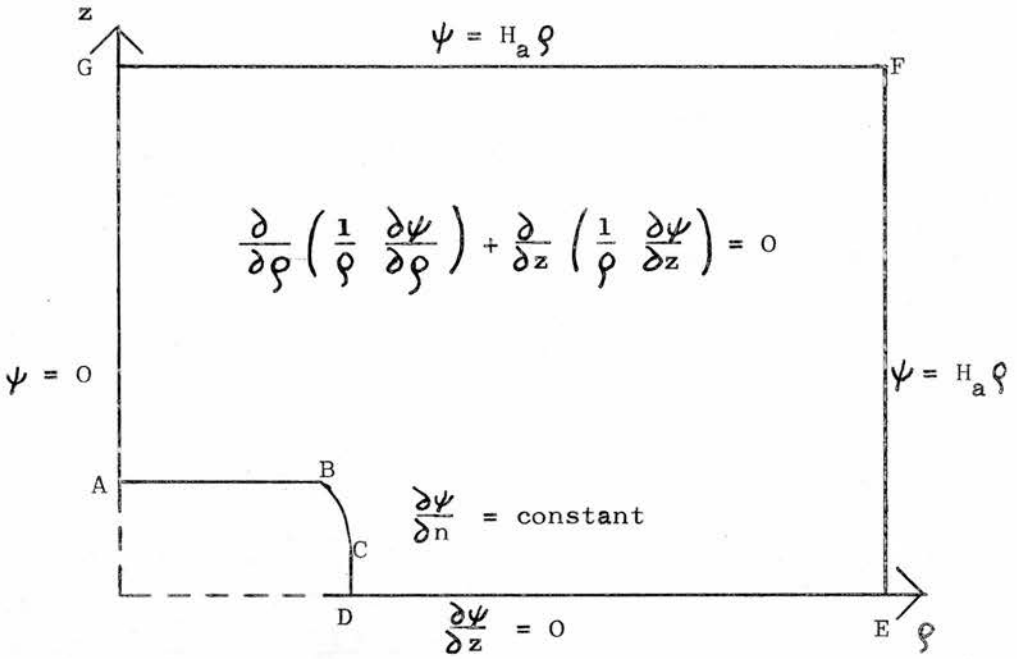

Fig. 4.1

The region of interest and the boundary conditions

In the finite difference approximation to a differential equation the derivatives are replaced by a finite difference approximation computed from the function values at neighbouring points.

For a typical mesh point O in a square mesh (see fig. 4.2), the finite difference approximations to the first and second order derivatives of a function w, can be found by expanding the function in a Taylor's series.

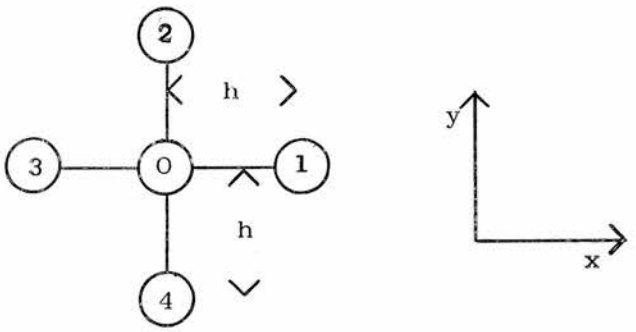

Fig. 4.2

$$w = w_o + \left(\frac{dw}{dx}\right)_o (x-x_o) + \frac{1}{2!}\left(\frac{d^2w}{dx^2}\right)_o (x-x_o)^2 +$$

$$\frac{1}{3!}\left(\frac{d^3w}{dx^3}\right)_o (x-x_o)^3 + \frac{1}{4!}\left(\frac{d^4w}{dx^4}\right)_o (x-x_o)^4 + \ldots\ldots \qquad (4.7)$$

Putting x equal to $x_o + h$ and $x_o - h$ in turn gives

$$w_1 = w_o + h\left(\frac{dw}{dx}\right)_o + \frac{h^2}{2}\left(\frac{d^2w}{dx^2}\right)_o + \frac{h^3}{6}\left(\frac{d^3w}{dx^3}\right)_o + \frac{h^4}{24}\left(\frac{d^4w}{dx^4}\right)_o + \ldots\ldots$$

$$w_3 = w_o - h\left(\frac{dw}{dx}\right)_o + \frac{h^2}{2}\left(\frac{d^2w}{dx^2}\right)_o - \frac{h^3}{6}\left(\frac{d^3w}{dx^3}\right)_o + \frac{h^4}{24}\left(\frac{d^4w}{dx^4}\right)_o - \ldots\ldots$$

and adding these two results and neglecting all terms involving fourth or higher order powers of h gives the finite-difference approximation to $\left(\frac{d^2w}{dx^2}\right)_o$

$$h^2\left(\frac{d^2w}{dx^2}\right)_o = w_1 + w_3 - 2w_o \qquad (4.8)$$

Similarly by subtracting the results and neglecting terms in h^3, or higher, the approximation to $(dw/dx)_o$ is found to be

$$h\left(\frac{dw}{dx}\right)_o = \frac{w_1 - w_3}{2} \qquad (4.9)$$

The derivatives with respect to y are similarly found from w_2 and w_4.

Writing equation 4.4 in the form

$$\frac{\partial^2\psi}{\partial\rho^2} - \frac{1}{\rho}\frac{\partial\psi}{\partial\rho} + \frac{\partial^2\psi}{\partial z^2} = 0 \qquad (4.10)$$

and substituting for the derivatives from equations (4.8) and (4.9) leads to the finite difference approximation to the function at O

$$\psi_o = \frac{1}{4}\left[\sum_{i=1}^{4} \psi_i \quad - \frac{h}{2\rho_o} \quad (\psi_1 - \psi_3)\right] \qquad (4.11)$$

where terms of order h^3 or higher have been neglected.

Near boundaries that do not fall on mesh lines, equation (4.11) does not apply, as one or more of the nearest points generally lie outside the boundary, and do therefore not exist in the region (see fig. 4.3). The equation can however be used by replacing the value at the non-existing point by a fictitious value obtained from the flux value at the boundary and the distance to the boundary ξh. In general, any one or two arms could be affected but here the position of the curved boundary is such that only points 3 and 4 are. As a considerable simplification in programming occurs by reducing the generality only the special case is considered here.

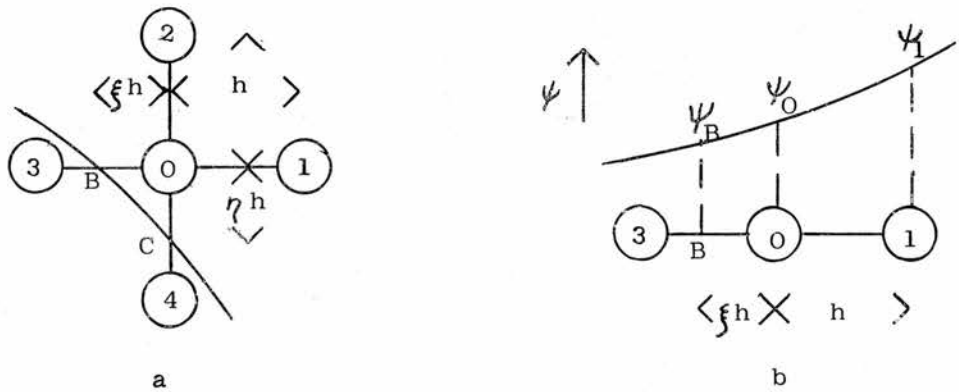

Fig. 4.3

Refering to fig 4.3b the value of ψ_B is found by Taylor's expansion (equation (4.7)) as

$$\psi_B = \psi_o - \xi h \left(\frac{d\psi}{d\rho}\right)_o + \frac{1}{2} \xi^2 h^2 \left(\frac{d^2\psi}{d\rho^2}\right)_o$$

neglecting terms in h^3 and higher. Replacing the differentials by their finite difference approximation gives

$$\psi_B = \psi_o - \frac{\xi}{2} (\psi_1 - \psi_3) + \frac{\xi^2}{2} (\psi_1 + \psi_3 - 2\psi_o)$$

from which the flux value at 3 is found to be

$$\psi_3 = \frac{2}{\xi(1+\xi)} \psi_B - \frac{2(1-\xi)}{\xi} \psi_o + \frac{(1-\xi)}{(1+\xi)} \psi_1 \qquad (4.12)$$

The value at 4 can similarly be expressed in terms of the values at C, O, and 2, and the proportion η

$$\psi_4 = \frac{2}{\eta(1+\eta)} \psi_C - \frac{2(1-\eta)}{\eta} \psi_o + \frac{(1-\eta)}{(1+\eta)} \psi_2 \qquad (4.13)$$

Inserting these values for ψ_3, ψ_4, or both, into equation (4.11) gives the expression for ψ_o at points close to the boundary. When the flux value at the boundary happens to be zero, as it is in this case, some simplification occurs.

The symmetry condition on the ρ axis is taken account of by putting $\psi_4 = \psi_2$ in equation (4.11) when computing the flux on the axis.

Initially the flux matrix was iterated by the Gauss-Seidel method, but later successive overrelaxation (S.O.R.) was employed with excellent results. In the first case the function values in equation (4.11) are those most recently computed, that is when computing the (n + 1) iteration row-wise at O the function values at 2 and 3 are those from the (n + 1) iteration but those at 1 and 4 are of the order n. The S.O.R. method is different, in that instead of using the (n + 1) and n order function values, it uses

$$U_n + \omega \left[U_{n+1} - U_n \right] \qquad (4.14)$$

where the U's are the function values and ω is a suitably chosen constant. The method reduces to the Point-Jacobi method when $\omega = 0$ and to the Gauss-Seidel method when $\omega = 1$.

The justification of the method comes from studies on well behaved matrices and cannot be extended to practical problems but the method has been found to converge for a wide range of non-ideal problems. The rate of convergence in the ideal case varies with ω somewhat as shown in fig. 4.4.

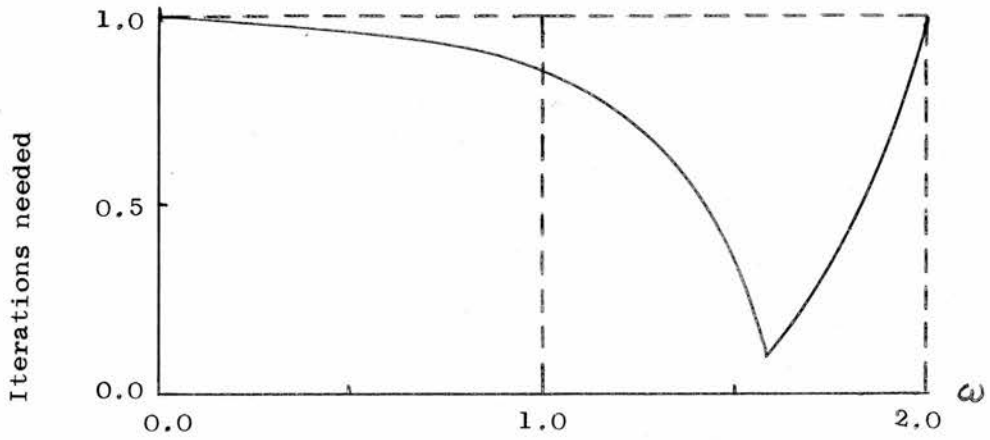

Fig. 4.4

Convergence in a relaxation scheme.

For practical problems the same kind of behaviour occurs although the exact shape of the curve and the position of the minimum varies. In non-ideal cases the optimum value for ω has to be found empirically in each case.

When equation (4.4) has been solved at all mesh points in the region it is a simple matter to find the field values. These are given by $\underline{H} = \nabla \phi$, which from equations (4.2) and (4.3) is in terms of flux, equal to

$$\underline{H} = \frac{1}{\rho} \frac{\partial \psi}{\partial z} \underline{i}_\rho - \frac{1}{\rho} \frac{\partial \psi}{\partial \rho} \underline{i}_z \qquad (4.15)$$

Equation (4.15) can however not be used on the normal-superconducting boundary; instead the field is found by extrapolation from the field at points just outside the boundary.

When using the finite difference approximation the curved boundary is only defined at its intersections with mesh lines and is thus approximated by a polygonal boundary. Changing the mesh length does therefore change the shape of the boundary and consequently the flux values in the region. The difference is most marked near the boundary and it falls off rapidly with distance. In this problem the boundary field is of main interest so a mesh length small compared with the sample dimensions had to be used. Using this fine mesh throughout the region was unneccessary and would have been wasteful of computer time and storage space. Use was therefore made of "graded nets", that is in the main region a coarse mesh was used but in a smaller region near the interface a finer one was employed.

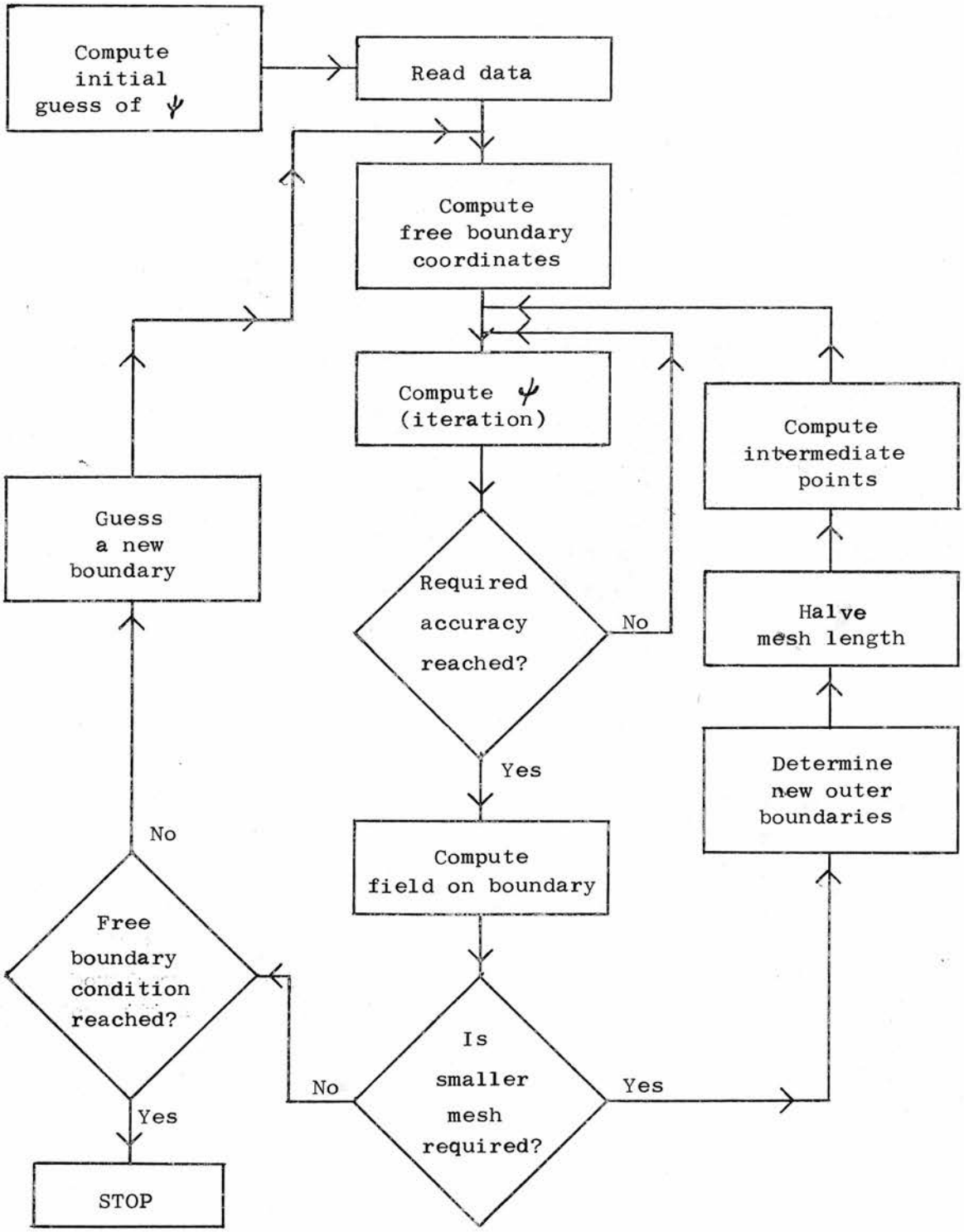

Fig. 4.5

Flow diagram of computer programs

In fact six different mesh sizes were used in succession, each half the length of the previous one, and each applied in a gradually smaller region around the interface.

4.3 Computer programs

The computer programs are best explained by a flow diagram (fig. 4.5). For clarity only the main steps are included.

In the first step the flux corresponding to the uniform applied field is computed in the region. This serves as a first guess to the flux values.

The second step reads in from data cards, the size of the sample, the parameters defining the initial guesses of the free boundary, the S.O.R. parameters, and other data necessary for the solution of the problem.

The phase boundary coordinates are computed in the third step. Initially a boundary curve was drawn on graph paper and the coordinates read off and fed into the computer as data. After the problem had been solved and the boundary field found, the shape of the curve was changed according to whether the field was too low or too high. This was tedious and, more important, it was found that the boundary field was extremely sensitive to irregularities in the surface. Very small changes in the curvature of the boundary caused large changes in the field and it was impossible to draw a curve smooth enough to give a constant boundary field.

The curves found in this way resembled ellipses and it was

therefore decided to define the boundary by a smooth function of the type

$$\left(\frac{\rho'}{a}\right)^m + \left(\frac{z'}{b}\right)^n = 1 \qquad (4.16)$$

These curves are smooth, tangential to the top and side surfaces, and a large variety of shapes can be obtained simply by changing the four parameters. The curves give satisfactory results when $b \approx 2a$ and $m \gtrsim n \approx 1.6 - 2.0$. The m is always higher than n, that is, the curvature is sharper near the top surface than at the side.

When the coordinates of the interface have been computed, the problem is set up and the flux equation (4.11) iterated. The iteration is continued until the flux at the top edge of the cylinder changes less than 1 part in 10^5 over ten iterations. This point has no special significance but is chosen because it is near the interface where the flux values are most important. With a good choice of the S.O.R. parameter about 100-150 iterations are needed for the initial coarse mesh but 40-100 for each of the subsequent finer meshes.

After the flux has been found the field on the boundary is computed. The field at points just outside the boundary is found by numerical differentiation of the flux values. The boundary field is then found from the field outside by extrapolation.

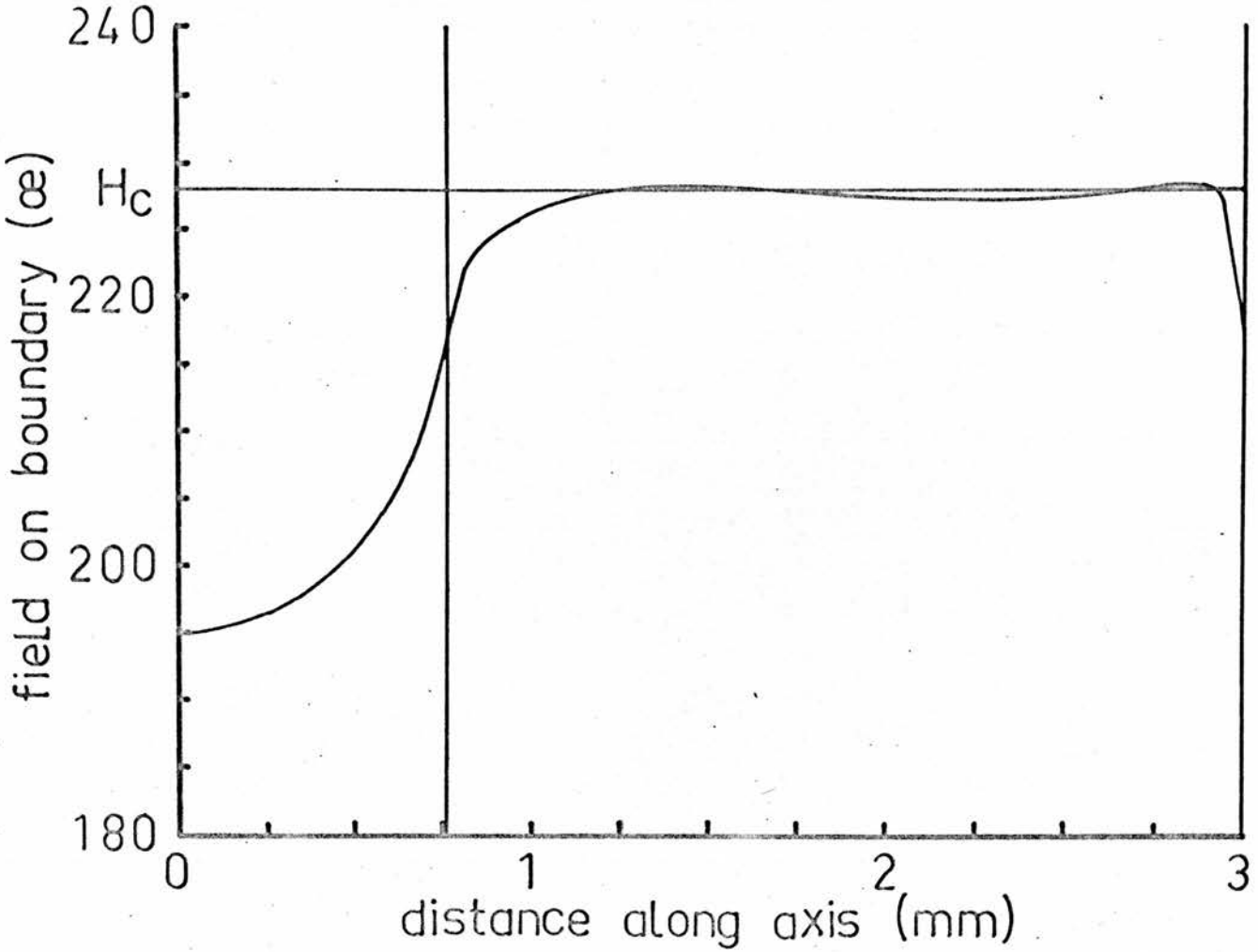

Fig. 4.6

The field on the penetration boundary as a function of the distance along the axis (z), for one of the profiles of the (l/d) = 6.0/22.0 mm cylinder. Between the axis and the first vertical line is the side surface of the cylinder. Between the two vertical lines, the penetration boundary. The horizontal line denotes the critical field (228 Oe).

To obtain sufficient accuracy the mesh size is reduced by half and the problem solved again in a smaller region. The process is usually repeated six times giving a final mesh size 1/32 of the initial mesh, in the region around the interface.

When the boundary field has been found for the smallest mesh, the next step is to determine whether it satisfies the free boundary condition. The criterion used is that the standard deviation from the average field taken over all points on the free surface, should be less than 1.0%. In most cases this was more than satisfied and the deviation was usually less than 0.5%.

At first new boundaries were guessed by looking at the previous results and changing the parameters in equation (4.16). Later the process was automated, and a function minimizing program used to minimize the standard deviation from the average field with respect to the parameters m, n, and a. This was quite successful and saved computer time as well as a considerable amount of effort.

Fig. 4.6 shows a typical plot of boundary field as a function of the distance along the axis of the cylinder. Between the vertical axis on the diagram and the first line is the superconducting surface but between the two lines the superconducting-normal interface. The horizontal line denotes the critical field. The field can be seen to be very nearly critical everywhere except near the two cylinder surfaces, where it drops noticeably. It is assumed that this is not a physical property of the system but rather a failure of the boundary curve to represent the actual boundary.

The optimum value of the relaxation constant ω was found by trial and error for each case. A plot of number of iterations against ω for a typical region (6.0 x 22.0 mm sample) is shown on fig. 4.7. The variation is similar to the ideal case except that the optimum occurs at a higher value of ω. It can be seen that at the minimum, the number of iterations needed is only about an eighth of that needed for the Gauss-Seidel method ($\omega = 1$).

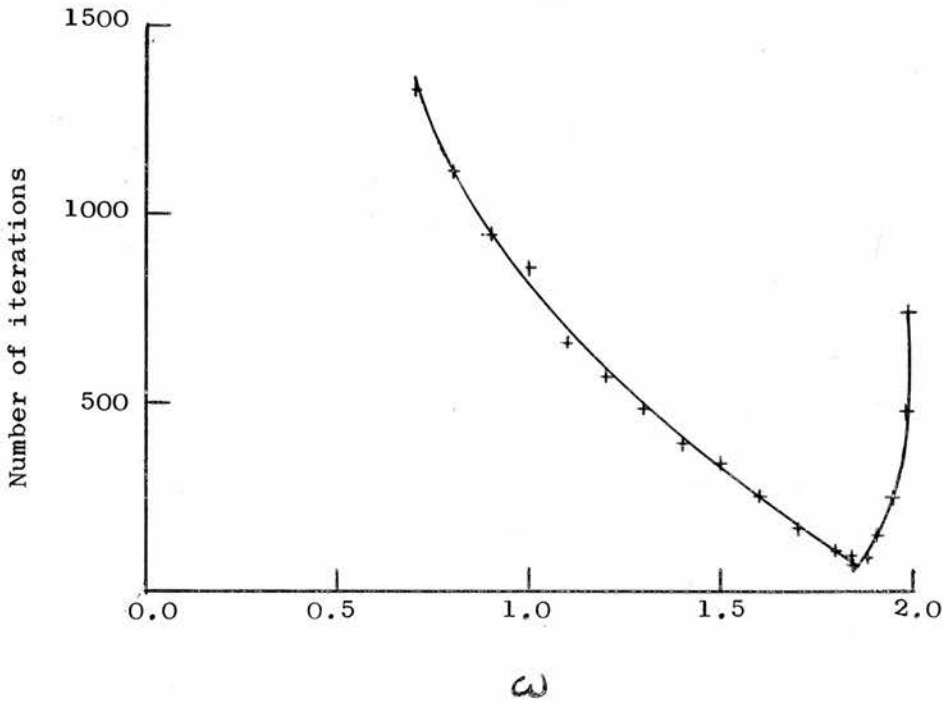

Fig. 4.7
Number of iterations needed plotted against ω.

4.4 Validity of the computed results

By their very nature numerical computations are approximations and should be treated as such. Apart from tests, to establish how well the mathematical model represents the physical system, it is therefore necessary to make certain that the computations converge on the right solution of the mathematical problem, and to estimate the accuracy of the final solution.

The computer programs also have to be carefully checked for logical errors. The standard tests usually show up all the obvious ones, but special cases that have not been foreseen can often arise during computations and make the results unpredictable. Computed results should therefore be checked and rechecked before they are used and their accuracy should be estimated.

The most obvious test to make is to compare the computed results with known analytical solutions. Theoretically this should show up any errors and give an estimate of the accuracy of the solution. The trouble is that even when such solutions exist, they are usually fairly special cases and have for example extreme symmetry. They might therefore not show up the weaknesses of the computations.

Another possibility is to compute the same quantities in widely different ways, and see if the answers agree. When this is possible, it can constitute a good check, but often there is only one way of solving the problem, or solving it twice is too time-consuming.

When dealing with physical problems, it is often possible to compute

some quantity, that can be determined experimentally, and compare the experimental and computed results. If they agree, one would not only expect the computations to describe the physical system satisfactorily, but also be more confident that the computations were right.

It is also sometimes possible to compute some physical behaviour, and see if it behaves as expected. An example of this is the free energy that should be at a minimum when the system is in equilibrium.

At the same time as the computations are checked for errors, their accuracy should be estimated and the computations adjusted so as to keep it within given limits. This involves changing mesh sizes and boundaries to obtain the required accuracy without wasting computer time and storage.

As far as practicable all the above tests were made. The results were compared with analytical results for spheres. When possible, the computations were done in two different ways, but it was not thought worthwhile to double the whole work. The Faraday rotation in a thin CMP glass disc on the top surface was computed from the results and compared with experimental results. Lastly the free energy was computed for the system as it went through the equilibrium.

To test if the programs were converging on the right solution the flux and field pattern outside a superconducting sphere was computed. These were then calculated analytically and the two results compared. The comparison for a sphere of 22.0 mm diameter

is shown on fig. 4.8. Because of limited computer storage capacity the computations were only done for mesh sizes 1/4 mm and above.

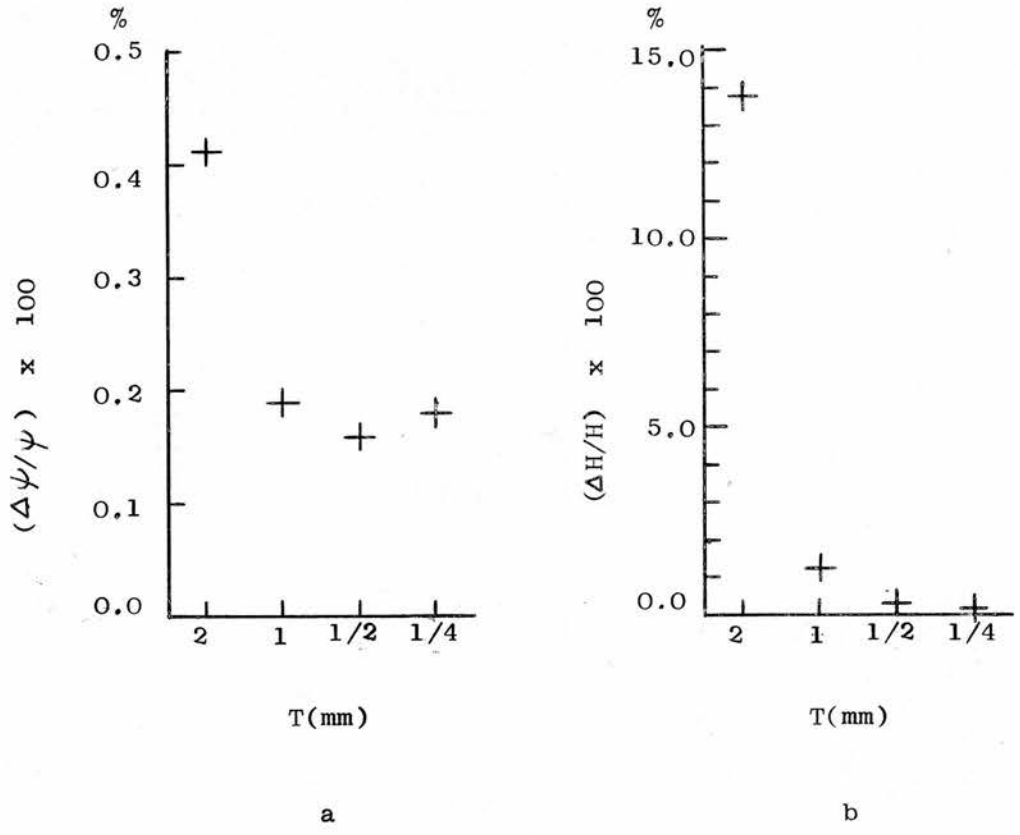

Fig. 4.8
The mean deviation from analytical values for a sphere 22.0 m diameter, (a) flux, (b) boundary field.

On fig. 4.8a the mean percentage deviation from the analytically calculated flux at all mesh points in the region is plotted against the mesh size T. Similarly fig. 4.8b shows the mean percentage deviation from the field at the surface of the sphere. In both cases the agreement can be said to be good. As the sphere is a very special case with high symmetry, this does not necessarily mean that this accuracy is obtained with the cylinders, but at least it indicates that no serious mistakes have been made and the computations are converging on the right mathematical solution.

The computations for a cylinder are tested for coherence and accuracy by looking at how the flux and field varies with mesh length. This is done by plotting the flux value at the top edge of the cylinder (fig. 4.9a) and the average field on the free boundary (fig. 4.9b) against mesh length. The top edge is chosen because it is near the boundary and should be representative of the points that are important in finding the boundary field.

The flux can be seen to be quite accurately computed for T = 1/4 mm. The field is more difficult. It can not be computed directly, but has to be extrapolated from points just outside the interface. This is most easily done by leaving out the points nearest to the boundary and extrapolating the field from the second and subsequent points to the boundary. The reason is that the nearest points are irregular, in that one or more arms of the finite difference stars are cut by the boundary and the field can therefore not be found by the usual differentiation

formula, used for the other points, but has to be specially computed. It was however found that as there is quite a steep gradient in the field away from the interface, the extrapolation was considerably more accurate when the irregular points were used (points + on fig. 4.9b) than when only the regular points were used (x on fig. 4.9b). So although the process was more complicated it saved one reduction of the mesh length and a considerable amount of computer time.

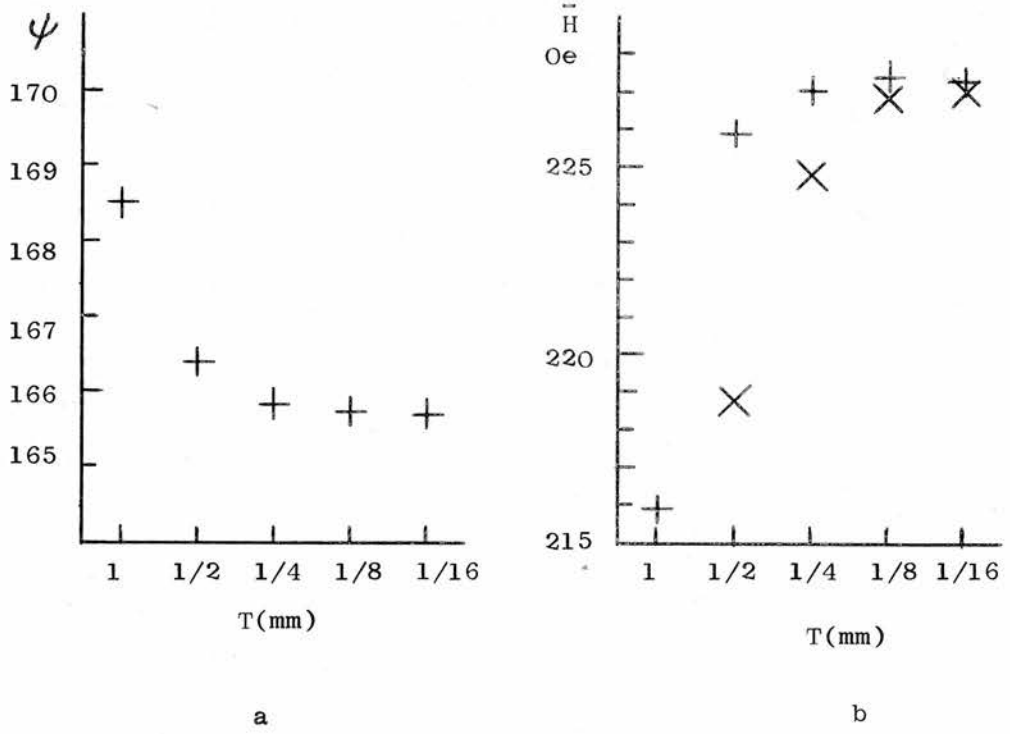

Fig. 4.9
Flux at the top edge of the cylinder (a), and the average field on the interface (b) plotted against mesh size T for a 6.0 x 22.0 mm sample (for explanation of + and x see test).

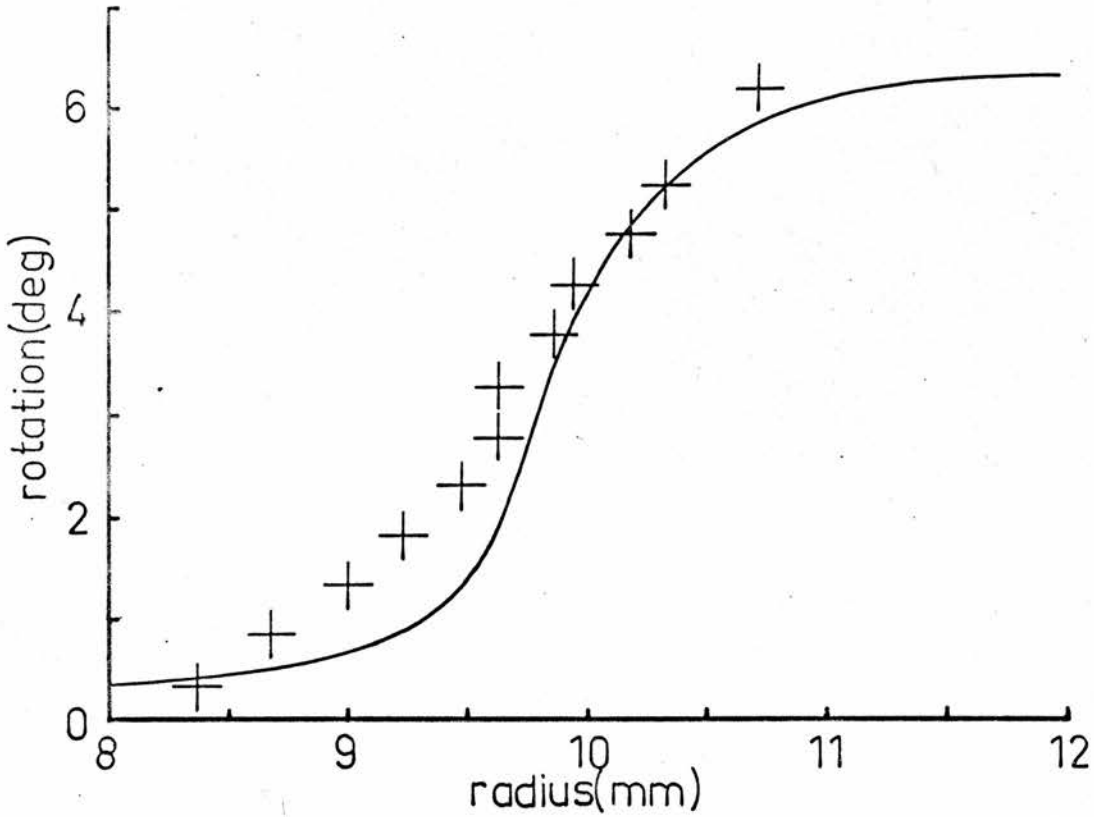

Fig. 4.10

Faraday rotation as a function of radial distance for In2 at T=1.4 ^{o}K and h_a=0.5. The full curve is that computed, while the crosses are experimental.

The effects of the outer boundaries are similarly estimated by plotting the field and the flux against the boundary position for each sample size. The boundaries are then put where the changes become less than the required accuracy.

The computations are non-dimensional and therefore only relative sizes are important. Fig. 4.9 indicates that mesh lengths of about 1/8 mm would be sufficient to get the boundary field accurate to 1%. Instead of using this coarser mesh and keeping the cylinder diameter about 20 mm the sample size was halved and the T = 1/16 mm mesh used. Most of the work was consequently done with 1/16 mm mesh on samples of 10 mm diameter.

The above checks should show whether the programs are converging on the right mathematical solution to the problem, but they do not show how well the approximations describe the physical problem. To do this the Faraday rotation in a CMP glass disk on the top surface was computed from equation (2.1) and the results compared with the experimentally observed values. The results are shown on fig. 4.10. The agreement can be said to be satisfactory, indicating that this quantity at least is reasonably well described by the computer model. As the rotation depends first and foremost on the position of the penetrating front and the field distribution in the penetrating region, this agreement indicates that the assumptions made about the penetration are reasonably valid.

If the critical field profile represents the equilibrium stage the free energy should have a minimum for that configuration. To check

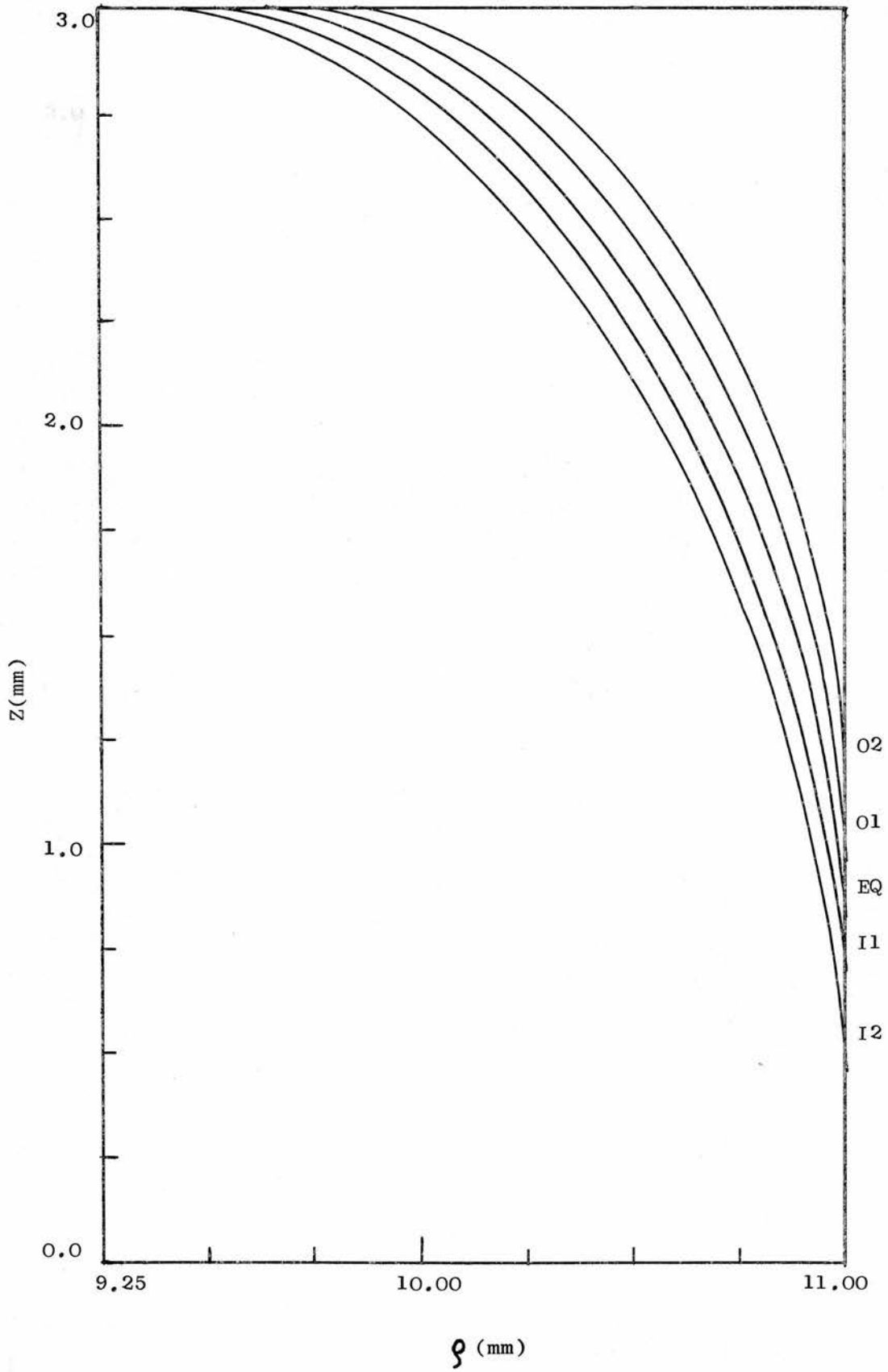

Fig. 4.11 a. Penetration profiles, EQ is the critical field profile.

if this was really so the energy was computed for the critical field profile and two similar profiles on each side of it (fig. 4.11a). On the ones that penetrate further in, the average field is lower than H_c, but higher than H_c on the ones that are further out.

The change in the free energy consists of two parts. Firstly there is the contribution of the magnetic energy due to the magnetic properties of the superconducting material. Secondly there is a change in the condensation energy due to the change in the relative volumes of superconducting and normal material.

The change in the free energy of a magnetic body of changing configuration in a constant applied field is given by

$$dF = \underline{H}_a \cdot d\underline{M}$$

(see Pippard (1957) p.26). For small changes in configuration the free energy changes are therefore given by

$$\Delta F = (\underline{M}_1 - \underline{M}_2) \cdot \underline{H}_a \qquad (4.17)$$

which can be computed for the cylinders.

To be able to compute changes in the condensation energy the penetrating region has to be taken to be in a supercooled normal state. Its free energy is then given by

$$F_n = V_n \cdot H_c^2/8\pi \qquad (4.18)$$

where V_n is the volume of the penetrating region.

The results for one of the interfaces of the 6.0 x 22.0 mm sample are shown on fig. 4.11a and 4.11b. The free energy does indeed have a minimum for the critical field profile.

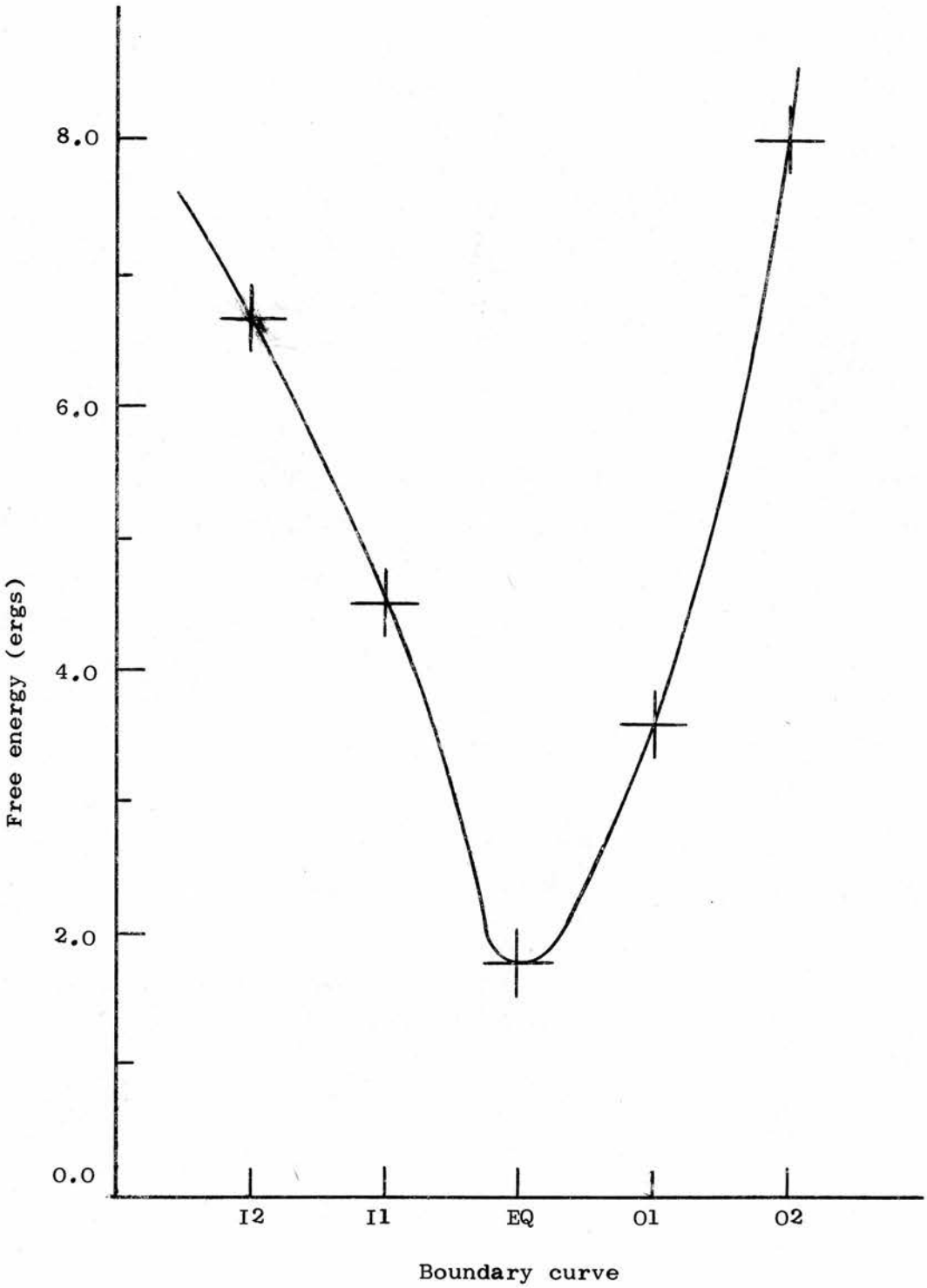

Fig. 4.11b.

Variation in free energy with penetration profile. EQ is the critical field profile.

In fact the penetrating region is not in a normal state but an intermediate state and the condensation energy will be slightly lower than that calculated above. However for this small change in configuration the condensation energy of the intermediate state will probably be nearly a linear function of the energy of the supercooled normal region in which case the effect on the position of the minimum will be small.

To sum up, it can be said that the checks showed that the programs converged on the right solution of the mathematical model and were accurate to at least 1% and probably in most cases to better than 0.5%. How well the model describes the physical system is more difficult to estimate, but the evidence, for what it is, indicates that the approximations are reasonable.

4.5 Results

Having established that the programs converge on the right solution a number of interfaces was computed for each of four different length/diameter ratios. This shows how the penetration proceeds and gives data for comparing with experimental results. It also supplies the basic data for other computations, like variations in magnetic moment, free energy, and the period of the fine intermediate state structure with penetration.

The computed penetration profiles for samples of length/diameter ratios 6/22, 6/10, 10/10, and 16/10 are shown on figures 4.12, 4.13, 4.14 and 4.15 respectively. For convenience the lengths are scaled in

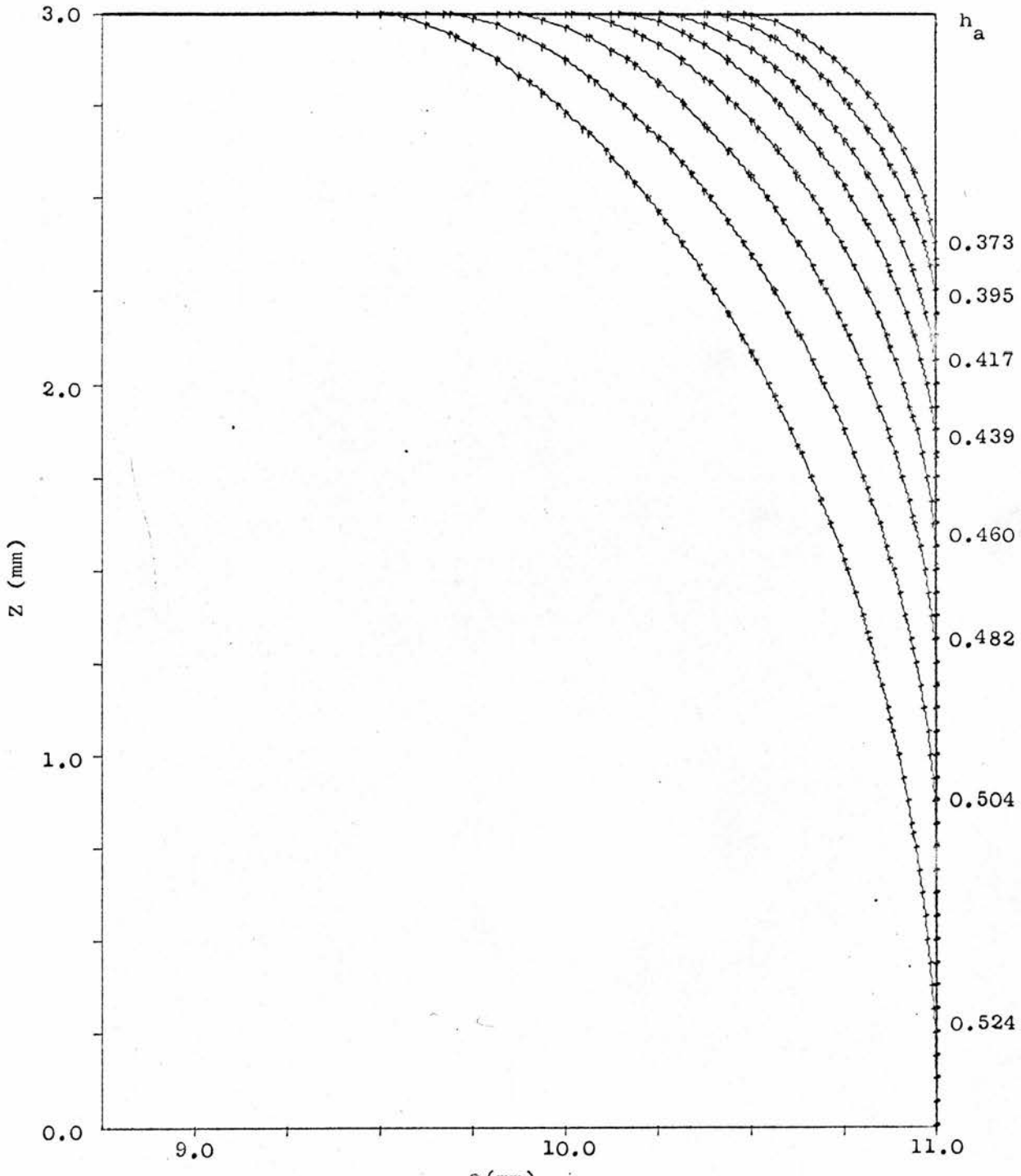

Fig 4.12

Interfaces for 6.0 x 22.0 mm sample

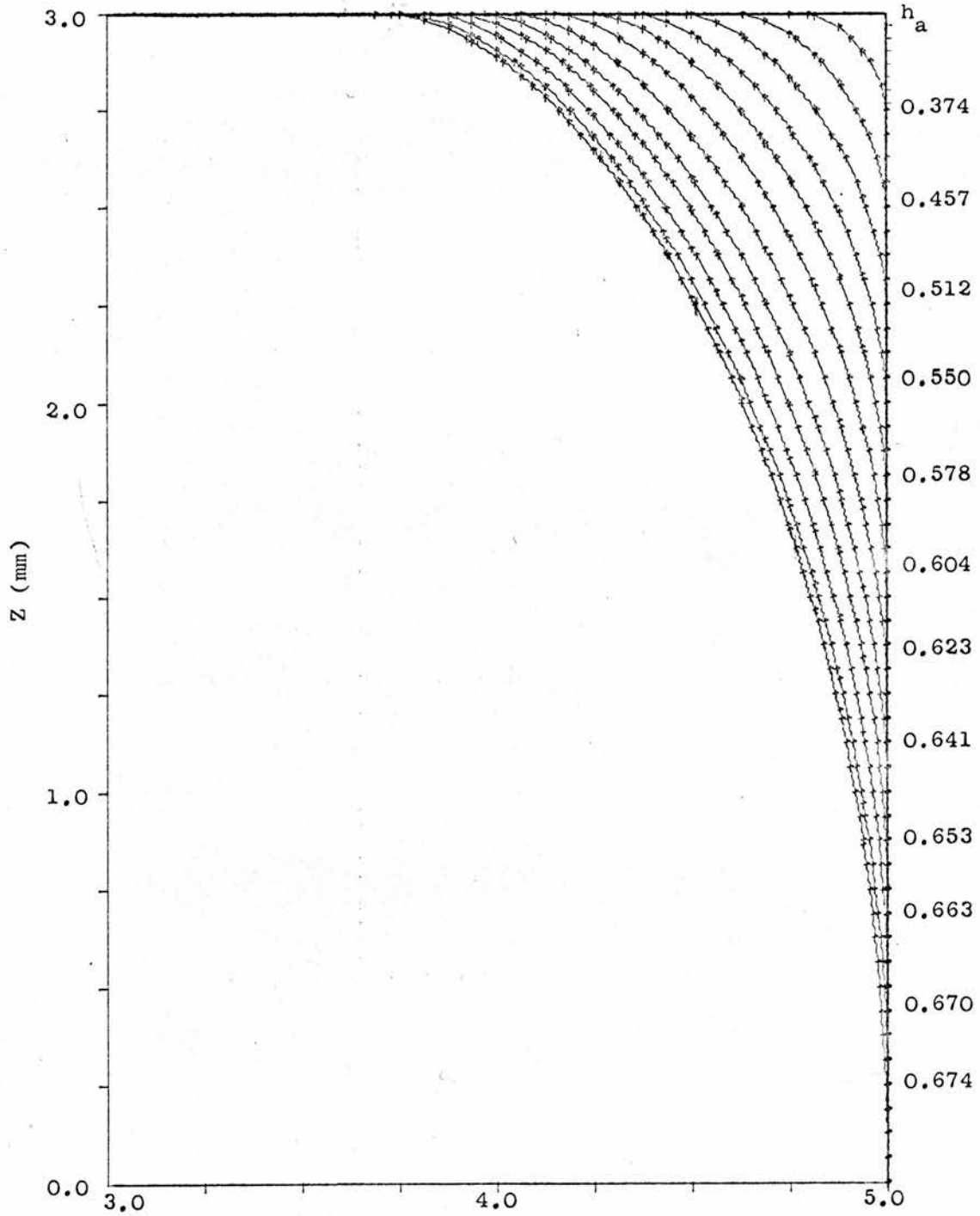

Fig 4.13

Interfaces for 6.0 x 10.0 mm sample

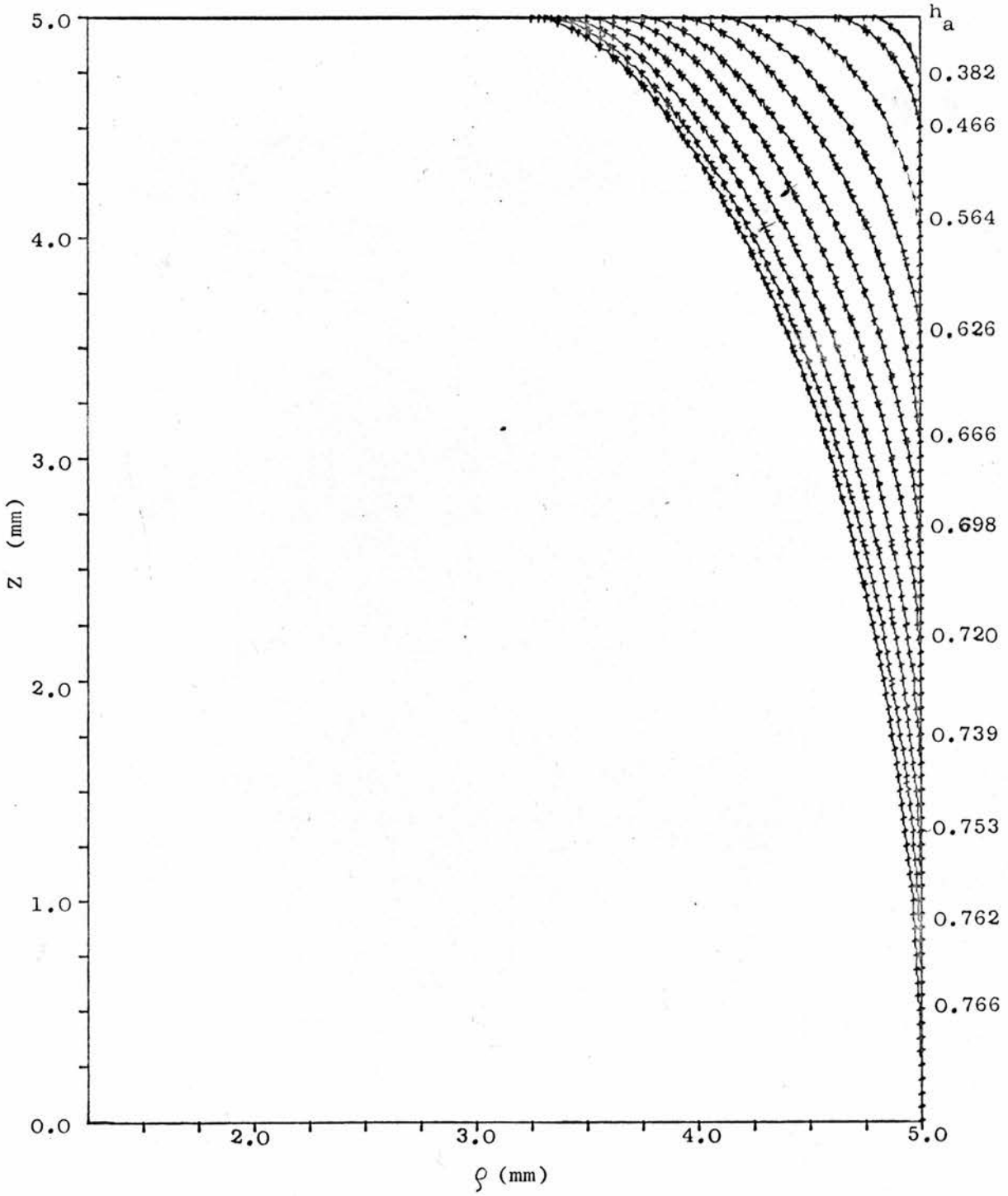

Fig 4.14

Interfaces for 10.0 x 10.0 mm sample

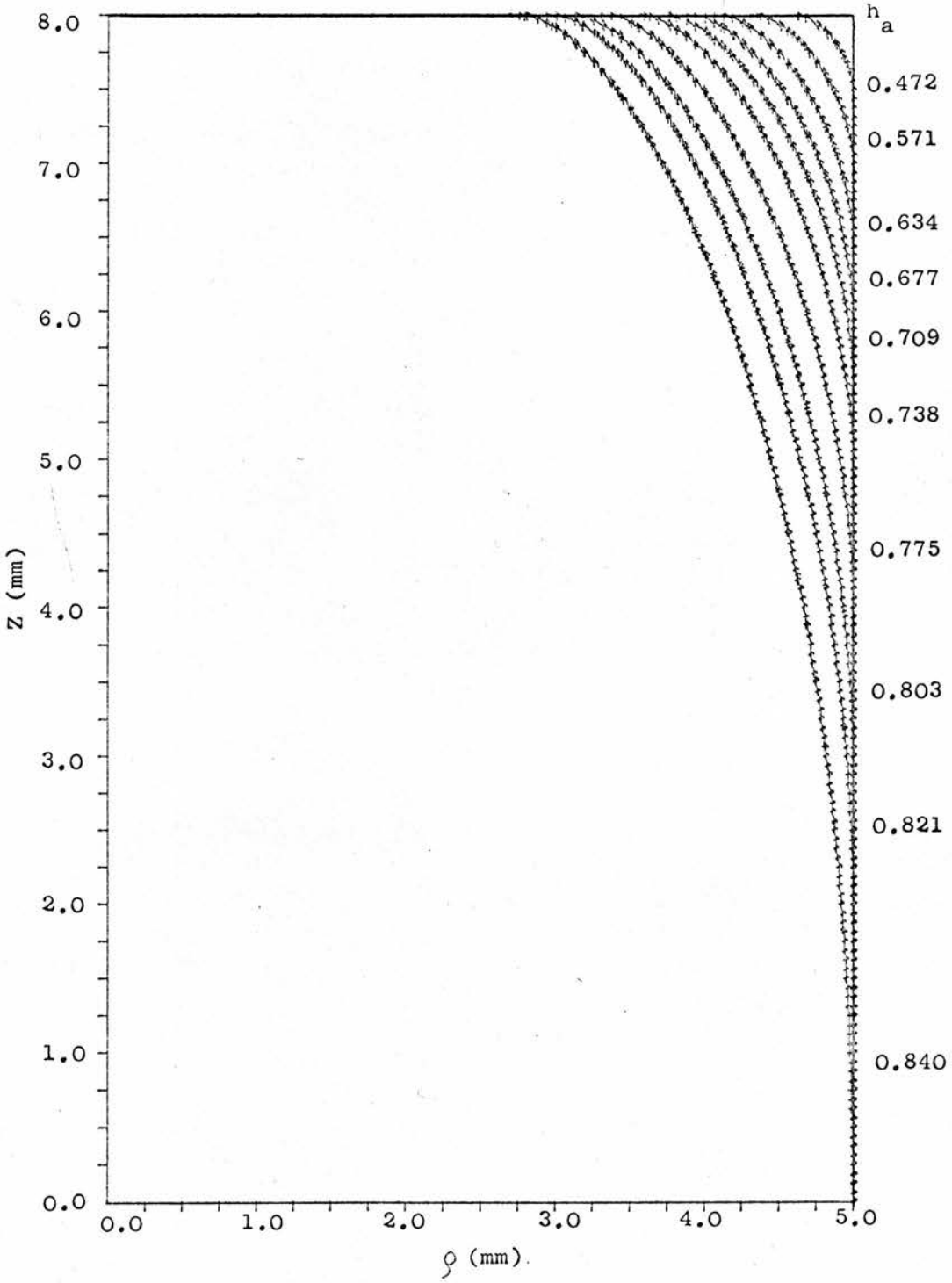

Fig 4.15

Interfaces for 16.0 x 10.0 mm sample

millimeters, although they are in fact non-dimensional. Except for the 16.0 x 10.0 mm sample, only the corner of the cylinder is shown, that is the ρ axis does not start at zero. The reduced applied field h_a is given to the right of each profile. On all the diagrams the innermost profile drawn is the one that is tangential to the side surface at the equator. It therefore marks the start of the second stage.

Small crosses are drawn at the points defining the curves, that is at intersections of the interface and mesh lines. The graphs are computer plots, and because of the digital nature of the machine they consist of small steps rather than a continuous curve.

CHAPTER 5 - EXPERIMENTAL DETERMINATION OF PHASE BOUNDARIES

5.1 Introduction

The experimental results are limited in that no measurements can be made inside the specimen and only the flux pattern on the top surface can be observed. Apart from the Faraday rotation in the CMP glass disc the only measurable quantity is therefore the radius of the superconducting region at the top surface (the "superconducting radius").

By comparing the experimental and computed results it is hoped to establish two things. Firstly whether the first stage of penetration consists of penetration of the corners of the cylinder, and is due to demagnetization effects, and secondly whether the start of the second stage of penetration coincides with flux penetrating the equator, as suggested by Baird.

To establish whether the first stage of penetration is as predicted both the observed and computed superconducting radii are plotted as a function of applied field. Agreement between the two results would indicate that in the first stage the flux does in fact penetrate the corners as predicted.

In the computed results the penetration of the equator is characterized by a certain value of the applied field (h_i) and also of the superconducting radius (ρ_i). These have both been computed for a large number of length/diameter (l/d) ratios from 0.2 up to 2.0. A comparison with the experimentally observed applied field and the superconducting radius at the start of the second stage should show if

the equatorial penetration represents the start of the second stage.

Experimentally the applied field at the start of the second stage of penetration can be determined from the minimum in the superconducting radius. It can also be quite accurately determined visually by noting the value of the applied field when flux bundles start to drift into the centre of the cylinder.

If the mode of penetration is as suggested it would only depend on the (l/d) ratio and the critical field but would otherwise be independent of material, temperature, preparation, and purity. To establish if this is the case experiments were done on differently prepared indium and tin at a number of temperatures.

In order to eliminate errors due to the experimental techniques both the magneto-optic method and the powder method have been used.

5.2 Experimental results

The reduced superconducting radius ρ has been measured and computed as a function of the reduced applied field h_a for three (l/d) ratios 6/22, 6/10, and 10/10, and is plotted on fig. 5.1, 5.2, and 5.3 respectively. The experimental points agree closely within themselves and there do not seem to be systematic differences between samples, temperatures, or methods of observation (fig. 5.1 and 5.2). The agreement with the computed results is satisfactory. The shape of the curves is the same and the minimum in the experimentally determined superconducting radius agrees closely with the last computed profile, that is penetration of the equator. The experimentally determined

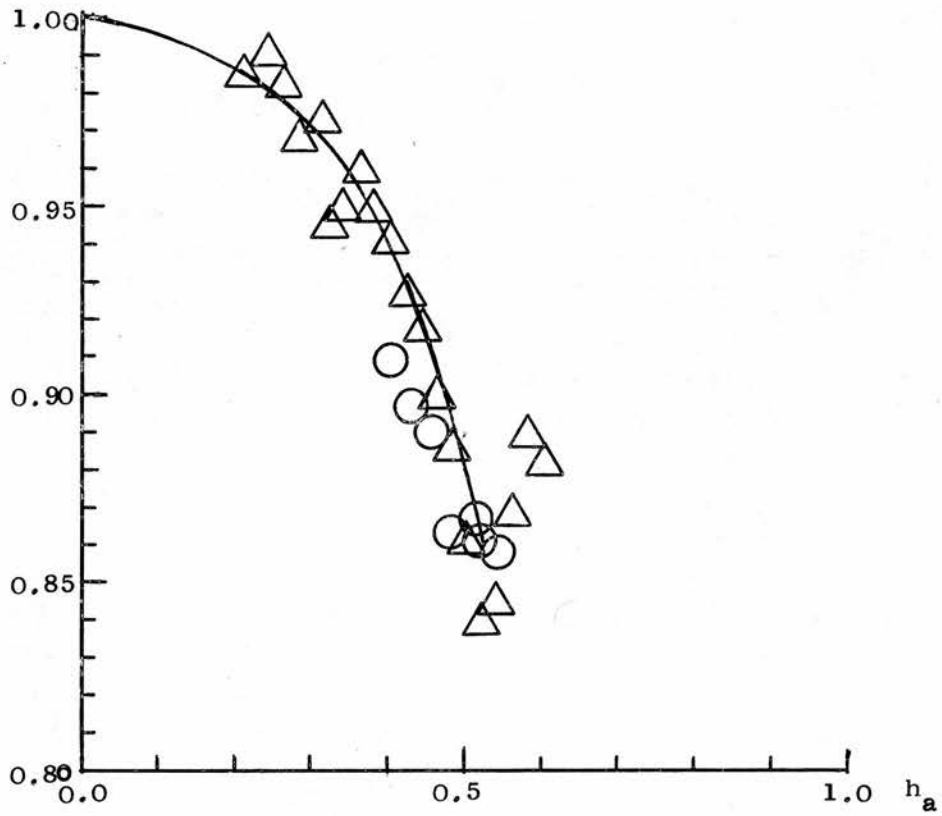

Fig. 5.1

1/d = 6/22. Superconducting radius ρ as a function of applied field h_a. Full line computed; △ In2 at 1.5 °K, using CMP glass disc, ◯ In2 at 2.2 °K, using powder.

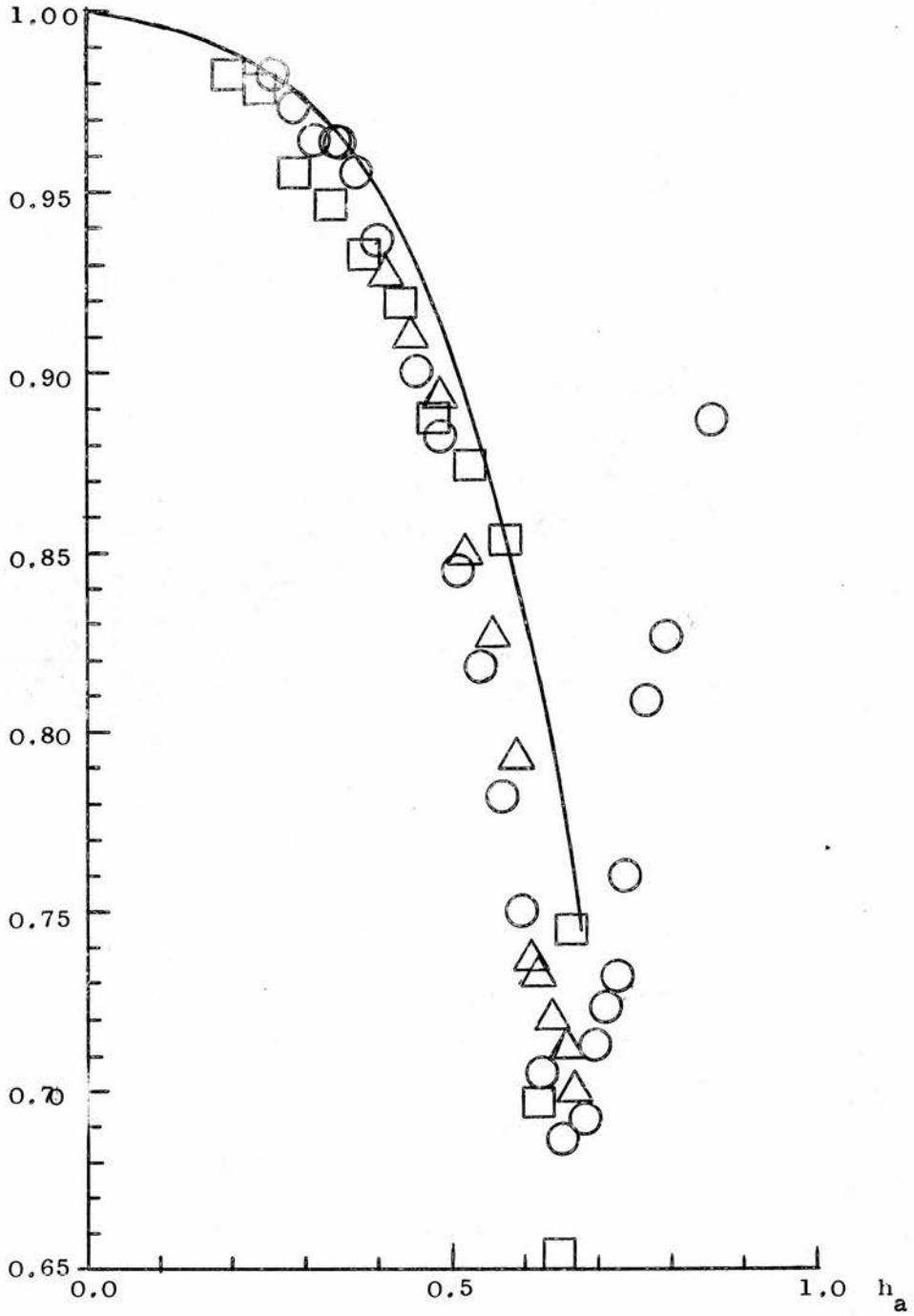

Fig. 5.2

$1/d = 6/10$, ρ against h_a. Full curve computed; △ In4 at 1.4 °K, using CMP; ○ In4 at 2.2 °K, powder; □ Sn1 at 1.7 °K, powder.

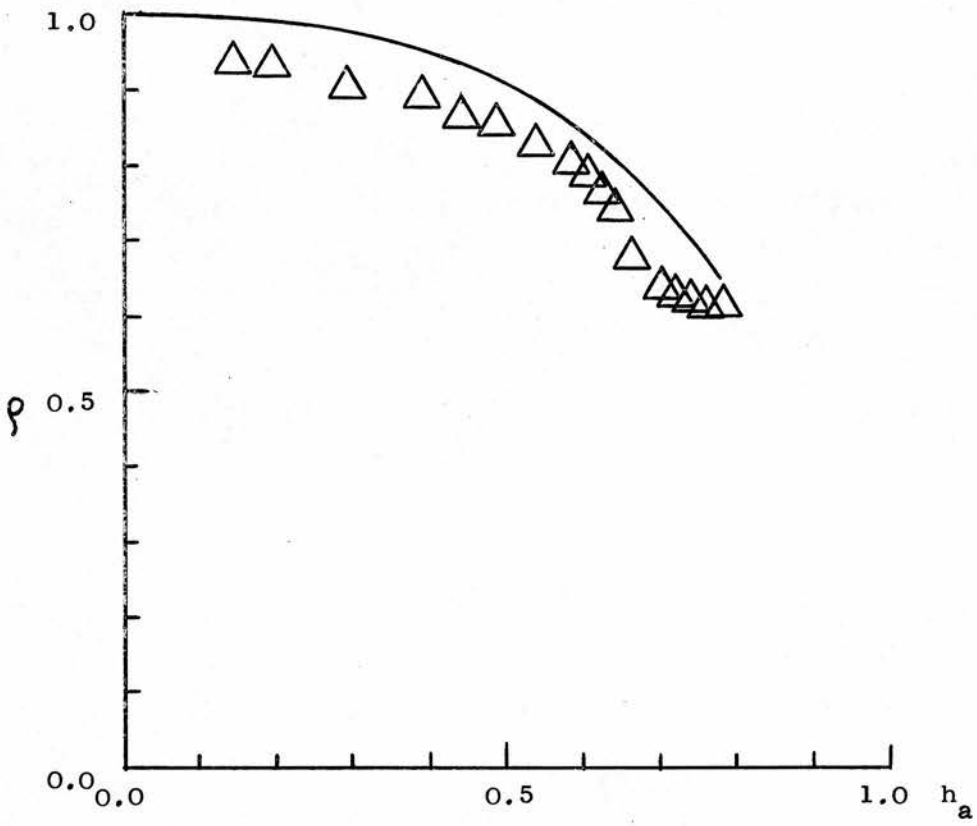

Fig. 5.3

1/d = 10/10, ρ against h_a. Full curve computed;

△ In5 at 1.4 °K, using powder.

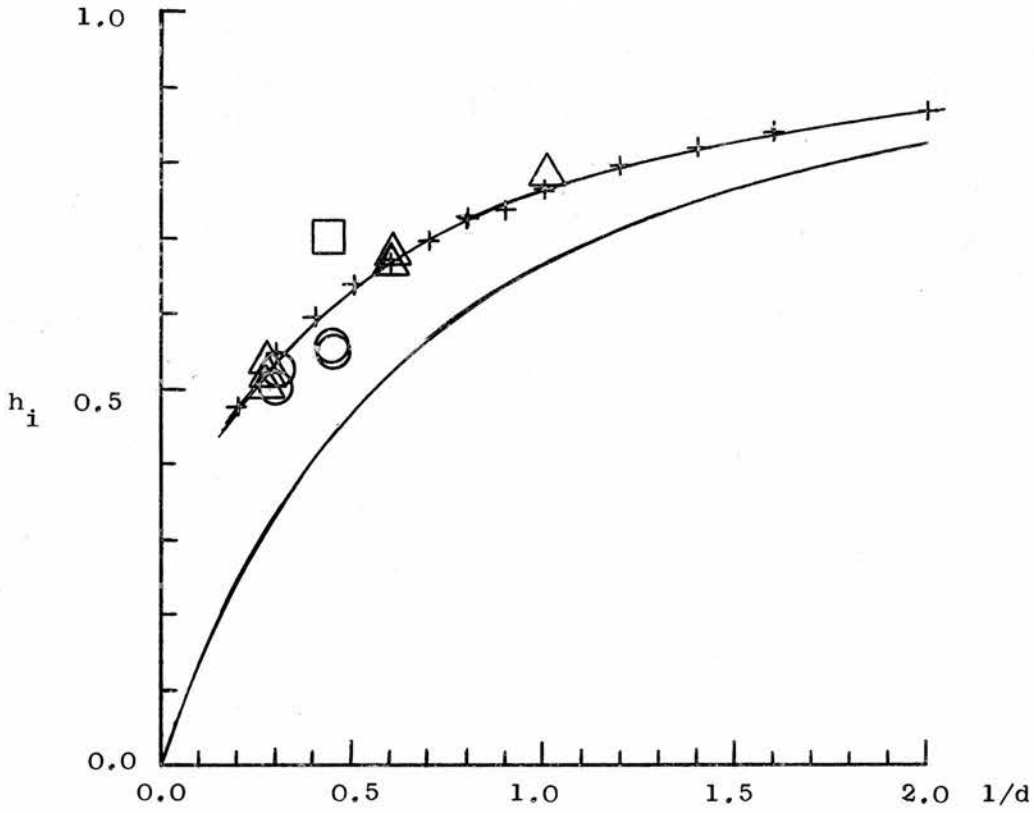

Fig. 5.4

The limiting field h_i plotted against length/diameter ratio. +——+ Computed (equatorial penetration), ——— (1-D) for ellipsoids, △ present experimental results, ◯ DeSorbo and Healy (1964), □ Baird (1964).

superconducting radius is however systematically smaller than the computed one.

The discrepancy cannot be ascribed to experimental errors as the CMP and the powder values agree quite closely. It seems more likely that the effect is real and probably due to the fact that the penetrating front does not have angular symmetry but consists of radial laminae. The average field on the interface can therefore not be equal to the critical field, but is probably somewhat lower. In that case the second stage would start at a slightly lower value of applied field than computed. This is not observed but the effect could be masked by other effects. It is for example not unlikely that a certain amount of equatorial penetration is necessary before flux bundles can drop off the ends of the laminae.

On fig. 5.4, h_i, the applied field corresponding to equatorial penetration, is plotted against the (1/d) ratio. This is compared with the experimentally determined applied field corresponding to the start of the second stage. Measurements were made for three (1/d) ratios and values published by DeSorbo and Healy (1964), and Baird (1964) have also been included. Baird's value is however not reliable as he could only measure the critical field of his sample to a 10% accuracy. The agreement with the computed results can be said to be good.

In the past demagnetizing factors of ellipsoids have been used to indicate when the field on the equator reached the critical value. It has been assumed that for cylinders this would be at the same value

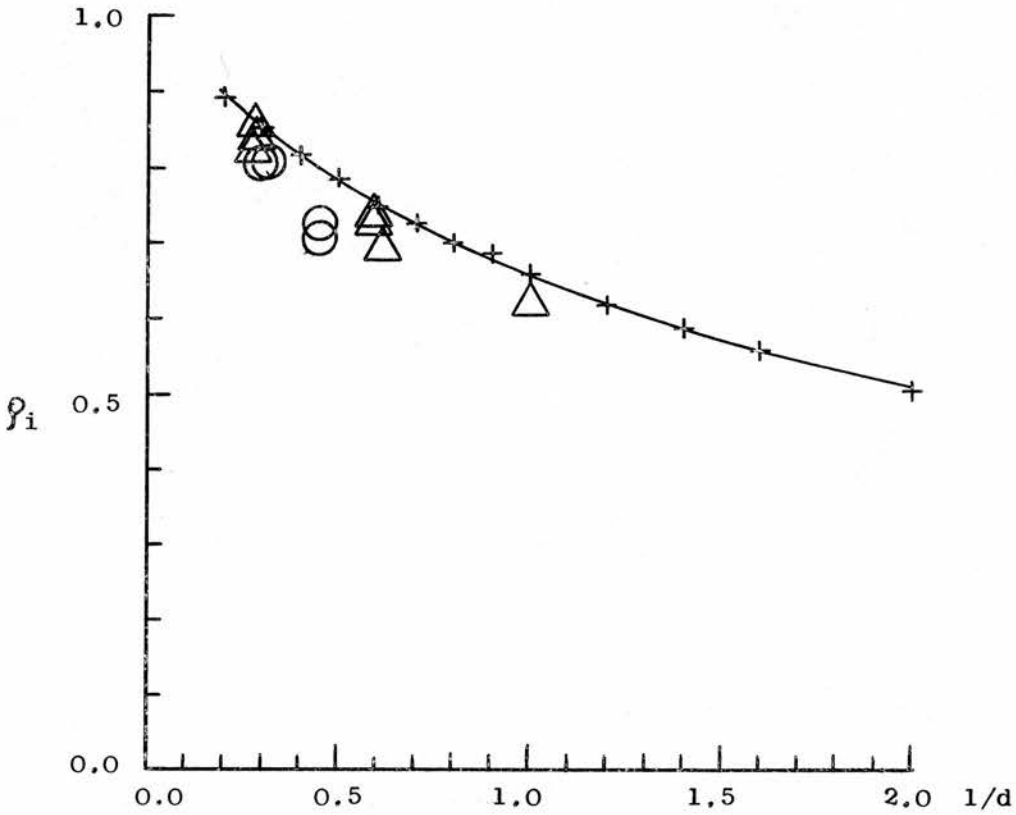

Fig. 5.5

The superconducting radius at the start of the second stage of penetration plotted against length/diameter ratio. —+—+— computed (equatorial penetration), △ present experimental results, ◯ DeSorbo and Healy (1964).

of applied field as for ellipsoids of equal eccentricity. As the field at the equator of a superconducting ellipsoid is given by $H = H_a/(1-D)$ where D is the demagnetizing factor, h_i should be equal to (1-D). This has been plotted on fig. 5.4 and it is obvious that the assumption is wrong. For cylinders the field at the equator only becomes critical for an applied field appreciably higher than for the corresponding ellipsoids.

On fig. 5.5 the computed superconducting radius corresponding to equatorial penetration and the experimentally observed values of the superconducting radius at the start of the second stage are plotted against the (1/d) ratio. The experimental values are again systematically lower than the computed values but otherwise the agreement can be said to be satisfactory.

5.3 Summary

From what has been shown above there seems to be ample evidence that the physical behaviour is reasonably well described by the mathematical model. The penetration proceeds inwards in very much the same way as predicted and the start of the second stage coincides with field penetrating the equator.

Bearing in mind the assumptions made in the computations about the symmetry of the interface and the penetrating region the agreement is in fact surprisingly good.

It is therefore considered that Baird's hypothesis has been proved and that it has been shown that the field first penetrates the edges

of the cylinder and proceeds inwards until the two penetrating regions meet and just penetrate the equator. At that point flux lines are completely within the material and flux bundles break off and drift towards the centre of the cylinder, thereby reducing the free energy of the system. As flux bundles are easily trapped by inhomogeneities the flux drift can only be expected to be completely free in pure and strainfree specimens.

It has been assumed that the penetrating region is in a supercooled normal state but in chapter 7 it will be shown that this is not so. Instead it consists of a radially laminar intermediate state. The effect of this on the penetration and the validity of the assumptions will be discussed further in chapter 7.

CHAPTER 6 - MAGNETIC PROPERTIES

6.1 Introduction

Having found H and B throughout a system a number of thermodynamic quantities can be computed. In this work the free energy of the system has been used to establish that the critical field interfaces really correspond to a minimum in the free energy. As the free energy is most conveniently found from the magnetic moment $\underline{M}$ of the sample using

$$F = \tfrac{1}{2} (\underline{M} \cdot \underline{H}_a) \qquad (6.1)$$

the magnetic moment was found for all the profiles. These results were later found to be of interest in themselves and as they throw some light on the problem they will be discussed at some length. Unfortunately hardly any measurements on magnetic moments of superconducting cylinders exist, and none have been made here. The results are therefore mostly computational and comparison with experiment is very limited.

When making magnetization measurements it is usually the flux B in the sample that is measured rather than the magnetization I. This can be done quite simply by wrapping a coil around the sample and measuring the induced voltage. Magnetic moment measurements on the other hand require more complicated apparatus. To make comparison with experiment easier, the average value of B in the sample has therefore been computed for all the profiles.

When dealing with the special cases of long rods or ellipsoids, the internal field is uniform and parallel to the applied field and consequently magnetization measurements are simplified. The internal field can be determined from $\underline{H}_i = \underline{H}_a/(1-D)$ and $\underline{I}$ can then be found from the relation $\underline{B} = \underline{H} + 4\pi \underline{I}$, if B is measured. For a cylinder this is no longer true

and the magnetization cannot be determined from the B/H curves, but has to be measured independently.

A further, and even more important simplification, occurs because the internal field is always equal to the highest field on the outer surface, that is the field at the equator. Penetration therefore coincides with the average magnetization $H_c/4\pi$ in the sample and a higher magnetization can never exist. In cylinders on the other hand the critical field is first reached at the edges of the cylinder, long before the average internal field has reached the critical value H_c. Furthermore, flux penetration into the centre cannot take place until the field at the equator becomes critical and at that point the average magnetization can be much higher than the critical value $H_c/4\pi$. The free energy is of course still lower than $H_c^2/8\pi$, because H_a is quite low. Normally this is not stressed and the very specialized behaviour of the ellipsoids is all too easily taken to be representative of superconductors.

The magnetic moment can be computed in two different ways depending on whether the bulk diamagnetism or surface current approach is used.

The bulk diamagnetism approach leads to an internal field $\underline{H}_i$, and as $\underline{B} = 0$ the magnetization is given by $\underline{I} = -\underline{H}_i/4\pi$. The magnetic moment can then be found by integration over the sample volume

$$\underline{M} = \int_V \underline{I}\,dv$$

To find the internal field, Laplace's equation has to be solved inside the sample under the appropriate boundary conditions. These are

found from the values already obtained outside the sample by applying the normal electromagnetic boundary conditions.

In the surface current approach there is no internal field and no magnetization. The break in the magnetic field at the boundary induces surface currents that give rise to a magnetic moment. If the field on the outside of the superconducting region is known, the total magnetic moment can be found by integration of the surface currents over the whole surface.

It is possible to find the magnetic moment by a third approach. The free energy of the specimen is given as

$$F = \tfrac{1}{2} \int_V \underline{H} \cdot \underline{B} \, dv - \tfrac{1}{2} \int_V \underline{H}_a \cdot \underline{B}_a \, dv$$

Where V is taken over all space outside the body, $\underline{H}$ and $\underline{B}$ are the local values of the field and the flux, and $\underline{H}_a$ and $\underline{B}_a$ are the applied field and flux. The first term represents the total energy of the system and the second the energy of the uniform applied field. The difference is therefore the energy of the specimen and from that the magnetic moment can be found using equation (6.1).

In the present computations this approach should have been possible. It was tried and was found to give results far inferior to the other two methods and was consequently discarded. The main reason for the failure is thought to be that the induced part of the field is very small compared with the total field ($\underline{H} \simeq \underline{H}_a$) so errors in the total field give rise to large errors in the induced field.

Of the first two methods the surface current method required less

computer time and was used to compute the magnetic moment of all the profiles. The bulk diamagnetism method was also programmed and used to test the results. The two methods agreed well with each other.

6.2 Bulk diamagnetism

Although it is not a formally correct description, a superconductor can be considered to be an ideal diamagnetic body with $\mu = 0$, but without surface currents. This describes correctly the behaviour of the field outside the body, and is sometimes more convenient to use than the surface current approach. Inside the superconductor the description is wrong, but that is seldom important.

In the intermediate state the superconducting region is surrounded by air with $\mu = 1$, and by the normal metal. In fact the susceptibility of the normal metal is so small that it is not necessary to distinguish between the two types of boundaries and the system can be considered to consist of a superconducting region with $\mu = 0$, surrounded by another medium of $\mu = 1$.

From electromagnetic theory the boundary conditions on a boundary between regions of different permeability are found to be:

(1) The potential is continuous across the boundary.

(2) The tangential component of H is continuous, but its normal component is not.

(3) The normal component of B is continuous.

The third condition has already been used to ~~derive~~ show that externally B, and consequently also H, is tangential to the surface.

As the flux is defined from the derivatives of the potential, the second condition means that the flux is not continuous across the boundary. The flux values outside can therefore not be used to find the internal field. Instead the potential just outside the boundary has to be found from the flux and the first condition used to find the appropriate boundary conditions inside.

As the potential is now given on the curved boundary, the internal field is determined by solving Laplace's equation for the potential ϕ inside the superconducting region. As before, only a quarter of the sample needs to be considered and the boundary conditions are, (i) that ϕ is known on the surface of the superconducting region, (ii) that the ρ axis is an equipotential line, and (iii) that on the z axis $\frac{\partial \phi}{\partial \rho} = 0$. The last two are the usual symmetry conditions.

The potential on the external boundaries is found from the boundary field computed in the first part of the work. It is given by $H_t = \frac{\partial \phi}{\partial t}$, and as $H_n = 0$ (where t refers to the tangential and n to the normal direction) the potential can be found by integration along the surface

$$\phi_a = \int_{l=0}^{a} H_t \, dl$$

taking $\phi = 0$ on the ρ axis. The integration is done numerically.

The potential inside is then found by solving Laplace's equation using finite differences and iteration. The equation is (4.1) and the method is almost identical to the one used for finding the flux outside the specimen. A 1/8 mm mesh size was used and the solution required 70-100 iterations.

After the potential has been found the field H_i is computed from it by numerical differentiation. The magnetization is given by $\underline{I} = -\underline{H}_i/4\pi$ and the total magnetic moment of the specimen is found by integrating $\underline{I}$ numerically over the superconducting volume.

6.3 Surface currents

This is formally the correct way of describing the magnetic properties of a superconductor. The material is now rightly assumed to have neither internal field nor magnetization and the magnetic properties are considered to be solely due to an induced supercurrent circulating on the surface.

From electromagnetic theory this current is given by

$$\underline{n} \times (\underline{H}_+ - \underline{H}_-) = 4\pi \underline{K} \qquad (6.2)$$

where $\underline{n}$ is a unit vector normal to the boundary, $\underline{H}_+$ is the boundary field outside, and $\underline{H}_-$ the boundary field inside the specimen, and $\underline{K}$ the surface current density. As $\underline{H}_- = 0$ the surface current density is given by $\underline{K} = (\underline{n} \times \underline{H}_+)/4\pi$ and the current goes round in a plane perpendicular to the z axis. This gives rise to a magnetic moment in the negative z direction equal to the enclosed area multiplied by the current density

$$\underline{m} = -|\underline{K}| \, A \, \underline{i}_z \qquad (6.3)$$

The total magnetic moment of the body is the sum of all the individual moments and can be found by integration of equation (6.3) along the surface.

The boundary field is again taken from the first part of the work. The area enclosed by the surface current loop is, because of the angular symmetry, a section through the specimen in a plane perpendicular to its axis and is given by $A = \pi\rho^2$. Putting this and the expression for the surface current density into equation (6.3), the total magnetic moment is given by

$$\underline{M} = -\tfrac{1}{2} \int_1 |\underline{H}| \rho^2 \, \underline{i}_z \, dl \qquad (6.4)$$

so $\underline{M}$ can be found by numerical integration of the field along the surface, from the equator to the pole.

6.4 Validity of the computations

As was the case with the free boundary problem, it is important to test thoroughly the validity of the computations. The two methods of finding the magnetic moment are quite different and if they give the same results some credibility has been established in the results.

Although both methods depend on the previous work, in that they use the boundary field computed there, they do not in fact totally depend on the assumptions made about the normal-superconducting interface and the field in the penetration region. The initial slope of the M/H curve is, for example, found from a cylinder without any penetration and should therefore be unaffected by the assumptions.

Apart from comparing the two numerical solutions, the magnetic moments were found for a sphere and a few ellipsoids and compared with the analytical results. A comparison with Shoenberg's (1937) experimental data for a 1/1 cylinder is also made.

In table 6.1 the computed values for a sphere and ellipsoids of eccentricity ϵ = 2/3 and 3/2 are compared with the analytical solutions.

Dimensions (1/d) mm	ϵ	1 %	2 %
6/6	1	-0.3	0.0
4/6	2/3	-0.6	+0.4
6/4	3/2	-0.5	-0.5

Table 6.1

The accuracy of the numerically computed magnetic moments of ellipsoids; Column 1 as determined from surface currents and column 2 from bulk diamagnetism.

The analytical values are found from the applied field and the volume of the ellipsoids using

$$M = - \frac{V}{4\pi} \frac{H_a}{(1-D)}$$

The accuracy of the numerical results is then expressed as the percentage difference from the analytical solution.

The numerical solutions can be seen to be accurate to better than 1% and the discrepancy between them is of a similar magnitude.

As these analytical solutions might not test the programs under realistic conditions, comparison has also been made between the numerical solutions for cylinders of various length/diameter ratios. The profiles used are some arbitrarily chosen critical field profiles. The results

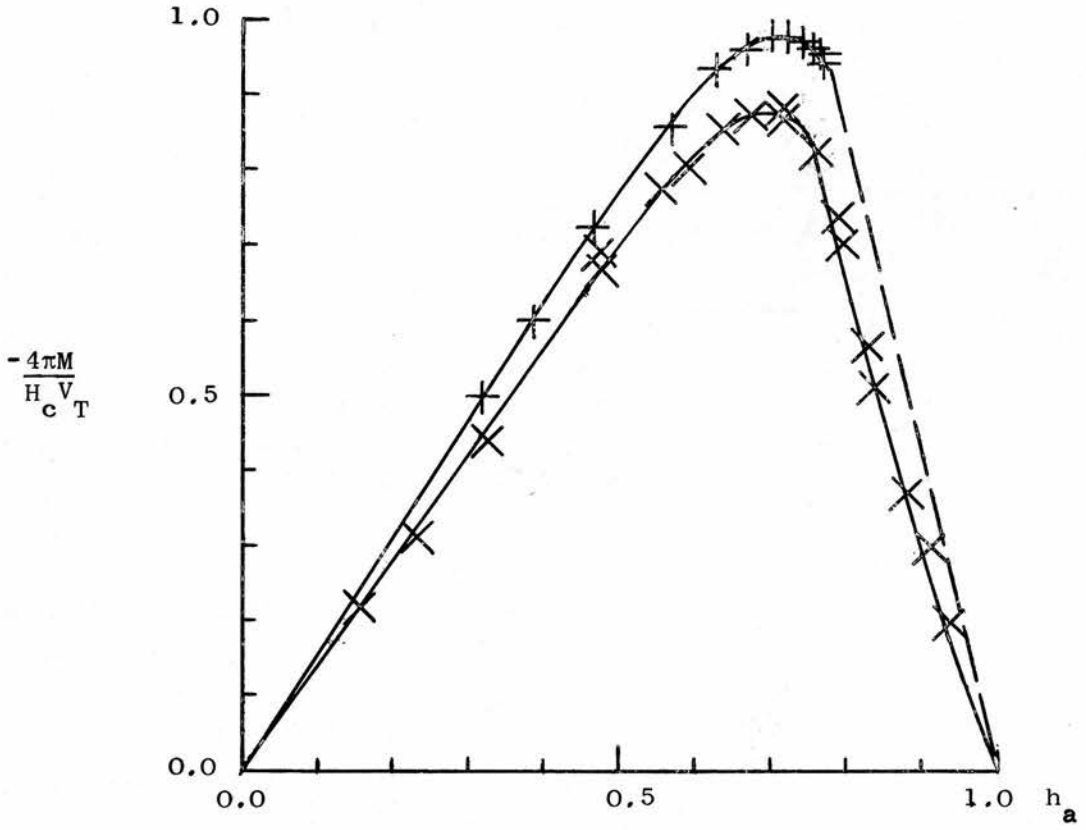

Fig. 6.1

Magnetization curve for a 1/1 superconducting cylinder. + computed, and × experimental (Shoenberg (1937)).

are shown in table 6.2

As was the case for the ellipsoids the numerical results agree closely, to within 1%.

1/d	Dimensions (1/d) mm	H_c Oe	Surface currents	Bulk diamagnetism	Difference %
0.273	6 x 22	228.0	28.02	28.02	0.00
0.600	12 x 20	173.5	28.25	28.24	0.04
1.000	10 x 10	130.4	3.86	3.85	0.14
1.600	16 x 10	119.1	5.17	5.19	-0.39

Table 6.2

Comparison of numerical values of magnetic moments for cylinders of various (1/d) ratios.

Shoenberg (1937) measured the magnetic moment of superconducting tin cylinders by measuring the force exerted on them by a slightly non-uniform field. The purity of the samples is unfortunately not known. Their diameter is of the order of 3-4 mm. Measurements were made on three (1/d) ratios, 1/2, 1/1, and 2/1, but only the 1/1 results can be reliably extracted from the paper. No measurements of magnetic moments of cylinders other than these have been found in the literature.

The measured and computed magnetic moments for a superconducting cylinder of (1/d) ratio unity are shown on fig. 6.1. The measured values were read from a graph in Shoenberg's paper. The computed values do of course only go up to the start of the second stage, h_i. The values have been reduced to take account of different sample sizes and critical fields. The similarity in the shape of the curves is striking, but

there is about a 10% difference in the vertical scale.

Shoenberg does give the initial slope of the magnetization curve for (l/d) ratios 1/2 and 2/1. These have been compared with slopes computed from cylinders with no penetration, and the comparison is shown in table 6.3 and fig. 6.3. Again the computed results are about 10% higher.

l/d ratio	Slope		Difference %
	Experimental	Computed	
1/2	1.86	2.08	-11.8
1/1	1.41	1.56	-10.5
2/1	1.20	1.29	- 7.5

Table 6.3

The initial slope of the magnetization curve for cylinders.

It is difficult to explain this discrepancy. The programs give accurate values for magnetic moments of ellipsoids and they give identical values for the magnetic moments of cylinders. The initial slope is determined from cylinders with no penetration, so assumptions made about the interface cannot be to blame.

There is some difficulty in estimating the quality of Shoenberg's experimental results, but in a previous paper (1936) he used the same apparatus to find the magnetic moment of lead spheres and got excellent agreement with theory.

It would have been desirable to measure the magnetic moment of one or more cylinders, so that the computations could have been thoroughly tested. Unfortunately there was neither the time nor the apparatus to do it.

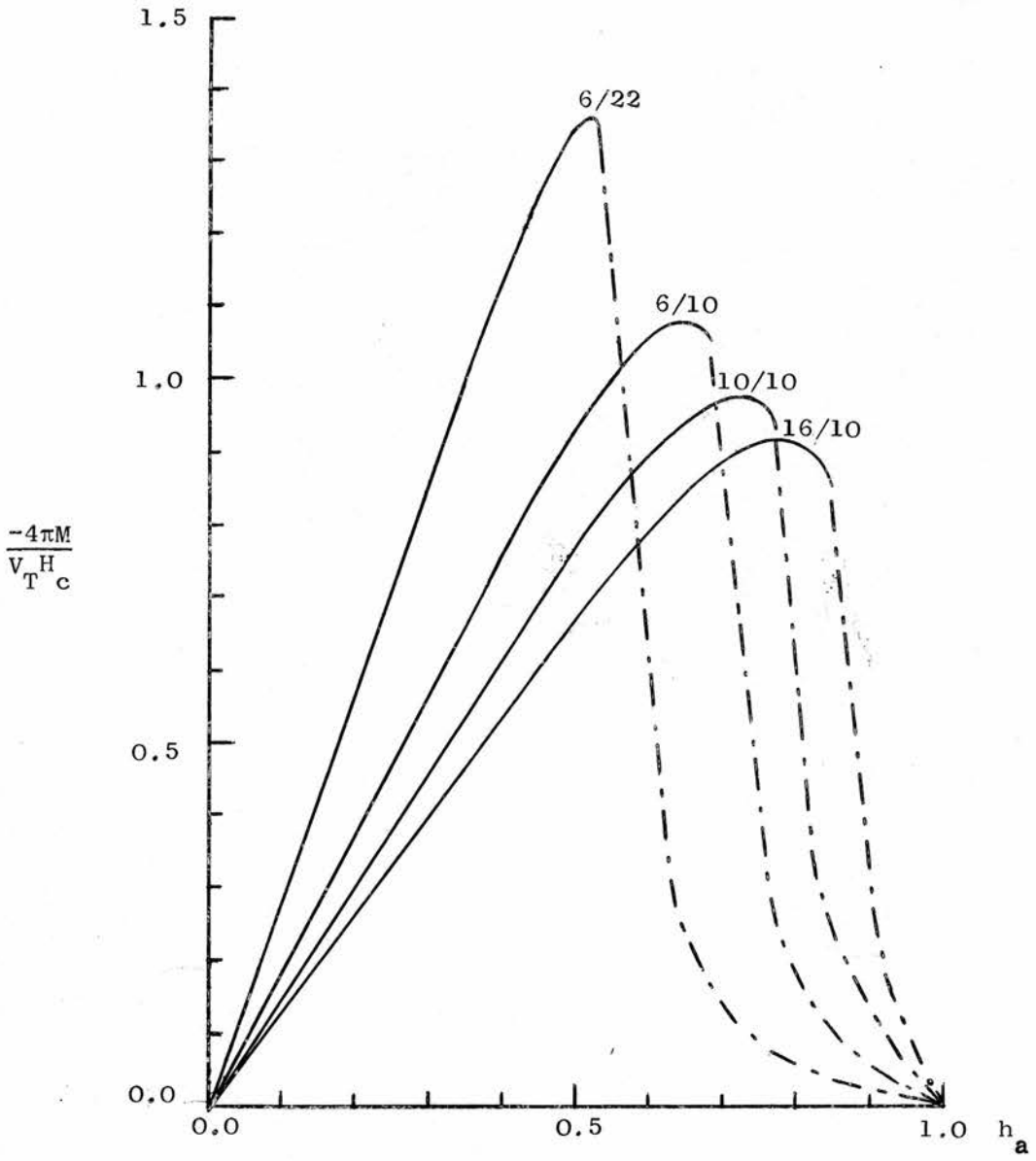

Fig. 6.2

Computed magnetization curves for cylinders of (1/d) ratio 0.273, 0.6, 1.0 and 1.6

One further computational check was made. The change in the free energy of a magnetic body with applied field is given by the integral under the magnetization curve. The energy difference between the superconducting state and the normal state is equal to the condensation energy $H_c^2/8\pi$ and this should equal the total area under the curve. Because of scaling factors the integral should be 0.5 in the present case.

For the experimental curve the integral was found to be 0.476, or about 5% too low. The computed curves are not complete so the integral cannot be determined, but assuming a linear fall from h_i to zero we obtain 0.549, which is 10% too high. The latter 10% is not necessarily related to the 10% difference in the initial slope, because a similar approximation was made for the other l/d ratios and the difference in energy was found to be increased as the cylinder became shorter. This suggested that the magnetization curve should not fall linearly, but start to fall with a large gradient and then decrease more slowly to zero. By trial and error, curves were found that gave the right area and were similar in appearance for all the (l/d) ratios. These curves are shown with a broken line in fig. 6.2 .

The B/H curves were found by numerical integration of the axial component of the field in the penetration region. The results are reduced by dividing by the total volume of the specimen and the critical field. They were not checked except to make sure that the integration was correct.

6.5 Summary

The magnetization curves up to the start of the second stage of

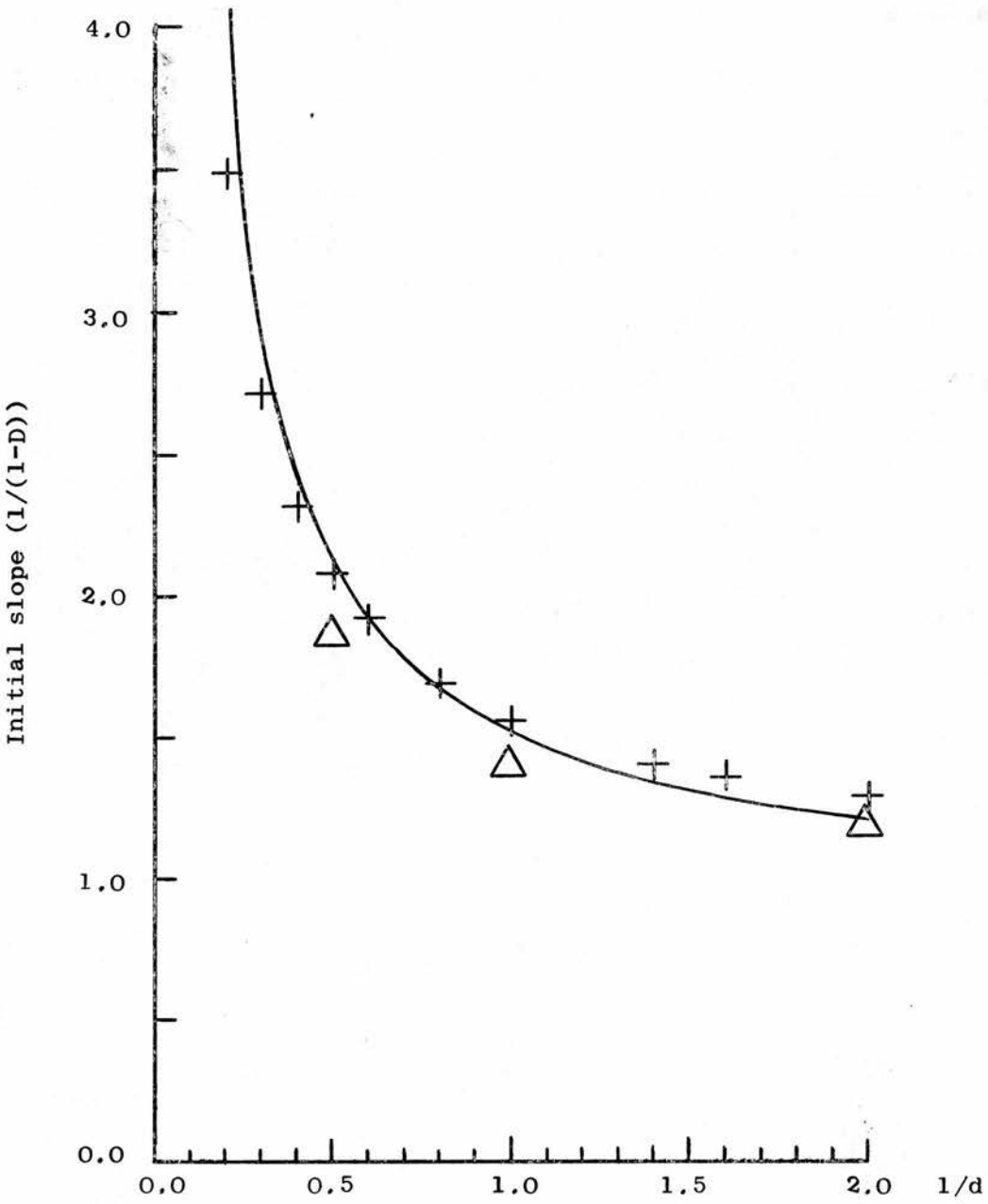

Fig. 6.3

Initial slope of magnetization curve. Solid line for ellipsoids (1/(1-D); + computed for superconducting cylinders; △ Shoenberg's experimental values.

penetration were computed for four length/diameter ratios. These are shown on fig. 6.2. The initial slopes of the magnetization curves were also computed for a number of (l/d) ratios. These gave a measure of the effective demagnetizing factor of the superconducting cylinders without penetration. In fig. 6.3 these are compared with Shoenberg's experimental values and the slopes of magnetization curves for ellipsoids (1/(1-D)) for (l/d) ratios from 0.2 to 2.0.

The most striking feature of fig. 6.2 is that the curves rise well above 1.0 for the lower (l/d) ratios. If the area under the curve is to be kept equal to the condensation energy, the curve can therefore not fall linearly to zero at H_c. This part of the curve can of course not be determined from the computations, but the broken lines are curves drawn so as to make the integral have the correct value. There is no other justification for them.

Fig. 6.3 shows that the initial slopes of the magnetization curves are very similar to those for ellipsoids. This is to be expected, since the slope is a measure of the total distortion of the magnetic field due to the presence of the superconducting body, and this probably should be similar for bodies of the same eccentricity. It seems though that cylinders of $(l/d) \lesssim 0.6$ disturb the field less than the corresponding ellipsoids do, but longer cylinders more.

The experimental values are lower than the computed ones but have a similar relation to the (1/(1-D)) curve in that as the (l/d) ratio increases they approach the curve and cut it at $(l/d) \simeq 2.0$.

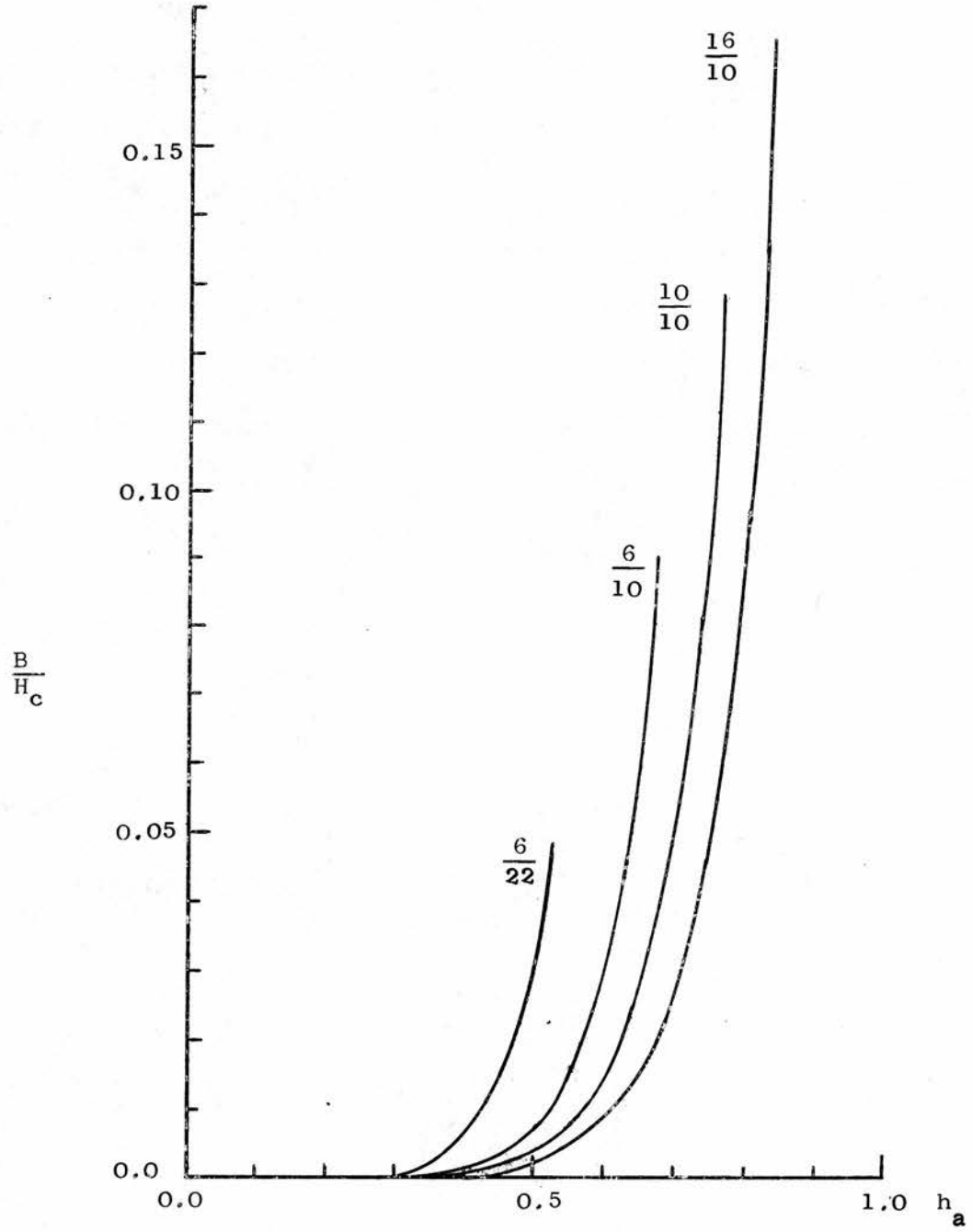

Fig. 6.4

B/H curves for cylinders of (l/d) ratio 0.273, 0.6, 1.0, and 1.6.

The average value of the axial component of the flux inside the specimen has been computed for the four (l/d) ratios and is plotted against h_a on fig. 6.4. It was found by integrating the axial component of $\underline{B}$ numerically over the penetrating region and dividing the integral by the total volume of the specimen. This quantity is easily determined experimentally by wrapping a coil around the specimen and measuring the e.m.f. No ~~experimental results~~ measurements have however been found in the literature and none were made. The results are therefore purely computational. As before the curves only go up to the start of the second stage of penetration (h_i).

CHAPTER 7 - FINE INTERMEDIATE STATE STRUCTURE

7.1 Introduction

As already mentioned, Baird (1964, 1965) reported that the penetration, as seen on the top surface, did not have angular symmetry but had corrugations or "fingers" imposed on it. His first observation of the fingers was made with a CMP glass disc where they showed up as shallow corrugations on the interface.

The resolution of the method was very poor and the results were difficult to explain. It looked however as if the fingers were connected with the interface rather than the bulk of the penetrating region.

Recently Baird has used a thin slice of a terbium aluminium garnet crystal in his experiments (Baird (private communication)). This material has a Faraday rotation four times that of CMP glass and the resolution has improved considerably. With this new setup the corrugations show up clearly and it is obvious that they go quite far into the penetrating region. Baird though did not believe that they reached all the way to the rim of the cylinder and he considered the penetrating region to be in a supercooled normal state.

The free boundary computations showed that the field in the penetrating region was lower than H_c, falling to about 0.75 H_c at the rim of the cylinder. If therefore the region was in a supercooled normal state it did have a considerable amount of excess energy that it could reduce by going into an intermediate state. As both phases were present in the specimen, it did in fact seem absurd that supercooling should be

present at all. It seemed much more likely that the corrugations were the coarsest part of an intermediate state structure so fine that most of it was unresolved by the experiments.

The resolution of the CMP glass was too poor to test this possibility and other methods were therefore tried. After an unsuccessful attempt at using thin films of europium chalcogenides it was decided to try powder methods. First superconducting niobium powder was used but it tended to stick together and was unsatisfactory. Next superconducting vanadium powder of average dimensions $\sim 50\,\mu m$ was tried and was found to be both freeflowing and easy to use.

The vanadium powder gave a resolution of about 100 μm which was sufficient to show that Baird's "fingers" were in fact the ends of radial laminae that extended through the penetrating region right out to the edge of the cylinder. As expected the structure is coarse near the interface but gets finer towards the outer edge of the cylinder.

Even though the average field in the penetrating region was known from the free boundary computations the problem was still complicated, and it was not easy to deduce the dimensions of an intermediate state structure. However some simple calculations showed that if the supercooled penetrating region split up into an intermediate state, the energy saved by the elimination of the supercooling was sufficient to create internal phase boundaries corresponding to an average laminar period of about 100-200 μm. When compared with the experimentally observed values that range from about 100 μm at the edge of the cylinder, to about 400 μm at the interface, there seemed little doubt that the fingers were in

fact an intermediate state structure and that a further investigation would be worthwhile. Landau's model of the intermediate state in an infinite plate was therefore adapted to the penetrating region of the cylinder and the laminar period computed as a function of radial distance. The model was found to account reasonably well for the observed structure.

7.2 Experimental results

If the laminae are indeed an intermediate state structure their dimensions should only be affected by sample dimensions and the surface energy of the material, but not by temperature, purity, material, and method of preparation, unless as far as these affect the surface energy. To test this, experiments were done at a number of temperatures on three samples of the same length/diameter ratio: (i) In4, an impure indium sample made by cold pressing; (ii) In6, a pure indium sample, cast; (iii) Sn1, a tin sample, cast and faced up in a lathe.

In two cases, In6 and Sn1 both at 1.4 ^{o}K, the samples were successfully removed from the cryostat without disturbing the powder pattern and a very good resolution was obtained. In the other cases the pattern was photographed inside the cryostat and, as the resolution was inferior, the results were not as reliable.

To some extent the powder follows changes in the flux pattern and the method can, if used with care, give a picture of dynamic processes. With increasing applied field the penetration seemed to proceed as follows: At $h_a \simeq 0.3 - 0.4$ flux penetration became noticeable along the top edge. (This refers to the (l/d) = 6/10 specimens. For

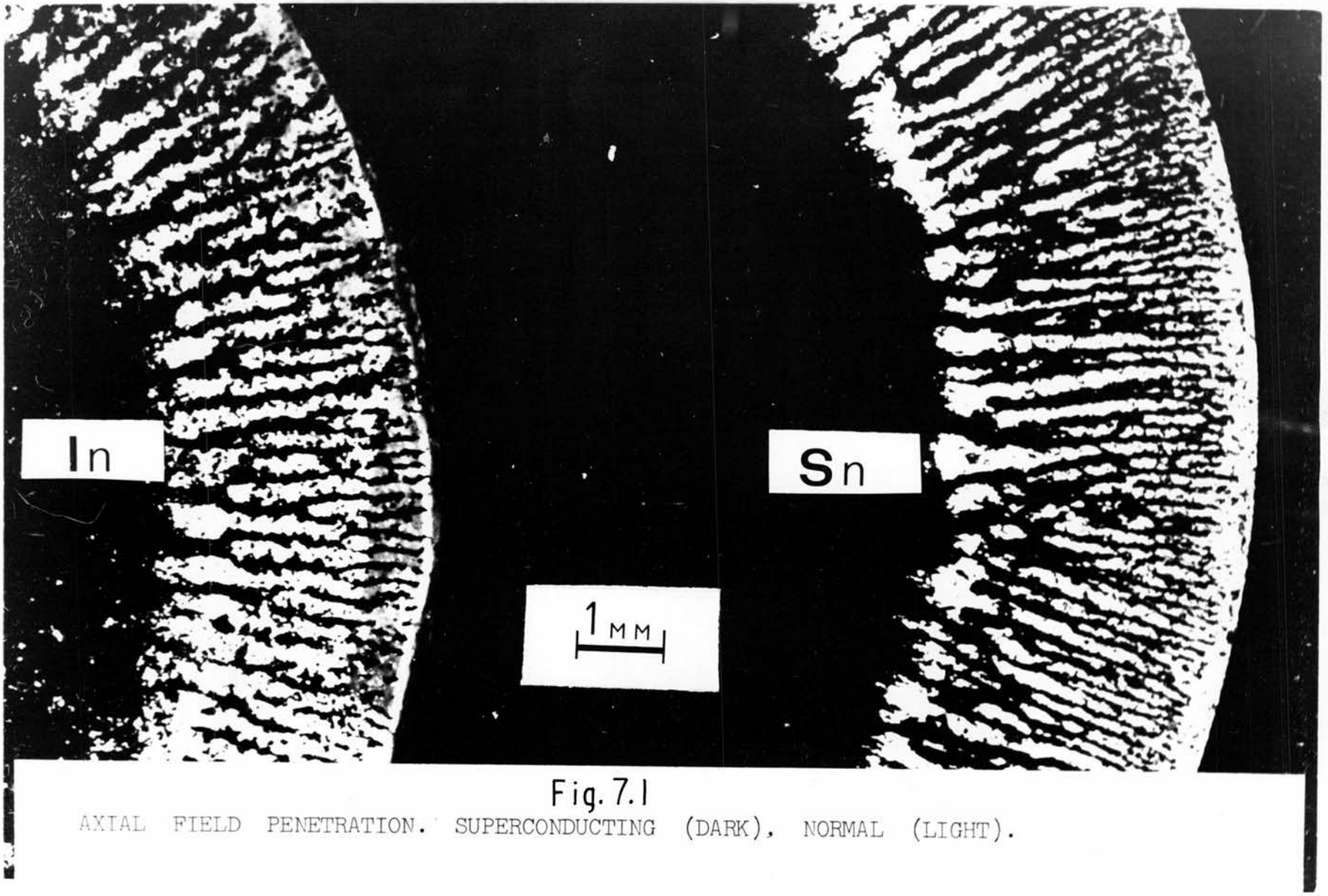

Fig. 7.1

AXIAL FIELD PENETRATION. SUPERCONDUCTING (DARK). NORMAL (LIGHT).

other (1/d) ratios the field values are different). It appeared to have angular symmetry and no fingers. As the field was increased it proceeded inwards and subsequently split up into radial laminae. The dimensions of these laminae were of ~~a similar~~ the same magnitude as the limit of resolution, so what appeared to be a continuous penetration region might have been laminar, but too fine to be resolved.

As the applied field was increased further, some of the laminae penetrated further into the specimen, but others were gradually left behind. The structure therefore became coarsest near the penetration edge but finer towards the rim of the cylinder.

At a well defined value of the applied field the laminar penetration stopped and flux bundles dropped off the ends of the laminae and drifted to the centre, as reported by Baird. In the tin sample the start of the second stage was less well defined than in the indium. The flux bundles were not as free to move and were often trapped quite near the penetrating front and some never reached the centre of the specimen. This trapping however, did not seem to affect the laminar penetration.

A photograph of the penetrating region of In6 and Sn1 at 1.4 ^{o}K is shown on fig. 7.1. It shows clearly how the laminae reach right out to the edge of the cylinder. It also shows the very noticeable difference in the dimensions of the fingers in the two metals. In indium the structure is coarser, as would be expected as its surface energy is considerably higher.

For each sample a similar change in finger dimensions with temperature was noticed, again indicating dependence on surface energy.

The period of the laminar structure was found by counting the number of laminae within a given angle at 0.5 mm intervals along the radius.

7.3 Computed results

When both the experimental results and the preliminary calculations indicated that the penetrating region was in an intermediate state, it seemed useful to attempt to compute the dimensions of the laminae from the field in the penetrating region. Although the average field at each mesh point in the region was known, the problem was still too complicated to compute directly and considerable simplifications had to be made.

As can be seen in fig. 7.1 the laminae are unbranched in the sense of Landau's branched and unbranched models. The reduction in laminar period along the radius is not branching in this sense but is due to the lower local field and the lower effective thickness, particularly the latter, towards the rim of the cylinder. It therefore seemed that Landau's unbranched model of the intermediate state might be used, with some modifications, to describe the structure.

In Landau's model the applied field is perpendicular to the surface of the plate and the total magnetic field is therefore distorted as it emerges at the surface. The total field does therefore contribute to the Gibbs free energy of the plate and appears in the expression for the laminar period. In a slanting field this is no longer so. Sharvin (1957) has successfully adapted Landau's unbranched model to this case

by assuming that only the component of the applied field perpendicular to the surface contributes to the magnetic part of the Gibbs free energy. This led him to the following expression for the laminar period a (the average distance between centres of adjacent normal laminae)

$$a = \frac{1}{(1-h_\rho^2)^{1/2}} \sqrt{\frac{L\,\Delta}{f(\eta_2)}} \qquad (7.1)$$

where h_a is the reduced applied field with components h_ρ and h_z parallel and perpendicular to the plate surface respectively. L is the thickness of the plate, f is a numerically evaluated function and $\eta_2 = h_z(1-h_\rho^2)^{1/2}$.

In the penetrating region of the cylinder the situation is similar to that of an infinite plate in a slanting field in that the field does not leave the specimen normal to the surface. Only its normal component should therefore contribute to the Gibbs free energy. The situation is however more complicated than in the plate, in that the field direction is not constant in the region that affects the magnetic energy, that is the region just below and just above the surface. In this work the value at the surface has been used as the best approximation available.

The surface energy does of course not depend on the direction of the field, so inside the direction is unimportant.

In the penetrating region the field is approximately constant along a flux line. At each point on the surface the laminar period should therefore be approximately determined by the local value of the

field and on the ratio of surface energy to magnetic energy.

Apart from the direction of the emerging field, the ratio of magnetic to surface energy is determined by the ratio of the area of the normal-superconducting boundary to the length of the intersection of this boundary with the surface of the plate. In equation (7.1) this is represented by the thickness L. For the cylinder the ratio corresponding to L is the change in the cross-sectional area of the penetrating region with radial distance, dA/dr. The area could be taken to be the area between fluxlines but an equally good approximation should be the area of the penetration profiles. This has the advantage of being already computed for a number of applied fields. The area can be expressed as a function of the corresponding "superconducting radius" and dA/dr found by numerical differentiation.

It was found that the direction of the flux lines with respect to the surface was similar on both surfaces so it was only necessary to consider the top surface.

It has now been shown that an equation similar to (7.1) could, with a suitable modification, be expected to give approximate values for the laminar period in the penetration region of the cylinder. If h is taken to be the reduced local field on the top surface and L replaced by dA/dr, the expression for the laminar period takes the form

$$\frac{a}{\Delta^{1/2}} = \left(\frac{dA/dr}{(1-h_\rho^2) f(\eta_2)} \right)^{1/2} \qquad (7.2)$$

The expression has been reduced by dividing by $\Delta^{1/2}$ so that specimens

of different materials and temperatures may be directly compared. The function $f(\eta_2)$ has been tabulated by Lifshitz and Sharvin (1951).

Expression (7.2) is dimensional and shows that the laminar period should increase as the square root of the radius of the specimen.

As the field on the superconducting-intermediate state interface was assumed to be equal to the critical field, the period tends towards infinity near the interface. In reality this can obviously not be so. As the superconducting laminae spread from the superconducting centre region through the interface and into the penetrating region the real interface must be different from the computed one, either in position or in the value of the average field on it. The previous results where the superconducting radius was consistently smaller than what was computed indicate that it was the position that was different.

7.4 Comparison of experimental and computed results

To compare the experimental results with the computed laminar period both are plotted as a function of reduced radial distance $\rho = r/r_o$ (r_o = radius of cylinder). To make comparison between different samples and temperatures sensible the laminar period a has been reduced by dividing it by the square root of the surface energy parameter Δ. Values of Δ were computed from

$$\Delta(t) = \Delta(0)/(1-t^{3/2})^{1/2}$$

For the pure samples $\Delta(0)$ was taken to be 2.3×10^{-5} and 3.4×10^{-5} cm for tin and indium respectively (Faber (1958), and Davies (1960)).

The specimen, In4, contains 0.9 at % lead, and for this alloy there are no surface energy measurements available. However it appears from Davies' (1960) measurements of relative surface energy parameters in Sn + In, Sn + Sb, and In + Sn alloys, that Δ depends more on the mean free path of the electrons (l) in the specimen than on the metals themselves.

The mean free path in specimen In4 can be found from the residual resistivity, $\rho_{4.2\ ^oK}$. This has been found to increase with Pb content as 0.55 - 0.60 $\mu\Omega$cm/at.% Pb (Gygax et.al. (1964), Noto et.al. (1966)).

If further ($\rho_{4.2\ ^oK} \times l$) is assumed to be constant and equal to that of pure indium, as seems reasonable for this low impurity content, the mean free path can be found. For pure indium Cotti (1963) has found

$$\rho_{4.2\ ^oK} \cdot l = 1.4 \times 10^{-11}\ \Omega\,cm^2$$

For In4 $\rho_{4.2\ ^oK} \simeq 0.5\ \mu\Omega$cm, which gives $l \simeq 0.3\ \mu$m. According to Davies (1960) this would give

$$\Delta(0)_{pure} / \Delta(0)_{alloy} \simeq 1.5$$

Taking $\Delta(0)_{In} = 3.4 \times 10^{-5}$ cm, the surface energy parameter for specimen In4 should be $\Delta(0)_{In4}$ 2.3×10^{-5} cm.

The experimental results for In4 were reasonably good so in spite of the approximations and assumptions made in estimating its surface energy parameter they have been included. The possibility of a considerable error in Δ should though be kept in mind.

As the expression for the reduced finger periodicity $a/\Delta^{1/2}$ (equation (7.2)) is dimensional, both the computed and experimental results have to be adjusted to take account of different sample dimensions. Here they have all been scaled down to a 10.0 mm

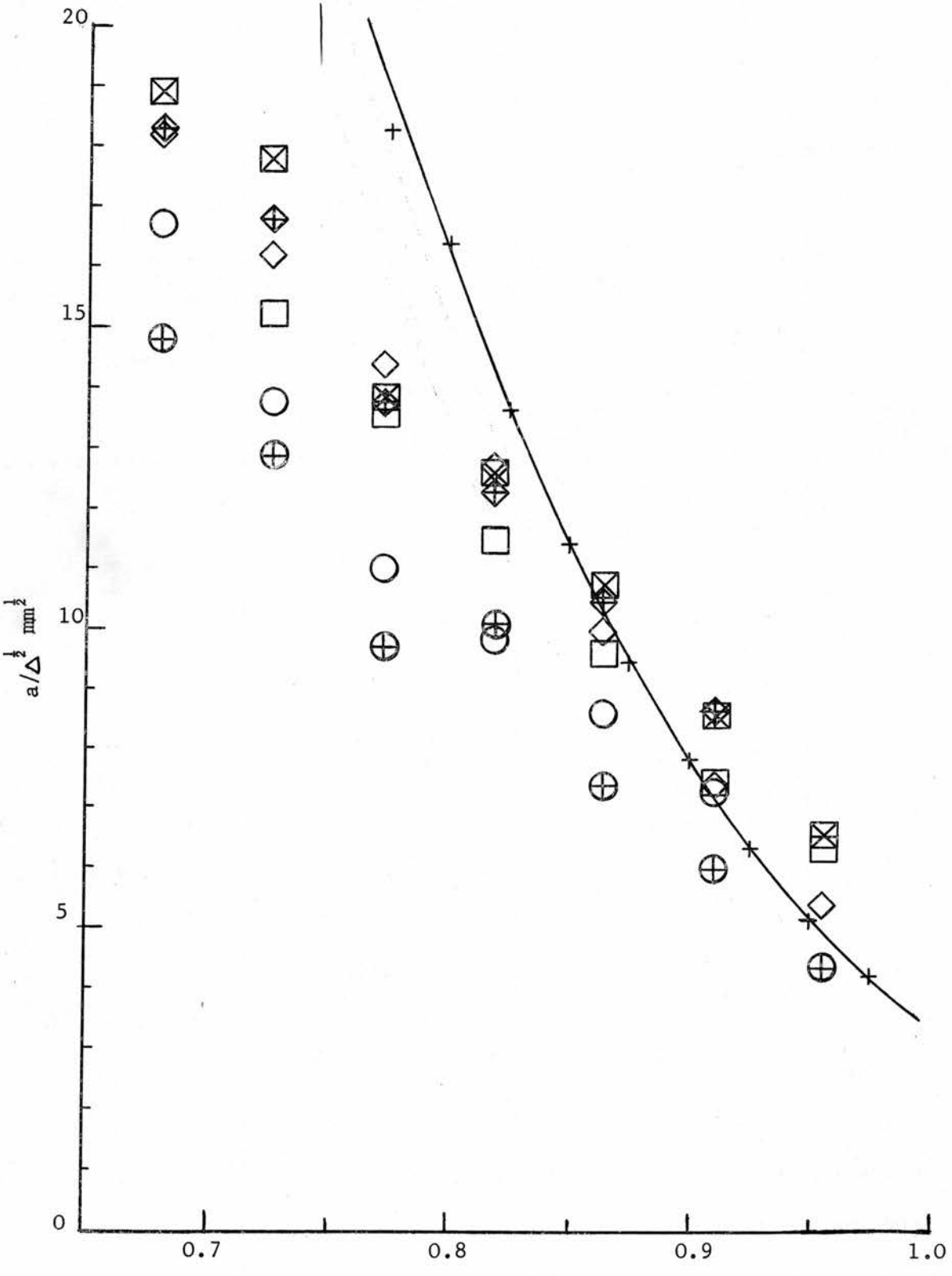

Fig. 7.2. Reduced laminar period plotted against reduced radius; +——+ computed; ⊕ In4 at 1.4 K; ◇ In4 at 2.16 K; ⊠ In6 at 1.4 K; □ In6 at 2.16 K; ⊕ Sn1 at 1.4 K; ○ Sn1 at 1.67 K.

cylinder diameter.

In fig. 7.2 the laminar period has been plotted for In4, In6, and Sn1. The measurements were done at two temperatures for each specimen. On the same graph are plotted the values of $a/\Delta^{1/2}$ computed from the profile on the 6.0 x 10.0 mm specimen corresponding to equatorial penetration.

For each run the experimental results can be seen to be reasonably smooth but there is a considerable difference between runs. The discrepancy is even larger than the experimental error, estimated to be about 15%. There are however not enough measurements to show up systematic errors.

As mentioned above, the assumption that the field is critical on the boundary between the two phases causes the computed laminar period to tend to infinity near the penetrating front. Together with the fact that the experimental superconducting radius is smaller than the computed one, this seems to be the main cause of the discrepancy between the experimental and computed results. As has already been emphasized the assumption is not realistic, but a better approximation has not been found. If however the laminae penetrate further in than the critical field profile, and the main difference in the field pattern is near the interface, as the Faraday rotation experiment indicated, this discrepancy could be expected to disappear. Considering the assumptions made in the computations, the computed values can therefore be said to agree reasonably well with the experimental results.

7.5 Summary

In this chapter it has been shown that the penetrating region is not in a supercooled normal state but in a laminar intermediate state. This has been done experimentally as well as by computing the dimensions of the intermediate state structure from the average field in the penetrating region.

It is considered likely that this form of penetration is not confined to cylinders but is characteristic of penetration of sharp corners where the boundary is convex.

The effect of the laminar structure on the field penetration is surprisingly small. Some adjustment of the penetrating front and the region just behind it, does though seem to take place and the penetrating front is probably rather more advanced than what was computed. Surprisingly, the applied field value at the start of the second stage (h_i) does not seem to be affected by this. The effect could though be cancelled out by other effects, such as the need for some equatorial penetration before flux bundles can form.

With the above reservations the penetration is therefore reasonably well described by the mathematical model and what was written in chapter 5 is still valid.

CHAPTER 8 - SUMMARY

8.1 Discussion of results

The purpose of the research was to establish the nature of the field penetration into superconducting cylinders. In particular the intention was to test Baird's hypothesis that the first stage of penetration consisted of penetration of the corners of the cylinder and was due to demagnetizing effects, and that the second stage was reached when the two penetrating regions met and just penetrated the equator.

To do this the first stage of field penetration has been studied in some detail experimentally. Computer programs that solve the field equations outside the specimen and find the penetration profiles have also been written. These profiles have been determined for a number of applied fields for each of four length/diameter ratios: 0.273, 0.6, 1.0, and 1.6.

The mathematical model was found to represent the physical system reasonably accurately and it is believed that Baird's hypothesis has been proved.

It has furthermore been shown that the penetration is not uniform but consists of laminae perpendicular to the penetrating front. It has also been shown that this laminar structure is due to the field behind the boundary being lower than the critical field. To reduce the extra energy due to a supercooled normal region, superconducting "fingers" therefore spread from the superconducting centre region into the penetrating region. The period of the structure has been shown to agree with that computed from the average field values in the region, using a modification of Landau's unbranched model. It is believed that this behaviour is not confined to cylinders but is also observed in flat plates (Solomon and Harris (1970)) and possibly in

all configurations where the penetration has a convex interface.

The magnetic moment was computed for each penetration profile for all the four (l/d) ratios. For length/diameter ratio unity the computations were compared with experimental results (Shoenberg (1937)). There was a 10% discrepancy between the results, for which no explanation has been found. As other measurements on magnetic moments do not exist and none were made, the results are mainly computational.

B/H curves have also been computed for the first stage of penetration for all the four (l/d) ratios, but no measurements were made. The results could be used to check the mathematical model further. Alternatively they could be of use when studying field penetration into type I, and possibly type II, superconductors.

It seems likely that all the above results would hold for the first stage of penetration into type II superconductors. The first stage of penetration is probably very similar to that of type I superconductors described here but with the first critical field H_{c1} having the same role as H_c has in type I.

In type II there would probably be a very considerable amount of trapping so the second stage of penetration is unlikely to be well distinguished from the first stage, as it is in pure type I superconductors.

8.2 Further discussion

It would hardly be worthwhile to do more work on the free boundaries, except when the results are needed for other work, as nothing important could be expected from computing other (l/d) ratios. It might though be interesting

to compute the penetration for long cylinders of (l/d) = 3.0 - 5.0 in order to estimate the errors involved when such specimens are treated as infinite cylinders.

It might be considered worthwhile to make more measurements on the fine intermediate state structure in the penetrating region, for example on other (l/d) ratios.

The discrepancy between the measured and computed magnetic moments remains puzzling and it would be interesting to make measurements of these.

It was hoped that the laminar period in the penetrating region could be used to find the surface energy parameter for other metals and alloys. It however turned out that the results are not accurate enough.

As mentioned above it would be interesting to study the first stage of penetration in type II cylinders. A particularly interesting possibility is the "intermediate state" of mixed and superconducting phases.

The numerical method used to compute the flux and the field is quite powerful and with modern highspeed computers it could be applied to many similar field equations. Two dimensional problems and problems with radial symmetry are easily dealt with and it should even be possible to solve small three dimensional problems.

The iterative method used to solve the free boundary problem, might not seem sophisticated. The fact is however that even to applied mathematicians the free boundary problem poses formidable problems, and it seems that the relatively simple approach used here is the best way

of attacking the problem. Particularly when the minimization is done automatically, it is in fact very well suited to the brute force of modern computers.

The experimental setup used here is not recommended, and a large proportion of the difficulties experienced in this work was caused by the very long viewing distance. It would be considerably easier to use dewars with bottom windows (Kirchner (1968b), Carroll et.al. (1967), Goodman et.al. (1966). This would cut the viewing distance considerably and allow a microscope to be used in place of the telescope.

REFERENCES

1. Books on superconductivity

DE GENNES, P.G. (1966), Superconductivity of Metals and Alloys, Benjamin, New York.

KUPER, C.G. (1968), An Introduction to the Theory of Superconductivity Clarendon Press, Oxford.

LONDON, F. (1950), Superfluids Vol. I, Dover Publications, Inc., New York.

LYNTON, E.A. (1962), Superconductivity, Methuen, London.

PARKS, R.D. (editor), (1969), Superconductivity, Marcel Dekker, New York.

ROSE-INNES, A.C., and RHODERICK, E.H. (1969), Introduction to Superconductivity, Pergamon Press, Oxford.

SHOENBERG, D. (1938), Superconductivity, Cambridge University Press.

REFERENCES

2. Books on computational techniques

DE G. ALLEN, D.N. (1954), Relaxation Methods in Engineering and Science, McGraw-Hill, New York.

GROVE, W.E. (1966), Brief Numerical Methods, Prentice-Hall, Englewood Cliffs, N.J.

SOUTHWELL, R.V. (1946), Relaxation Methods in Theoretical Physics, Clarendon Press, Oxford.

VARGA, R.S. (1962), Matrix Iterative Analysis, Prentice Hall, Englewood Cliffs, N.J.

WACHSPRESS, E.L. (1966), Iterative Solution of Elliptic Systems, Prentice Hall, Englewood Cliffs, N.J.

REFERENCES

3. Original Papers

ABRIKOSOV, A.A. (1957), J.E.T.P. USSR 32, 1442-52; Sov.Phys. J.E.T.P. 5, 1174-85; J.Phys.Chem.Solids 2, 199-208.

ALERS, P.B. (1956), Phys.Rev. 105, 104-108.

ALERS, P.B. (1959), Phys.Rev. 116, 1483.

ANDREW, E.R. (1948), Proc.Roy.Soc. A194 , 98-112.

BAIRD, D.C. (1964), Can.J.Phys. 42, 1682-6.

BAIRD D.C. (1965), Can.J.Phys. 43, 971-2.

BALASHOVA, B.M., and SHARVIN, YU.V. (1956), J.E.T.P. USSR 31, 40-4; Soviet Phys. J.E.T.P. 4, 54-9 (1957).

BARDEEN, J., COOPER, L.N. and SCHRIEFFER, J.R. (1957), Phys.Rev. 108, 1175-1204.

CARROLL, K.J., LIEBENBERG, D.H., and OVERTON, W.C. (1967), Rev.Sci. Instrum. 38, 260-1.

COCHRAN, J.F., and KAESER, R.S. (1957), Physica 23, 727-45.

COOPER, L.N. (1956), Phys.Rev. 104, 1189.

COTTI, P. (1963), Phys.Letters 4, 114-6.

DAVIES, E.A. (1960), Proc.Roy.Soc. A255, 407-26.

DE SORBO, W. (1960), Phys.Rev.Letters, 4, 406-8.

DE SORBO, W., and NEWHOUSE, V.L. (1962), J.App.Phys. 33, 1004-9.

DE SORBO, W., and HEALY, W.A. (1964), Cryogenics 4, 257-323.

DE SORBO, W. (1965), Phil.Mag. 11, 853-62.

FABER, T.E. (1952), Proc.Roy.Soc. A214, 392-412.

FABER, T.E. (1958), Proc.Roy.Soc. A248, 460-81.

GINZBURG, V.L., and LANDAU, L.D. (1950), J.E.T.P. USSR 20, 1064.

see also GINZBURG, V.L., Nuovo Cimento 2, 1234-50 (1955).

GOODMAN, B.B., LACAZE, A., and WERTHEIMER, M.R. (1966), Compt. Rend. 262, 12-5.

GORTER, C.J. (1933), Arch.Mus.Teyler 7, 378.

GORTER, C.J., and CASIMIR, H.B.G. (1934a), Physica 1, 306-20.

GORTER, C.J., and CASIMIR, H.B.G. (1934b), Phys.Z. 35, 963-6; Z.Techn.Phys. 15, 539.

GYGAX, S., OLSEN, J.L., and KROPSCHOT, R.H. (1964), Phys.Letters 8, 228-30.

HAENSSLER, F., and RINDERER, L. (1960), Helv.Phys.Acta 33, 505-7.

HAENSSLER, F., and RINDERER, L. (1965a), Phys.Letters 16, 29-30.

HAENSSLER, F., and RINDERER, L. (1965b), Helv.Phys.Acta 38, 448-54.

HAERING, R.R., TOXEN, A.M., MILLER, P.B., DUMKE, W.P., and KINGTON, B.W. (1963), Solid-State Electronics 6, 365-75.

HUEBENER, R.P., ROWE, V.A., and KAMPWIRTH, R.T. (1970a). J.App.Phys. 41, 2963-7.

HUEBENER, R.P., ROWE, V.A., and KAMPWIRTH, R.T., (1970b), Proc. 12th Intern.Conf. on Low Temp.Phys., Kyoto 1970 (to be published).

KAMERLINGH ONNES, H. (1911), Leiden Comm. 122b, 124c.

KAMERLINGH ONNES, H. (1913), Leiden Comm.Suppl. 34.

KAMERLINGH ONNES, H., and TUYN, W. (1923), Prog.Acad.Sci.Amsterdam 25, 443.

KEESOM, W.H. (1924), 4e Congr.Phys.Solvay, p.288.

KIRCHNER, H. (1968a), Phys.Letters 26A, 651-2.

KIRCHNER, H. (1968b), Proc. 11th Intern.Conf. on Low Temp. Phys., Vol. II (815-8) St. Andrews, Eds. J.F. Allen, D.M. Finlayson, and D.M. McCall (University of St. Andrews Printing Department).

KIRCHNER, H. (1969), Phys.Letters 30A, 437-8.

KUPER, C.G. (1951), Phil.Mag. 42, 961-77.

LANDAU, L.D. (1937), J.E.T.P. USSR 7, 371; Phys.Z.Sowjet. 11, 129.

LANDAU, L.D. (1943), J.E.T.P. USSR 13, 377.

LANDAU, L.D., and LIFSHITZ, E.M. (1960), Electrodynamics of Continuous Media, Chapter IV, Vol.8 of Course of Theoretical Physics - Pergamon Press, London.

LIFSHITZ, E.M., and SHARVIN, YU.V. (1951), Doklady Akad. Nauk USSR 79, 783.

LONDON, F., and LONDON H. (1935a), Proc.Roy.Soc. A149, 71-88.

LONDON, F. and LONDON H. (1935b), Physica 2, 341-54.

LONDON F. (1936), Physica 3, 450-62.

LONDON H. (1935), Proc.Roy.Soc. A152, 650-63.

MEISSNER, W., and OCHSENFELD, R. (1933), Naturwiss. 21, 787.

MESHKOVSKY, A., and SHALNIKOV, A.(1947), J.Phys.USSR 11, 1-15.

NOTO, K., MUTO, Y., and FUKUROI, T. (1966), J.Phys.Soc. Japan 21, 2122-31.

PEIERLS, R. (1936), Proc.Roy.Soc. A155, 613-28.

PIPPARD, A.B. (1950), Proc.Roy.Soc. A203, 210-23.

PIPPARD, A.B. (1951), Proc.Camb.Phil.Soc. 47, 617-25.

PIPPARD, A.B. (1953), Proc.Roy.Soc. A216, 547-68.

PIPPARD, A.B. (1957), Classical Thermodynamics, Cambridge University Press.

QUINN III, D.J., and ITTNER III, W.B. (1962), J.Appl.Phys. 33, 748-9.

RINDERER, L., and HAENSSLER, F. (1959), Helv.Phys.Acta 32, 320-2.

ROSE-INNES, A.C., and RHODERICK, E.H. (1969), Introduction to Superconductivity, Pergamon Press, Oxford.

SARMA, N.V., and MOON, J.R. (1967), Phil.Mag., 16, 433-45.

SCHAWLOW, A.L., MATTHIAS, B.T., LEWIS, H.W., and DEVLIN, G.E. (1954), Phys.Rev. 95, 1344-5.

SCHAWLOW, A.L. (1956), Phys.Rev. 101, 573-9.

SCHAWLOW, A.L., and DEVLIN, G.E. (1958), Phys.Rev. 110, 1011-6.

SCHAWLOW, A.L., DEVLIN, G.E., and HULM, J.K. (1959), Phys.Rev. 116, 626-7.

SHARVIN, YU.V. (1957), J.E.T.P. USSR 33, 1341-6; Sov.Phys.J.E.T.P. 6, 1031-5.

SHOENBERG, D. (1936), Prog.Roy.Soc. 155, 712-26.

SHOENBERG, D. (1937), Proc.Camb.Phil.Soc. 33, 260-76.

SOLOMON, P.R., and HARRIS, R.E. (1970), Proc. 12th Intern.Conf. on Low Temp.Phys., Kyoto 1970 (to be published).

STRATTON, J.A. (1941), Electromagnetic Theory, McGraw-Hill, New York.

TRÄUBLE, H., and ESSMANN, U. (1966a), J.Sci.Instrum. 43, 344.

TRÄUBLE, H., and ESSMANN, U. (1966b), Phys.Stat.Sol. 18, 813-28.